

**PERFORMANCE OF UNSTIFFENED STEEL PLATE SHEAR
WALLS UNDER CYCLIC QUASI-STATIC LOADING**

by

ADAM S. LUBELL

B.A.Sc., University of Waterloo, 1995

A THESIS SUBMITTED IN PARTIAL FULFILLMENT OF
THE REQUIREMENTS FOR THE DEGREE OF
MASTER OF APPLIED SCIENCE

in

THE FACULTY OF GRADUATE STUDIES

Department of Civil Engineering

We accept this thesis as conforming

to the required standard

THE UNIVERSITY OF BRITISH COLUMBIA

June 1997

© Adam Lubell, 1997

In presenting this thesis in partial fulfilment for an advanced degree at the University of British Columbia, I agree that the Library shall make it freely available for reference and study. I further agree that permission for extensive copying of this thesis for scholarly purposes may be granted by the head of my department or by his or her representatives. It is understood that copying or publication of this thesis for financial gain shall not be allowed without my express permission.

Department of Civil Engineering
The University of British Columbia
2324 Main Mall
Vancouver, Canada
V6T 1Z4

Date: MAY 30/97.

ABSTRACT

Several structures around the world have been designed with steel plate shear walls acting as the primary lateral load resisting system. It represents an innovative technique for providing high elastic strength, large displacement ductility capacity, and good energy dissipation properties in medium and highrise steel structures, which is of particular importance in areas of high seismic risk.

An experimental testing programme was conducted at the University of British Columbia on two single and one multistorey steel plate shear wall assemblies. Each specimen consisted of a single bay, 30 % scale model of an inner residential building core with panel width to height aspect ratios of 1:1. Each specimen employed moment-resisting beam column connections, and thin unstiffened infill panels with full perimeter attachment to the surrounding frame. Quasi-static cyclic testing was conducted under standard testing protocols used to determine the seismic performance of steel structures. The determination of the load deformation response properties and resulting strain distribution in various components were the primary objectives of the testing program.

The three test specimens were tested to maximum displacement ductilities of $7 \times \delta_y$, $6 \times \delta_y$, and $1.5 \times \delta_y$, respectively. The termination of each test was a result of local problems and limitations of the testing setup, and did not necessarily reflect the global

displacement capacity limit of each specimen. Based on accepted guidelines, each specimen was characterised at test termination as experiencing moderate inelastic damage while maintaining a force resistance capacity at or near the maximum level achieved. Inelastic damage modes included yielding of the infill plate followed by column yielding in the single storey specimens, and column yielding in the multistorey specimen.

Simplified tension field analytical models were developed using a non-linear frame analysis program. Numerical modelling was conducted for monotonic and cyclic loading cases, and compared with the load-deformation response characteristics obtained from physical testing. Additional studies were conducted on one of the models to investigate the sensitivity of the results to various model parameters.

Finally, the adequacy of existing design guidelines were assessed on the basis of the experimental and analytical results generated through this research programme. Proposed modifications to the existing code provisions have been identified.

TABLE OF CONTENTS

ABSTRACT	ii
TABLE OF CONTENTS	iv
LIST OF TABLES	viii
LIST OF FIGURES	ix
LIST OF SYMBOLS	xii
ACKNOWLEDGMENTS	xiv
CHAPTER 1 Introduction	
1.1 Background	1
1.2 Overview of the Research Program	2
1.3 Scope and Objectives of this Thesis	3
1.4 Outline of Thesis	4
CHAPTER 2 Literature Survey	
2.1 Background	6
2.2 Review of Published Research	8
2.2.1 Study by Takahashi et al. (1973), Japan	9
2.2.2 Early Studies at the University of Alberta, Canada	9
2.2.3 Research at the University of Wales, United Kingdom	11
2.2.4 Research at Kansai University, Japan	13
2.2.5 Research at the University of Maine, USA	14
2.2.6 Research at Lehigh University, USA	17
2.2.7 Recent Studies at University of Alberta, Canada	19

CHAPTER 3 Single Panel Experimental Programme

3.1 Introduction	21
3.2 Test Specimens	21
3.3 Loading Systems	26
3.4 Lateral Support System	28
3.5 Instrumentation and Data Acquisition	29
3.6 Testing Procedures	32

CHAPTER 4 Discussion of Single Panel Results

4.1 Summary of Test Results	36
4.2 SPSW1 Test	36
4.2.1 Load Deformation Characteristics	36
4.2.2 Strain Distributions	40
4.2.3 Failure Mode	43
4.2.4 Other Observations	45
4.3 SPSW2 Test	46
4.3.1 Load Deformation Characteristics	46
4.3.2 Frame Behaviour	50
4.3.3 Plate Behaviour	52
4.4 Comparison of SPSW1 and SPSW2	53
4.4.1 Frame Element Effects	53
4.4.2 Loading Histories	54
4.4.3 Displacement Ductilities	55

CHAPTER 5 Multistorey Experimental Programme

5.1 Introduction	58
5.2 Test Specimen	58
5.3 Loading System	63
5.4 Lateral Support System	65
5.5 Instrumentation and Data Acquisition	66

5.6 Testing Procedures	71
 CHAPTER 6 Discussion of Multistorey Results	
6.1 Summary of Test Results	74
6.2 Material Tests	75
6.3 Failure Mechanism	76
6.4 Load-Deformation Characteristics	80
6.5 Local Column Deformation	83
6.6 Infill Panel Behaviour	84
6.7 Strain Gauge Analysis	86
6.7.1 Infill Panel Strain Distribution	86
6.7.2 Frame Element Strains	89
6.8 Vibration Testing	94
6.9 Comparison with Single Storey Results	95
 CHAPTER 7 Analytical Modelling of the Test Specimens	
7.1 Introduction	98
7.2 Simplified Tension Field Strip Model	99
7.3 CANNY-E Software	102
7.4 Common Model Parameters	103
7.5 Modelling of Monotonic Loading	107
7.6 Modelling of Reverse Cyclic Loading	110
 CHAPTER 8 Results of Analytical Modelling	
8.1 Introduction	113
8.2 Single Storey SPSWs	113
8.2.1 Monotonic Loading of Single Storey Specimens	113
8.2.2 Reverse Cyclic Loading of Single Storey Specimens	117
8.3 Four Storey SPSW	120

8.3.1 Monotonic Loading	120
8.3.2 Reverse Cyclic Loading	123
8.4 Parametric Studies	126
8.4.1 Thickness of the Infill Plate	126
8.4.2 Angle of Inclination	129
CHAPTER 9 Conclusions and Recommendations	
9.1 Summary of Findings	131
9.1.1 System Performance	131
9.1.2 Overturning Moment to Base Shear Ratio	133
9.1.3 Angle of Inclination	133
9.1.4 Boundary Frame Response	134
9.1.5 Numerical Modelling	135
9.2 Recommendations for Further Study	136
9.3 Rational Design Guidelines	139
REFERENCES	143
APPENDIX A: Material Properties Testing	
A.1 Frame Member Properties	146
A.2 Infill Plate Properties	147
A.3 Fish Plate Properties	150
APPENDIX B: Strain Gauge Analysis Software	
B.1 About the Software	153
B.2 Suggested Improvements to the Software	154
APPENDIX C: Sample CANNY-E Input Record	155

LIST OF TABLES

4.1. Strength degradation over SPSW2 cyclic loading	49
5.1. Load history for SPSW4	72
6.1. Summary of material properties determined from coupon testing	75
6.2. Energy dissipation for the SPSW4 specimen	84
7.1. Summary of geometric and material properties	105
7.2. Computational aspects of numerical modelling using CANNY-E software	112
8.1. Sensitivity to infill plate thickness	128
8.2. Sensitivity of longitudinal properties to the angle of inclination	130

LIST OF FIGURES

3.1. Dimensions of the single storey test specimens: (a) SPSW1, and (b) SPSW2	23
3.2. Fish plate connection detail	24
3.3 Test setup for the SPSW1 specimen	27
3.4. Lateral bracing system for single storey specimens	28
3.5. Instrumentation layout for SPSW1	30
3.6. Instrumentation layout for SPSW2	31
3.7. (a) Force and (b) displacement histories for SPSW1	34
3.8. (a) Force and (b) displacement histories for SPSW2	35
4.1. Force-deformation curve for SPSW1	37
4.2. Selected cycle from force-deformation curve for SPSW1	39
4.3. In-plane infill panel strain, top corner of SPSW1	41
4.4. Axial strain at base of south column, SPSW1	42
4.5. Global damage in SPSW1 after testing	44
4.6. Force-deformation curve for SPSW2	47
4.7. Damage in the South column, SPSW2 specimen	48
4.8. Hysteretic energy dissipation from SPSW2	50
4.9. Inelastic column deformation on SPSW2 at the south, top joint at test completion	51
4.10. "Hourglass" shape resulting from deformation of the columns at completion of SPSW2 test	52
4.11. Representation of a ductile structure's load-deformation capacities	56
4.12. Normalized "backbone curves" up to test termination, for (a) SPSW1 and (b) SPSW2	57
5.1. Photograph of specimen SPSW4 within the test frame	59
5.2. Specimen SPSW4	60
5.3. Gusset detail at base of SPSW4 specimen	61

5.4. Instrumentation diagram for SPSW4	67
5.5. Strain gauge instrumentation on the first storey, SPSW4	68
5.6. Photograph of typical strain rosette orientation	69
5.7. (a) Force and (b) displacement histories for SPSW4, cycles G1 to M1-	73
6.1. North column buckled shape	78
6.2. Inelastic buckling of the 1st storey infill panel	79
6.3. Force-deformation curve for the 1st floor, SPSW4	81
6.4. Storey shear — storey drift relationships for SPSW4	82
6.5. Displaced North column profile, cycle L1+	85
6.6. Magnitude of principle tension strains and applied base shear relationship, cycle L	87
6.7. Schematic of principle strains under 150 kN base shear	88
6.8. Angle of inclination—base shear relationship	89
6.9. Axial strains in first floor beam, load level L	91
6.10. Bending strains in first floor beam, load level L	92
6.11. Axial column strain—base shear curve, load level L	93
6.12. Column bending strains, load level L	94
6.13. Comparison of longitudinal load-deformation envelopes	96
7.1. Schematic used in deriving the tension field strip model	101
7.2. Hysteresis curve for CANNY Sophisticated Bilinear/Trilinear Model	106
7.3. Multi-spring column model	107
7.4. Column steel spring hysteresis model	107
7.5. Schematic for single storey numerical models	108
7.6. Schematic for 4 storey numerical models, $\alpha = 37^\circ$	109
8.1. Monotonic load-deformation curve from numerical modelling of SPSW1	115
8.2. Monotonic load-deformation curve for numerical modelling of SPSW2	116
8.3. SPSW2 cyclic model, 1 cycle at each load level	118

8.4. SPSW2 cyclic model, 3 cycles at each load level	119
8.5. Monotonic load-deformation curve from numerical modelling of SPSW4	122
8.6. Cyclic force-deformation curve of the 1st storey, from numerical modelling of SPSW4	125

LIST OF SYMBOLS

A	= cross-sectional area
A_b	= cross-sectional area of beam
A_c	= cross-sectional area of column
A_s	= cross-sectional area of tension strut
E	= Young's modulus of elasticity
F	= force magnitude
F_y	= yield force magnitude
h_s	= storey height (centreline beam — centreline beam)
I_c	= moment of inertia of column, axis perpendicular to infill plate
I_{xx}	= strong axis moment of inertia
K_{py}	= post-yield stiffness ratio as defined by Canny Consultants (1996)
L	= width of shear wall panel (centreline column — centreline column)
M	= moment in member
M_p	= fully plastic moment capacity of a member
N	= axial force in member
N_p	= plastic axial capacity of a member
Q_y	= storey shear force at control location, at global yield
Q_{yi}	= storey shear force of i^{th} storey, at the point of significant global yielding
R	= elastic force reduction factor
SPSW1	= first single storey specimen tested
SPSW2	= second single storey specimen tested
SPSW4	= 4 storey specimen tested
t	= thickness of infill plate
α	= angle of inclination of the tension field from the vertical

δ_i	= longitudinal deflection at i^{th} storey
δ_y	= longitudinal deflection at control location, at global yield
δ_{yi}	= longitudinal deflection at i^{th} storey, at global yield
Δ	= deformation magnitude
Δ_y	= yield deformation magnitude
ε	= strain magnitude
σ_y	= material yield stress
σ_{ys}	= axial yield stress of tension strip
σ_u	= ultimate material stress

ACKNOWLEDGEMENTS

First I would like to thank my supervisors, Dr. Helmut Prion and Dr. Carlos Ventura, for their guidance and encouragement throughout the course of the research work and in the preparation of this thesis.

Special thanks also goes to my fellow graduate students, Mahmoud and Reza, who were involved in this joint research programme. The ingenuity and help of Paul and Dick in the Structures Lab was also invaluable in making this project successful.

Recognition also goes to others in my office, especially Kim, Bob, Aaron, Marc and Ardel, who made the whole experience enjoyable.

Financial support for this study was provided by the Natural Science and Engineering Research Council of Canada, and by the University of British Columbia.

Adam Lubell

June 1997
Vancouver, British Columbia

CHAPTER 1

Introduction

1.1 Background

Since the early 1980's, work has been underway in Canada to develop the unstiffened steel plate shear wall system as a competitive lateral force resisting system for use in steel highrise building construction. Experimental work has shown steel plate shear walls to exhibit desirable characteristics including high elastic stiffness properties, large displacement ductility capacities, load path redundancy, and stable hysteresis behaviour. A number of structures around the globe have been constructed utilizing the steel shear wall concept for all or part of their lateral resistance needs.

The Canadian approach to steel plate shear wall design, initiated through work at the University of Alberta, has been to use an unstiffened infill panel within one or more of the frame bays, over the height of the structure. By using an unstiffened plate, the designer can utilize the significant post-buckling shear capacity of the infill panel, making efficient use of the materials while minimizing fabrication expenses.

The most recent edition of the Canadian design code for steel construction (Canadian Standards Association, 1994) allows for the use of unstiffened steel plate shear walls in structural design. It provides simplified methods for their analysis and design, based on tension field principles.

To date, however, very limited testing in Canada and elsewhere has been conducted on medium to large scale steel shear wall assemblies. Most research has been done on single panel specimens, specimens of a very small scale, or specimens with stiffened infill plates.

The current series of research programmes described in Section 1.2, a portion of which is presented herein, have been designed to expand the current state of knowledge. Existing design methodologies are assessed, and some of their limitations established.

1.2 Overview of the Research Program

This research is a subset of a larger collaborative study established in 1994 to assess the performance of steel plate shear walls in areas of high seismic risk. The study involved researchers from the University of British Columbia, the University of Alberta and practicing structural engineers in industry. Studies included quasi-static testing of single and multistorey steel plate shear walls, dynamic shake table experimentation, numerical and analytical investigations, and a comparative design study to assess the economic feasibility of the system.

The scope of research described in this thesis consists of the quasi-static testing programme at the University of British Columbia on two single-storey, and one multistorey test specimens. The tests were conducted from January 1996 through September 1996 in the Structures Laboratory of the Department of Civil Engineering.

The results of the experimental investigations, as well as comparative numerical models are presented herein.

1.3 Scope and Objectives of this Thesis

This thesis reports the results from an experimental and analytical investigation into the performance of unstiffened steel plate shear walls under cyclic quasi-static loading. Two single-storey and one multistorey specimens were fabricated, tested and numerically modelled to assess their behaviour under elastic and post-yield conditions. In particular, the suitability of this structural system for areas of high seismic risk was to be verified. Current design guidelines were assessed on the basis of the performance characteristics obtained for the specimens studied. This research program also served to provide benchmark results for subsequent research on a similar multistorey specimen using dynamic shake table methods.

The objective of the experimental programme was to verify the structural response of the steel shear wall specimens under industry standard testing guidelines for cyclic seismic loading. In particular, the load-deformation properties, hysteretic behaviour, and displacement ductility capacities of the specimens were to be established.

The goal of the analytical portion of this study was to verify current simplified numerical modelling techniques, for accurately predicting behavioural characteristics of steel plate shear walls. In particular, numerical predictions of load-deformation

relationships through all levels of the cyclic excitation were to be compared to those obtained from physical testing. Limitations of this technique were to be identified.

Lastly, from the composite results of the experimental and analytical programmes, areas for future study were to be established with recommendations for changes to current design guidelines.

1.4 Outline of Thesis

Chapter 2 presents an overview of the published results from past research into the behaviour of steel plate shear walls. Emphasis is placed on studies focusing on the use of unstiffened infill panels.

Chapters 3 and 4 present the procedures and results employed for the experimental investigation of the single-storey steel shear wall panels respectively. Chapters 5 and 6 present the testing of the multistorey steel shear wall specimen.

The simplified numerical modelling technique used for analytical studies is described in Chapter 7. Chapter 8 presents the results of analytical modelling of the single and multistorey specimens under monotonic and cyclic loading.

A summary of the findings from this research programme are described in Chapter 9. Conclusions, recommendations for future study and recommended modifications to the design guidelines are drawn.

CHAPTER 2

Literature Survey

2.1 Background

Numerous buildings around the world have been constructed utilizing steel plate shear walls as the principal lateral load resisting system, in one or more directions (Journal of Commerce, 1984; Anon., 1989). Buildings such as the Olive View Hospital in Los Angeles, CA (Troy and Richard, 1979) have been constructed in active seismic regions, and take advantage of the reduced mass and large ductility capacities available with this system. Troy and Richard indicated that a structure using steel shear walls would exhibit reduced non-structural damage due to a seismic event, as compared to a conventional steel moment frame alternative. However, the lack of codified design guidelines in most jurisdictions has discouraged the widespread adoption of this structural system for building construction.

A steel plate shear wall frame is comprised of column and beam elements augmented by steel infill shear panels, provided over the height of a framing bay. Its form is analogous to that of a plate girder, vertically cantilevered from its base, with the columns acting as flanges, the beams as stiffeners, and the infill panel as the plate girder web. When subjected to lateral loading in the plane of the wall, forces are resisted through the flexural and coupled axial response of the columns and by diagonal tension field action in the infill panels anchored between the beams, which act as stiffeners.

Steel plate shear walls can be designed to utilize the full post-buckling shear strength of the infill panel, when designed with no additional intermediate stiffeners and incorporating thin infill plate thicknesses.

Some of the potential advantages of the steel plate shear wall system over traditional alternatives include reduced material usage, reduced foundation requirements, and increased erection speeds. By using a steel core in place of the traditional reinforced concrete flexural wall system in medium and high-rise steel construction, savings can also be achieved by reducing the required tolerances for frame to shear wall connections, eliminating the incompatibility between steel and concrete construction trades, and allowing for increased off-site fabrication. Preliminary results of a study assessing the cost advantage of this system for an eight storey structure designed for different seismic zones are presented by Timler *et al.* (1997). Major savings are cited for the steel shear wall buildings related to significant reductions in total construction time compared with a conventional reinforced concrete alternative.

Different design and analysis approaches towards the use of steel plate shear walls have been adopted by researchers, practicing engineers and standards bodies in various countries. Many recommend the use of extensive stiffeners to prevent buckling of the infill steel panels under lateral loads. Xue and Lu (1994a) have studied different infill panel to boundary frame attachment configurations. Other variations include recent work by Sugii and Yamada (1996) in which the use of infill steel panels embedded

within a concrete covering were studied and compared to “traditional” unstiffened steel plate shear wall designs.

Since the early 1980's, an approach utilizing unstiffened thin infill panels has been developed by researchers at the University of Alberta, Canada. The concept was to achieve improved economy by reducing the required level of fabrication, and allow for the use of the post-buckling strength of the steel plates through the activation of a tension field. This approach was validated through experimental and numerical studies on the behaviour of single and two panel steel shear wall assemblies (Thorburn *et al.*, 1983; Timler and Kulak, 1983; Tromposch and Kulak, 1987). As a result of this work, design guidelines for unstiffened steel plate shear walls have been included as an Appendix to the Canadian standard for Limit States Design of Steel Structures, CAN/CSA S16.1-M94 (Canadian Standards Association, 1994).

2.2 Review of Published Research

Several analytical and experimental investigations have been conducted on steel frames incorporating infill shear panels in Canada, Japan, the United States and the United Kingdom. The following sections outline important published results to date. In particular, this review focuses on systems incorporating unstiffened infill panels, in which the panel is permitted to buckle under applied horizontal loading.

2.2.1 Study by Takahashi *et al.* (1973), Japan

Takahashi *et al.* conducted a series of experimental tests and analytical studies on the use of thin infill panels in steel shear walls. Specimens of dimension 2100 mm by 900 mm were constructed, with plate thicknesses of 2.3 to 4.5 mm and various infill panel stiffener configurations. All specimens used a rigid frame, with the infill plates attached using high strength bolts. Two full size, two-storey specimens from a proposed 32 storey building design were also tested, one of which included openings within the infill panel. In some specimens, the infill panels buckled in the elastic region, due to excessive stiffener spacing, while plastic buckling occurred in others. S-shaped hysteresis plots of load vs. deformation were obtained. A finite element model was developed based on the assumptions of no plate buckling, a bilinear stress-strain relationship, and the Von Mises yield criterion. Reasonable correlation was obtained between this model and the experimental results. The research of Takahashi *et al.* was based on the premise that the thin infill panels should be stiffened so as to prevent buckling under elastic stress conditions.

2.2.2 Early Studies at the University of Alberta, Canada

Research was undertaken at the University of Alberta into rational, simplified methods to predict the behaviour of steel plate shear walls with thin unstiffened infill panels. This research was based on the design philosophy that the thin infill panels should be permitted to buckle under elastic loading. A tension field would be formed and would

allow for the utilization of the post-buckling strength of the plates in resisting lateral shear forces.

Thorburn *et al.* (1983) put forward an approximate numerical modelling technique, incorporating a discretized tension field. Derivations were based on least work principles. Variations were presented for further case specific simplifications to the model. One example is the use of a single diagonal tension brace in place of each panel, with axial brace properties producing an equivalent lateral stiffness, to generate initial approximations to a steel plate shear wall design.

Timler and Kulak (1983) tested a large scale steel plate shear wall specimen consisting of two symmetric single storey panels, arranged as a simply supported beam and loaded along the internal beam at the symmetry line. Cyclic loading to a serviceability drift limit was conducted, followed by monotonic pushover loading to failure. Each panel of the test specimen was 3750 mm wide, with a storey height of 2500 mm and contained an infill panel with a thickness of 5 mm. Failure of the specimen was defined by localized weld tearing in a connection and did not reflect the maximum displacement ductility that could be achieved by the global structural system. The results of the experiment, including the stress pattern recorded in the infill plate provided a good correlation to the numerical model presented by Thorburn *et al.* (1983), although the predicted elastic stiffness of the specimen was somewhat larger than measured. A

revised angle of inclination formulation was presented, to incorporate the flexural component of the column action in Thorburn *et al.*'s energy derivation.

Tromposch and Kulak (1987) reported the results of an experiment on a single large scale steel plate shear wall specimen, under fully reversed cyclic loading. Industry standard bolted beam-column connections were used, with pinned external column supports. An axial preload was introduced in the columns through high strength steel bars anchored to the column ends. The configuration of the specimen was similar to Timler and Kulak's, with a bay width of 2750 mm, a storey height of 2200 mm and 3.25 mm thick unstiffened infill plates. Hysteresis loops from the test were stable, but pinched to an S-shape. As with Timler and Kulak's test, localized weld tearing was recorded. The test was terminated upon reaching the limits of the hydraulic actuator system and did not reflect the ultimate capacity of the global structural system. A hysteresis model was developed by Tromposch and Kulak, which closely approximated the hysteretic characteristics achieved during physical testing. Parametric studies with that model suggested that significant additional energy could be dissipated by using full moment resistant beam-column connections within the steel plate shear wall frame.

2.2.3 Research at the University of Wales, United Kingdom

Roberts and Sabouri-Ghomi (1991) conducted experimental and analytical studies on small scale unstiffened infill shear panels. Specimens were 300 mm high, with panel width to height aspect ratios of 1.0 and 1.5, and used 0.54 mm (aluminum), 0.83 mm

(steel) and 1.23 mm (steel) thick infill panels. The panels were held within a boundary frame using a perimeter bolting system. Fully reversed quasi-static cyclic testing produced S-shaped hysteresis curves, with high ductility capacities. A theoretical model of the hysteretic response was developed, incorporating the influence of shear buckling of the infill panel, and yielding of the panel and boundary frame. Good correlation was reported between experimental and analytical results.

The results of nonlinear dynamic analysis studies on steel shear wall systems were reported by Sabouri-Ghomi and Roberts (1992). Steel plate shear walls were idealized as vertical cantilevers with associated mass, stiffness and dynamic loads applied at each storey. The above hysteretic model was incorporated. Using a finite difference time stepping technique, the nonlinear dynamic response of a specimen was modelled. However, no dynamic physical testing was conducted to validate the analytical results.

Other work by Roberts and Sabouri-Ghomi (1992) included experimental and analytical studies on similar steel shear wall panels which included perforations. Similar overall hysteretic behaviour patterns were achieved. Their research led to the development of conservative reduction factors for the strength and stiffness of a steel shear wall panel containing openings, based on an effective diameter of a hole placed at the centre of the infill plate.

2.2.4 Research at Kansai University, Japan

Yamada (1992) presented the results of an investigation into the behaviour of shear panels within composite reinforced concrete and steel boundary frames. Research included the use of thin infill steel panels, with and without concrete covering. A series of 1/5 scale specimens were tested to determine the relationship between the applied shear and storey rotation angle. The shear panels were 1200 mm wide, with a 600 mm storey height. Testing was conducted until failure of the surrounding frames was noted and did not achieve failure of the infill panel. The infill panels without concrete covering were noted to form a diagonal tension field, with little reduction in the strength of the specimens beyond the ultimate shear capacity of the plates. The tension field was indicated as acting between diagonal corners of the panel, with a given effective width. In panels with a concrete covering, a diagonal compressive field in the concrete was established over a given effective width, between the other pair of corners, in addition to the steel panel's tension field. Yamada noted that the relationship between the stiffnesses of the infill panel and the surrounding frame were very important.

Sugii and Yamada (1996) reported results from a further study into the monotonic and cyclic behaviour of thin unstiffened steel shear panels within composite frames. Two-storey specimens with panel width to height ratios from 1.0 to 2.0, and plate thicknesses of 0.4 mm to 1.2 mm, were evaluated. Maximum resistance was achieved in the

monotonic tests at storey sway angles of 0.02 to 0.03 radians, with some reduction in strength reported beyond these values. Using Yamada's (1992) single effective tension strip approach with a trilinear stress strain relationship, numerical models were created and compared with the results from physical testing. The analytical models capture the general trends, but missed important elements of the specimen behaviour, including the peak strength, gradual yielding properties and strength degradation at high displacements. Cyclic modelling appears to overestimate the "fullness" of the hysteresis curves. Yamada's model appears to be too simplistic to accurately reflect steel plate shear wall performance, although it could be useful as a preliminary design tool.

2.2.5 Research at the University of Maine, USA

Caccese et al. (1993) reported the results of an investigation into the cyclic post-buckled response of steel plate shear walls. The influence of the beam-column connection detail and the panel thickness relative to the panel width were of primary concern. Experiments were conducted on five, three-storey, one quarter scale steel shear wall assemblies. Each panel was 49 inches (1245 mm) wide with a storey height of 33 inches (838 mm). Simple shear type and full moment beam-column connection details were used on respective specimens. Infill plate thicknesses studied were 0.076 mm, 1.87 mm and 2.65 mm. One specimen consisted of a moment frame only, with no infill panels used. Loading consisted of a single horizontally acting actuator affixed at the roof of the structure. No direct external vertical loading was applied. A cyclic

loading sequence to a drift limit of 2 % was employed, followed by monotonic loading to specimen failure or equipment limitations.

Results of the experimental testing programme indicated that an increase in initial elastic stiffness occurred with thicker infill panels. However, no force deformation plots have been provided to indicate the method used in calculating these values, for example, whether tangent or secant stiffnesses are reported. The type of beam-column connection used was shown to have only a minor influence on the behaviour of the specimen, with a slightly greater effect for thinner panels. The thickness of the infill panel was shown to have an effect on the failure mode: the thin panel yielded early causing failure in the specimen when the column formed a plastic hinge, while the thick panel never yielded, initiating failure when the yielded column became unstable. However, since the steel plate shear wall system as implemented in these specimens was highly redundant, the steel plate shear wall would still have possessed global displacement capacity if the local instability issues could have been prevented. Concerns about the generalized nature of the conclusions reported from this work have been outlined in Kennedy *et al.* (1994) and Kulak *et al.* (1994).

Numerical modelling of the above specimens was conducted using a finite element analysis and the simplified tension field strip model described in Timler and Kulak (1983). These results are presented in Elgaaly *et al.* (1993). In the finite element analysis, which used three-dimensional isoparametric doubly curved shell elements to

model the infill panels, the stiffness and yield strength parameters for each specimen were consistently overpredicted by more than 18 %. These discrepancies were attributed by Elgaaly *et al.* to out of true fabrication, a coarse element mesh and the assumption of in-plane global deformation only (only the plates were permitted to move out of plane as they buckled). Additional modelling using the tension field strip technique generally produced better correlations, for both monotonic and cyclic results. A trilinear stress-strain relationship was employed for the tension ties, with parameters selected to produce a best fit result with the experimental data. In the discussion by Kennedy *et al.* (1994), it is suggested that the need for the trilinear model results from infill plates made from cold rolled steel, and that the empirical parameters developed would need to be adjusted for every new design (i.e. every new steel sample). Elgaaly *et al.* (1994) state that variations in the strain distribution along the length of each strip require the trilinear model. Hysteretic modelling was conducted by implementing a symmetric tension field model, and a hysteresis material model derived from the trilinear stress-strain approximation.

Sensitivity studies on various model parameters were also conducted. The number of strips to include in a tension field strip model was varied, and found to have little influence on the calculated performance, once sufficient strips were included. It was noted that for thin panels which yielded well before the columns, very few strips needed to be implemented. More strips were required for thick panels, since greater force levels were transferred through the tension field into the columns. Varying the angle of

inclination of the strip elements in a range from 38 to 45 degrees did not alter the results significantly.

2.2.6 Research at Lehigh University, USA

Xue and Lu (1994a) conducted an analytical study of the performance of various steel plate shear wall configurations in a twelve storey structure. Model configurations utilized thin, unstiffened infill panels which were permitted to buckle and included various panel attachment details: full perimeter, girder only, and column only. An upper bound solution in which the plates were prevented from buckling was also studied. Moment resisting and simple connections between the girders and columns of the shear wall bay were examined. Studies within the elastic and moderate damage ranges were of primary interest. The analysis was conducted using a finite element program, which included a grid of four-noded shell elements for the infill panels and incorporated initial geometric imperfections to initiate plate buckling. The single steel bay on either side of the steel shear wall included moment resisting connections.

In all cases studied, the tension field action resulting from the buckled infill plates dominated the longitudinal resistance of the frame. Xue and Lu's results showed that there was an insignificant change in the initial stiffness of the frame through a variation in the beam to column fixity of the infilled bay. They also presented results indicating only a moderate increase in stiffness associated with a full perimeter attachment of the infill panels as compared to girder attachment only. Column attachment only was

eliminated as a viable alternative since the relative displacement of adjacent columns was insufficient to activate a tension field in the shear plate as efficiently as the much larger relative beam displacements. Using beam attachment only resulted in a larger amplitude moment demand envelope for the beam members as compared to full perimeter attachment. However, it also resulted in relocating the peak moment demands for the beams inwards from the connections. Sequential buckling and yielding was achieved upward through the stories of the structure. By separating the column from the infill panel, the system exhibited action closer to a shear deformation mode and less like a cantilever flexural mode, particularly at higher storeys. It was noted that the elimination of flexural deformations in the infill panels through pinned beam-column joints lead to improved load carrying capacity for the panels. Xue and Lu concluded that, among the variations studied, using pinned beam-column joints with infill panels attached to the girders only was the "optimal" solution. No experimental testing has been conducted to verify their numerical results.

Using their optimal girder only connection arrangement for the infill panels, Xue and Lu (1994b) conducted parametric studies on the monotonic and cyclic performance of a one-bay, one-storey steel shear wall panel. Simple shear connections between the columns and girders were implemented. Panel width to height ratios of 1.0 to 2.5 were studied. The maximum panel edge dimension to thickness ratio was varied from 300 to 900. The ratio involving panel thickness was shown to have little effect on the elastic and post-yield stiffnesses of the specimen, and decreased the yield strength only

slightly when thinner panels were implemented. Using narrower aspect ratio panels (i.e. smaller width to height ratio) produced a system with slightly lower elastic stiffness, approximately equal post-yield stiffness, but a significantly lower yield strength. Empirically derived equations were developed for response parameters including the strength at significant yielding and the post-yield stiffness. No experimental testing has been conducted to validate these equations.

2.2.7 Recent Studies at University of Alberta, Canada

In collaboration with the research activities at the University of British Columbia (of which this thesis is a part), Driver (1997) conducted experimental and analytical studies on a large scale, four-storey single bay steel plate shear wall assembly. Each panel was 3050 mm wide, with 1800 mm nominal storey height. Infill panel thicknesses of 4.8 mm (lower 2 storeys) and 3.4 mm (upper 2 storeys) were used. Equal lateral loads were applied at each floor. A uniform gravity loading over the specimen height was simulated through hydraulic actuators. The specimen was subjected to 30 reversed cycles of quasi-static loading, including 20 cycles in the inelastic region. All cycles were not symmetrically fully reversed due to equipment limitations, with larger excursions being reported in one direction. Severe local buckling at the base of each column was noted. Failure of the specimen resulted from a fracture at the base of one column. A large scale corner detail was also tested experimentally by Driver.

Driver reported good correlations between the experimental results and those obtained from numerical modelling using both finite element and tension field strip model techniques. Suggestions were noted on methods to improve the tension field technique, by including elements such as compression struts in the corners, and vertical struts to better reflect the infill panel's contribution to carrying the vertical forces resulting from the overturning moment. Driver presented an additional numerical method for predicting the hysteretic behaviour, which correlated well with the experimentally obtained results.

The ductility of the experimental specimen was assessed in relation to the current seismic design provisions of the National Building Code of Canada (National Research Council of Canada, 1995). The NBCC currently permits a maximum force reduction factor, R , of 4.0 under seismic loading, for a ductile steel plate shear wall structure. Driver suggested that this value is conservative.

CHAPTER 3

Single Panel Experimental Programme

3.1 Introduction

Two single storey specimens were constructed and tested, to obtain performance data, and to validate design assumptions prior to completion of the four-storey testing programme. This included testing the specimen fabrication techniques to be used, evaluation of the force application and transverse bracing strategies, and a confirmation of the simplified analytical models used during the design phase. The testing also allowed for significant incursions into the post-buckling and post-yield regimes of the unstiffened infill panels.

A description of the test specimens used is provided in Section 3.2. Section 3.3 contains a description of the load application and lateral support systems. The instrumentation and data acquisition employed during the experiments are described in Section 3.4. Finally, Section 3.5 summarizes the testing procedures.

3.2 Test Specimens

A total of two, single-storey specimens were constructed and tested, referred to as SPSW1 and SPSW2 respectively. Each specimen was a 30 % scale model of an inner residential building core, having floor-to-floor and column-to-column spacings of 900

mm. Frame members were constructed from S75x8 hot rolled steel sections, with a nominal yield strength of 300 MPa. (Actual material properties were assumed the same as those obtained from coupon testing of the four-storey specimen, described in Appendix A.) The infill shear panel was constructed from 16 gauge (1.5 mm) thick hot rolled sheet steel, with nominal strength of 225 MPa. Beam-column joints were all fully fixed, with full flange continuity stiffeners added across the column webs. The configuration of the two specimens differed principally in the column-base gussets, and the addition of a second top beam on SPSW2. Figure 3.1 illustrates the geometry of the two specimens. A fish plate detail, as developed at the University of Alberta, was used to join the infill plate to the steel frame, as shown in Figure 3.2. This detail allowed for improved tolerances in the infill plate dimensions, and ease of fabrication. A 20 mm x 200 mm base plate was attached to the bottom beam and the column section perimeter by continuous fillet welds.

The overall design of the panel sections was done using both finite element software and simplified tension field strip model methods. Construction specifications, including materials and dimensions, were determined based on the testing equipment and facilities proposed for the four-storey experiment (described in Section 5.2). The intent was to test multiple specimens in different configurations and with different techniques, without altering the basic components of frame stiffness, infill panel properties, and storey aspect ratio. The overall panel dimensions were governed by size limitations of the reaction frame, for the subsequent four-storey specimen. A

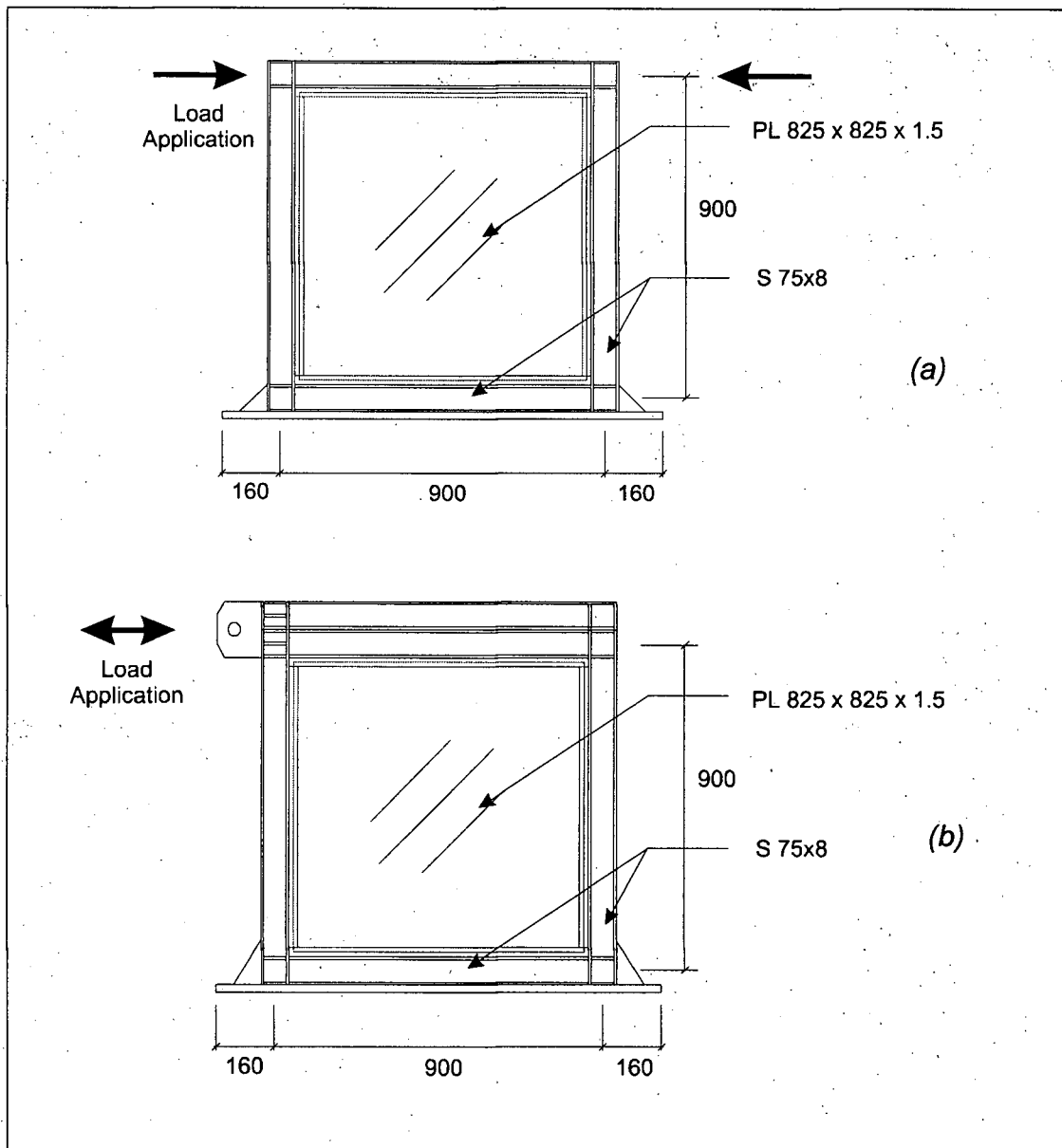


FIGURE 3.1: Dimensions of the single storey test specimens: (a) SPSW1, and (b) SPSW2

similar height restriction existed for an identical four-storey specimen tested dynamically on the shaking table in the Earthquake Engineering Laboratory at the University of British Columbia (Rezai, 1997). The overall strength of the specimen, as

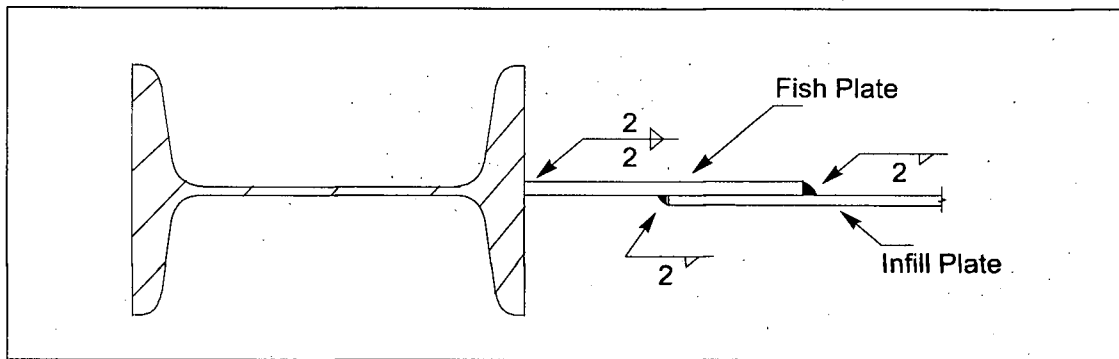


FIGURE 3.2: Fish plate connection detail

predicted using the tension field strip model technique, discussed in Section 7.2, was kept within the maximum base shear capacity of the shaking table actuators (150 kN).

With these restrictions considered, the design progressed using locally available materials. Frame members consisted of the smallest hot rolled I-shaped section commonly available from Canadian steel mills. The plate thickness (1.5 mm) was the thinnest available with the desired hot-rolled steel properties, including a well defined yield plateau and subsequent strain hardening characteristics, typical of full scale plate material. To meet the design requirements with these materials, a 1:1 panel aspect ratio was selected. This would be at the narrow end of typical building bay proportions although it is within the practical range and is also similar to ratios reported in other studies as presented in Chapter 2.

While the overall specimen design met the general design criteria suggested for steel shear walls, the actual components chosen do not fully reflect the proportions that

might exist in a steel shear wall intended for commercial construction. In particular, the column sections would likely be governed by vertical loading, stability concerns, or code design restrictions and would thus be stiffer about both axes. Member sizes might also be dictated by standardized sections used throughout the rest of a framing system.

The additional top beam added to SPSW2, fully welded along adjacent flange tips, was used to better anchor the tension field terminating along the top edge of the plate. A stiffer section minimized the beam curvature and thus more closely simulated the effect of an additional shear wall infill panel above, as would be the case in multistorey construction. The Canadian steel shear wall design guidelines in CAN/CSA S16.1-M94 (Canadian Standards Association, 1994) require that the tension field be anchored at the extreme top and bottom of the steel shear wall and suggests that a stiff beam can be used to anchor the tension field forces internally.

The SPSW1 specimen revealed some fabrication concerns, which were corrected for subsequent specimens. One of the main concerns was related to out of plane deformation of the infill plate due to welding distortion. At the centre of the infill panel on SPSW1, a residual out of plane deflection after manufacturing was measured as 26 mm. In contrast, the improved fabrication methods for subsequent specimens typically limited this distortion to less than 5 mm.

3.3 Loading Systems

A similar load application system was used for both SPSW1 and SPSW2. All tests were conducted within a self-reacting test frame, significantly stiffer than the specimens.

An MTS 458.10 digital servo controller was used to operate a Cunningham HST hydraulic actuator with a capacity of ± 445 kN force and ± 305 mm displacement. A load cell and displacement sensor were integral with the actuator. The actuator was pinned to rotate freely in the vertical direction at both the reaction frame connection and the loading tab joining the specimen. Its elevation was set to apply the horizontal load at the mid-height level of the top beam, or the beam combination in the case of SPSW2.

Figure 3.3 shows the test setup for the single-storey specimens.

For SPSW1, a load transfer arrangement was used to always apply the load to the top beam in a compressive manner. A loading plate was used on each end of the top beam, with four, 25 mm diameter threaded rods connecting them. The threaded rods were installed to carry tension forces only, when the actuator was in its "retract" mode. The rods were periodically tightened during the test, as the applied force level increased and the rods stretched.

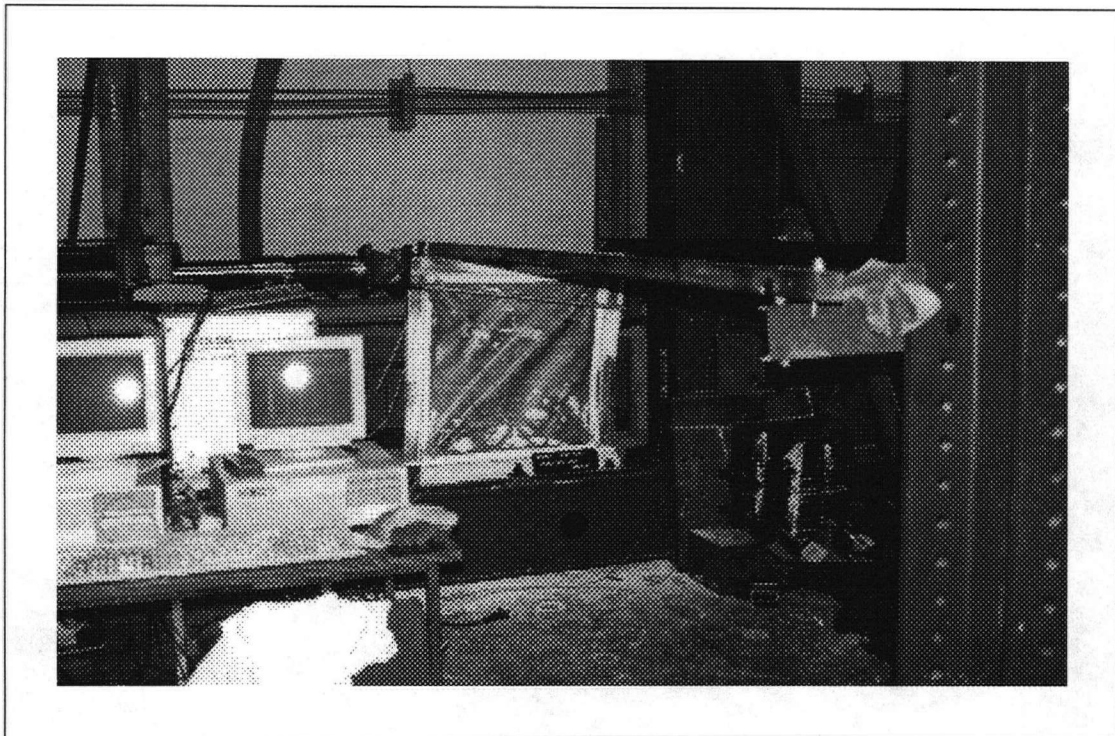


FIGURE 3.3: Test setup for the SPSW1 specimen

For SPSW2, a 25 mm thick loading tab was welded over the full height of the top beam combination. It was positioned on the column flange in the plane of the column web. Additional horizontal web stiffeners were added at this beam column joint.

For the SPSW1 test, control of the hydraulic actuators was by manually adjusting the actuator stroke on the servo controller. The SPSW2 test employed a sine wave function generator connected to the MTS controller setup.

3.4 Lateral Support System

The lateral bracing system is illustrated in Figure 3.4. It relied on a “racking” type mode of the support arms, which joined the column tops to a support beam, via pin type connections in the horizontal plane. The support arms were each 3020 mm long between pins. This system imposed some out-of plane deformation to the structure under large specimen displacements, due to the racking behaviour. This was considered to be within an acceptable range.

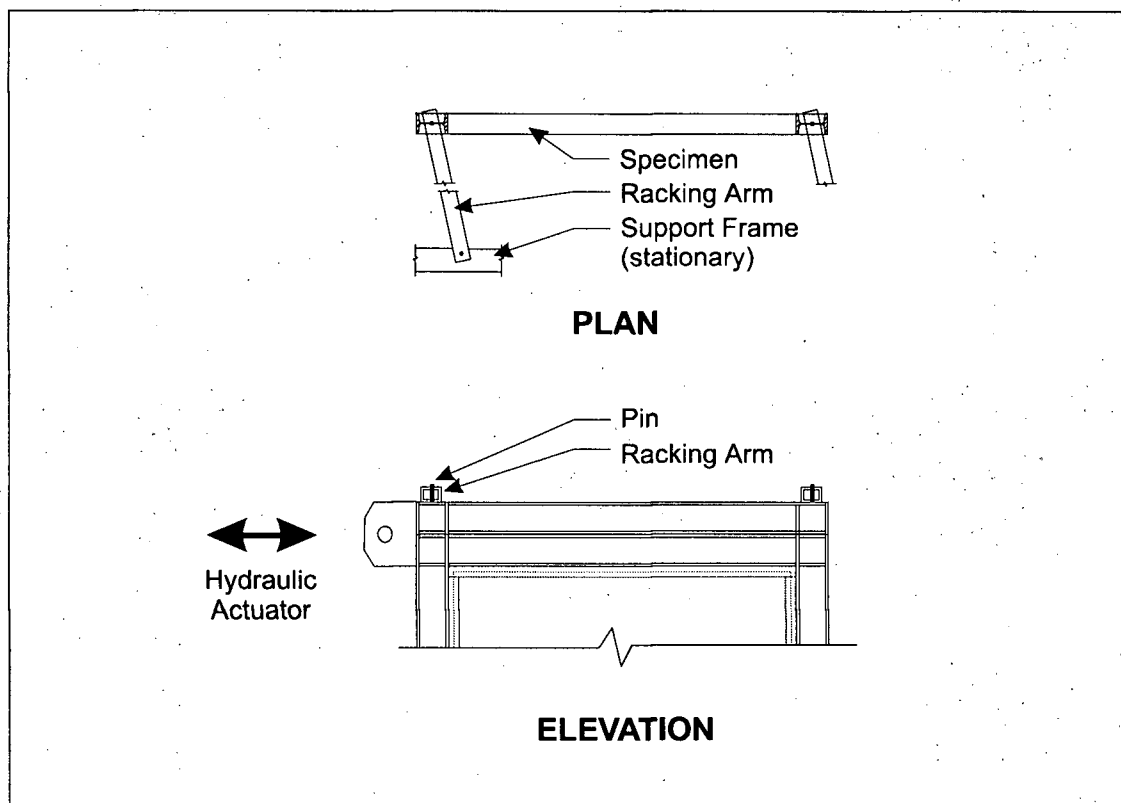


FIGURE 3.4: Lateral bracing system for single storey specimens

The base plate of each specimen was fastened to the test frame using ten 25 mm diameter bolts, using a hand wrench. Four bolts were arranged around each column, with two bolts provided at the mid-length location. To increase friction, the contact surfaces between the base plate and test frame were cleaned prior to installation.

3.5 Instrumentation and Data Acquisition

The load deformation properties were of primary interest in both experiments, and the specimens were instrumented accordingly. The SPSW1 specimen was instrumented with more than the usual number of uniaxial strain gauges and displacement measuring devices, to develop an improved instrumentation strategy for subsequent tests.

The hydraulic actuator contained an integral MTS load cell and displacement measurement sensor using a Temposic LDT Position Sensing System, with resolutions of 0.2 kN and 0.15 mm respectively. Additionally, a cable potentiometer with a resolution of 0.13 mm was used as the principal device to measure longitudinal movement of the top-beam mid-height location, since the actuator stroke measurement also included deformations in the testing frame and movements associated with connection tolerances between the actuator and test frame or specimen. Due to the nature of the control system, all displacement controlled loading in the post global yield range was governed by the actuator's displacement sensor.

For the SPSW1 specimen, uniaxial strain gauges were located on the inner and outer flanges of column and beam elements. Uniaxial strain gauges were also placed on the infill plate in vertical and horizontal directions at key locations. All gauges were attached using M-Bond 2000 adhesive, following the manufacturer's recommended surface preparation and installation procedures. Figure 3.5 shows the instrumentation layout for SPSW1.

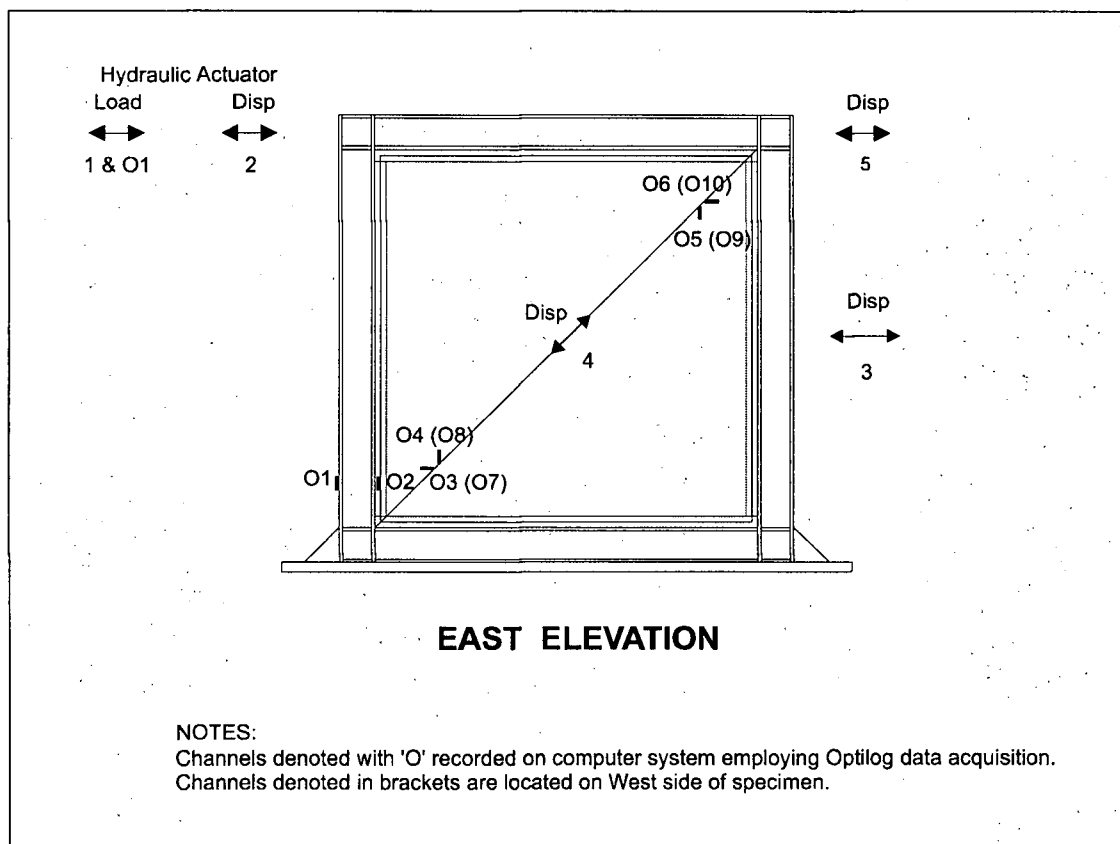


FIGURE 3.5: Instrumentation layout for SPSW1

In total, the SPSW1 test included data acquisition from 22 channels. The acquisition system consisted of two computer systems running simultaneously, using the applied actuator force as a common channel for cross-reference. The first system recorded

strain gauge data, and used an Optilog data acquisition system which contains signal filters and amplifiers. A manufacturer supplied software program (Opus 200) on an attached PC was used for control and storage. The second computer system employed a PC with analog-to-digital converters and Labtech Notebook software. The software provided an on-screen customized display of critical load and deflection readings in a graphical format. All data sampling was conducted at a rate of 2 Hz.

The SPSW2 data acquisition system was similar except that only one computer was used to record four channels. Figure 3.6 shows the instrumentation layout for the SPSW2 experiment.

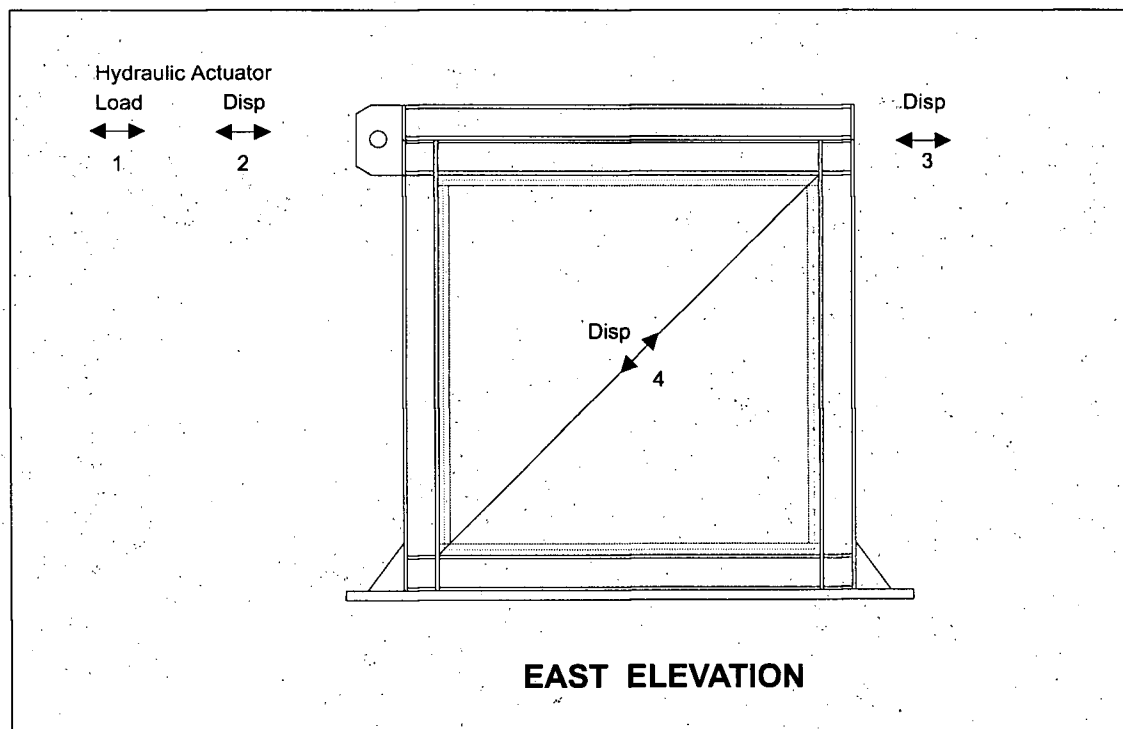


FIGURE 3.6: Instrumentation layout for SPSW2

3.6 Testing Procedures

Both specimens were tested according to procedures based on those recommended in ATC-24: *Guidelines for Cyclic Seismic Testing of Components of Steel Structures* (Applied Technology Council, 1992). ATC-24 is a guideline designed to produce standardized measures of the seismic performance of steel structures when tested under cyclic quasi-static conditions. It specifies that testing is conducted in a force controlled manner up to an observed global yield level, followed by displacement controlled loading at multiples of the global yield displacement. Three cycles are to be completed at each level, with a minimum of 3 load levels used prior to achieving global yield. One of these load levels should be above 75 % of the global yield force level. The global yield point, where “significant” yielding of the specimen was detected, gives the basis for selection of a yield deformation, δ_{yi} , and a yield force, Q_{yi} . The storey drift of the first storey, δ_{y1} , and the corresponding storey shear, Q_{y1} , were selected for all tests as the control parameters. While substantial judgement is involved in selecting these parameters, the level of precision is considered sufficient for test control use. In all cases, the values for δ_y and Q_y are reported for a location at the intercept of tangent stiffnesses to the elastic and post-yield regions of the global force deformation curves.

Seismic loading is often simulated through slow cyclic loading. While other load histories could be followed, it was decided that the approach of using gradually increasing load, as described in ATC-24, would provide the best comparative results.

Derecho *et al.* (1980) suggested that using a loading history that alternates large and small amplitude cycles is more reflective of true seismic loading, where the maximum — or near maximum — deformation may occur early in the loading sequence. However, the gradually increasing model is the most widely adopted type of loading history, allowing for better comparisons with other experimental programmes. It allowed for several initial low level cycles where any testing difficulties could be identified, without fear of significant structural damage. Furthermore, knowledge of the maximum capacity of the specimens is not needed in advance.

The SPSW1 specimen was cycled with increasing force magnitude, with one or two cycles at each load level until an assumed global yield was reached, at 180 kN and 10 mm lateral displacement. Cyclic loading in the post yield region was applied using only one cycle per displacement increment, until $4 \times \delta_y$. After this, a cycle of ± 100 kN force was applied, followed by a pushover load to failure. A plot of the force history for SPSW1 is presented as Figure 3.7(a). The displacement history is presented as Figure 3.7(b). The load-deformation relationships are described in Section 4.2.1.

The SPSW2 specimen was cycled according to the ATC-24 guideline, with an assumed global yield occurring at 200 kN and 8 mm lateral displacement. Plots of the force and displacement histories for SPSW2 are presented in Figure 3.8. The load-deformation relationships are described in Section 4.3.1

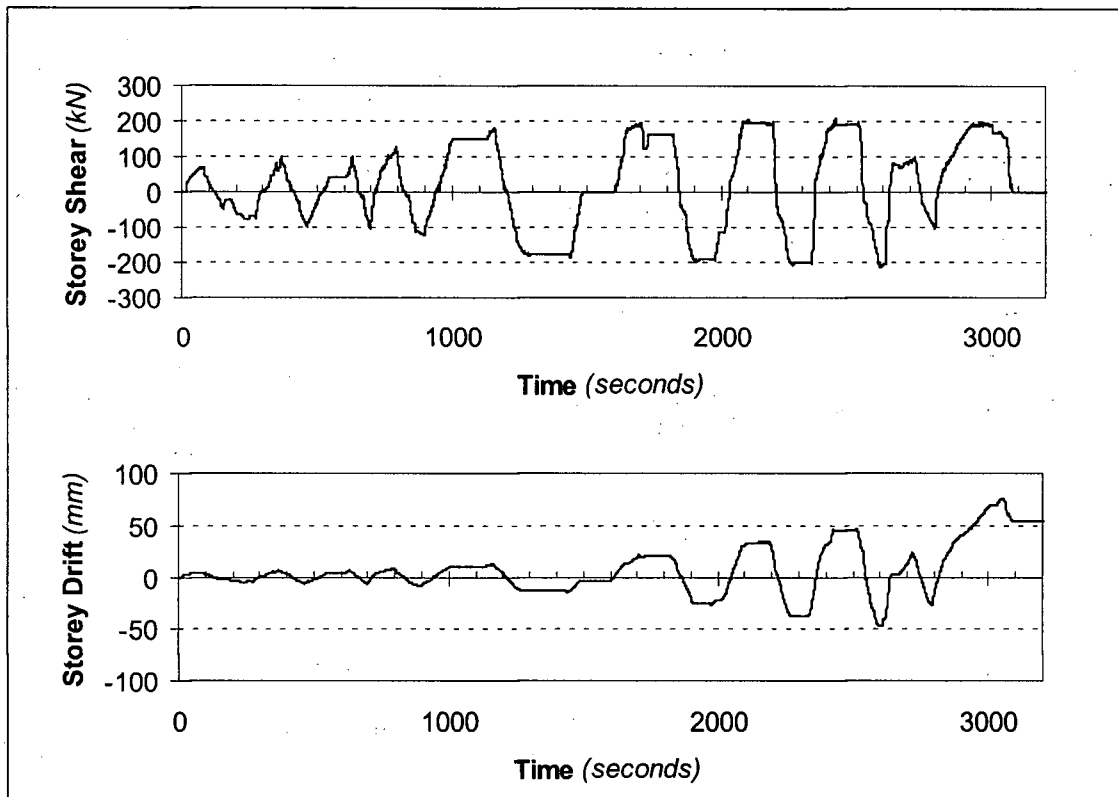


FIGURE 3.7: (a) Force and (b) displacement histories for SPSW1

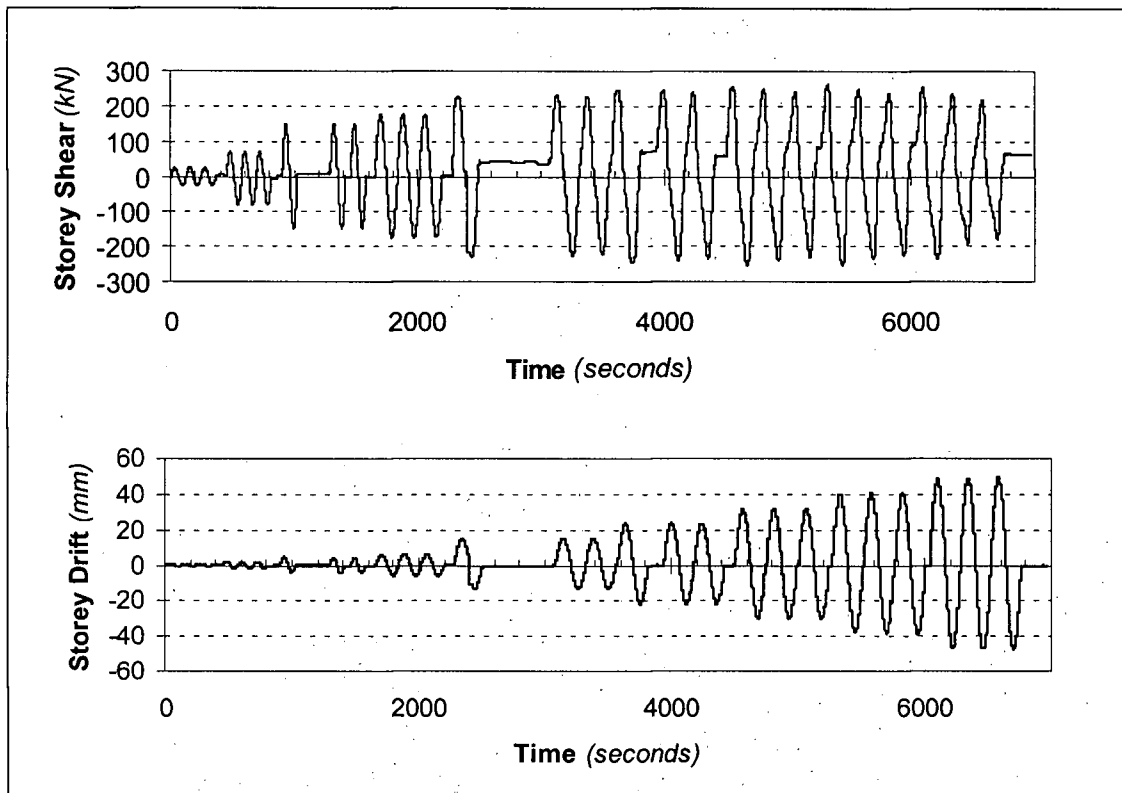


FIGURE 3.8: (a) Force and (b) displacement histories for SPSW2

Chapter 4

Discussion of Single Panel Results

4.1 Summary of Test Results

The results of the single panel tests revealed interesting characteristics about the influence of the frame members and boundary conditions, the fabrication details, and the loading histories on the specimen behaviour.

Results of the tests on the SPSW1 and SPSW2 specimens are presented in Sections 4.2 and 4.3 respectively. Section 4.4 contains a relative comparison of the performance of the two specimens as it relates to differences in their design and loading histories.

4.2 SPSW1 Test

4.2.1 Load Deformation Characteristics

The key performance characteristic of a steel plate shear wall, as demonstrated by the test control procedures, is the relationship between the storey shear and storey drift. Figure 4.1 illustrates the hysteretic behaviour of this relationship observed during the SPSW1 test. A well defined elastoplastic envelope is evident.

By examining an isolated cycle (Figure 4.2) from this test in the post-yield region, well defined segments of the hysteresis curve can be identified. During the unloading stage,

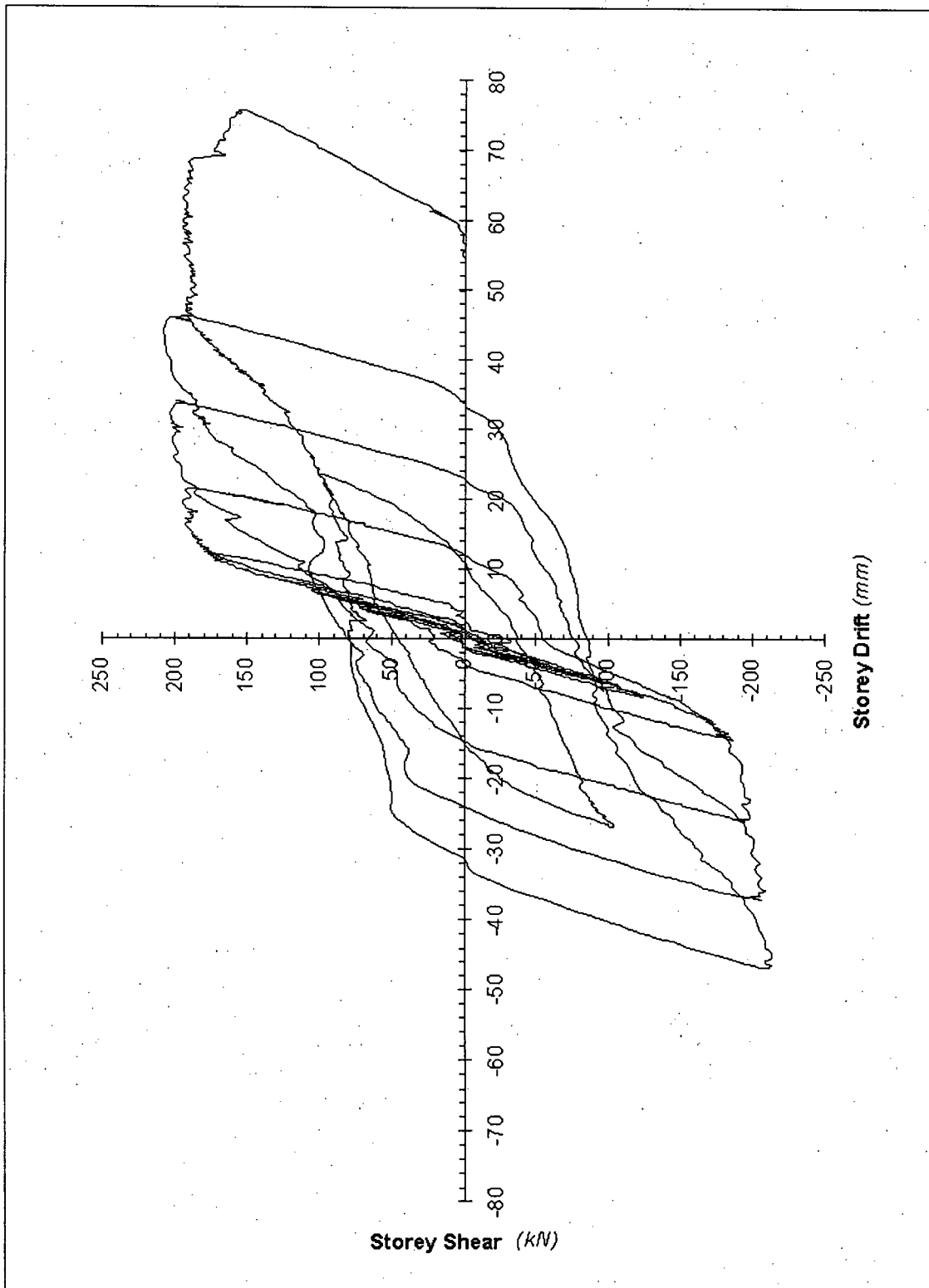


FIGURE 4.1: Force-deformation curve for SPSW1

a constant stiffness was evident, with only a moderate degradation of stiffness from a cycle at the previous load level. Shortly after the specimen passed through the zero applied shear region, the stiffness rapidly degraded to approximately 30 % of the previous value, as the tension field in the infill plate reoriented itself in the opposite direction. The stiffness then increased, until the force level approached the maximum achieved during the previous load level. The stiffness then followed the post-yield stiffness given by the structure's load-deflection envelope. The process repeated itself through unloading and subsequent loading in the other direction.

The overall cyclic loading was applied to a maximum displacement of $4 \times \delta_y$, which corresponds to a storey rotation angle of 0.05 radians. Subsequently, the pushover loading achieved a maximum displacement of $7 \times \delta_y$, corresponding to a storey rotation angle of 0.086 radians, before the testing was terminated. It is important to note that the test was stopped due to buckling of an undersized member in the lateral bracing system, and not collapse of the specimen itself.

Due to limited loading repetition at each force or displacement level, the results obtained may not be strictly applicable to assess seismic performance. They do, however, reveal the inherent ability of a steel plate shear wall system to accommodate large inelastic longitudinal deformations under multiple reversed cycles.

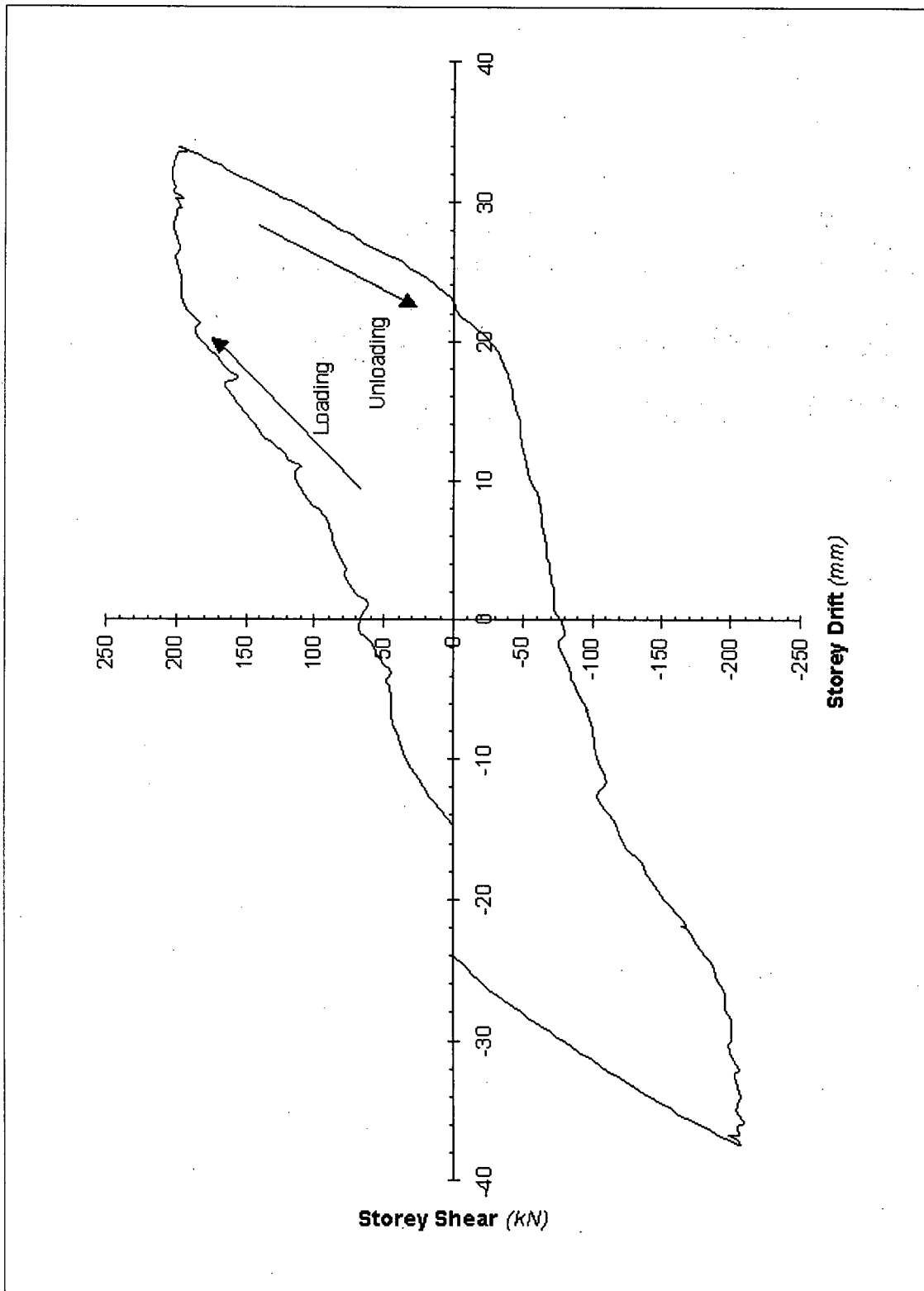


FIGURE 4.2: Selected cycle from force-deformation curve for SPSW1

The maximum base shear resisted by the specimen was 205 kN. This represents a value approximately 13 % higher than the observed global yield force level.

4.2.2 Strain Distributions

The measurements from the various strain gauges attached to the SPSW1 specimen were analysed to determine the strain distributions in the frame members and the infill plate.

From the strain gauges attached to the infill plate, near the top corner, a relationship was observed between the applied base shear and angle of inclination of the resultant in-plane strain. As the base shear changed, the angle of inclination was affected in a near linear relationship. This is shown in Figure 4.3. Since strain gauges were affixed in only two orthogonal directions, the angle of inclination and magnitude of the *principal* strains could not be determined. However, the fact that the resultant angle shifts, indicates that the principal strain resultants would also vary, in some relationship.

The relationship between infill panel strains and base shear could be related to the overall steel shear wall behaviour in general, and the flexibility of the top beam. Since the beam was flexible enough to rotate under load, it might have caused a redistribution of the strains to some degree. While the extent of this action is unknown, the fact that the above relationships existed at low load levels, when beam rotation would be

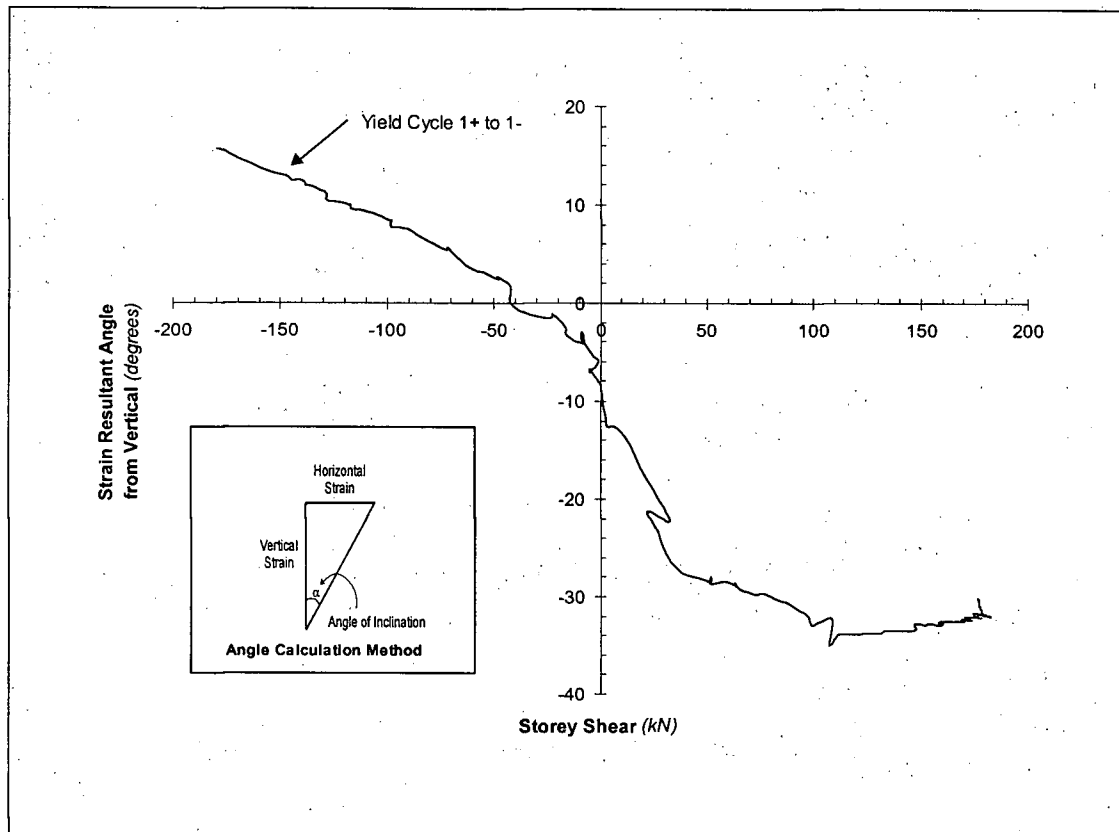


FIGURE 4.3: In-plane infill panel strain, top corner of SPSW1

minimal, suggests that the mechanisms involved in establishing load paths in “general” steel shear walls are at least partially responsible.

A relationship was also observed between the applied base shear and the axial column strains at the base of the south column (Figure 4.4). The axial strains induced in the column result from the overturning moment created by the actuator at the top of the specimen. In the figure, the theoretical axial strain for 100 % tension field anchorage in the column (from an assumed equivalent single brace model) has been superimposed over the measured strains. Some part of the stiff fish plate and adjacent infill panel may

be acting with the column, increasing its net area and requiring a reduction in the theoretical strains. However, since the measured values are close to the theoretical approximation even without considering the fish plate action, it is apparent that the column was effective in anchoring a significant proportion of the tension field. Little of the vertical component of the tension field seems to have been anchored in the bottom beam.

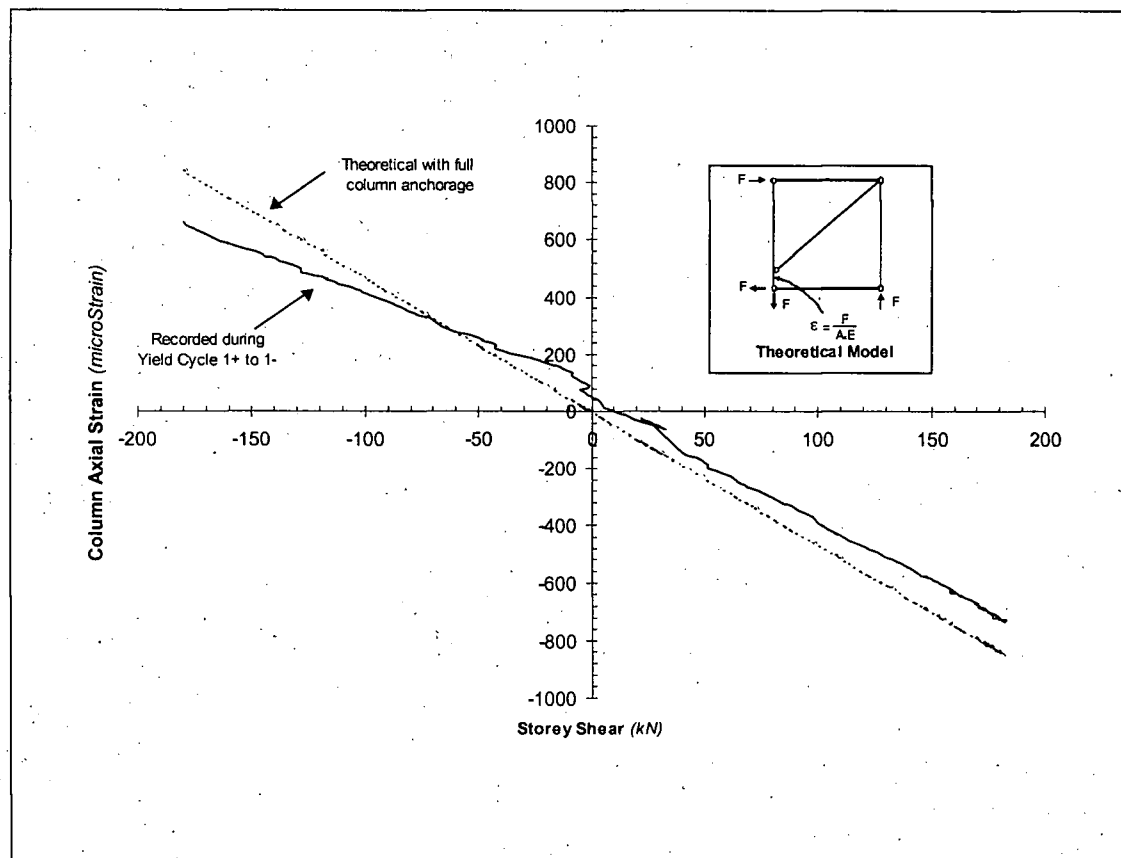


FIGURE 4.4: Axial strain at base of south column, SPSW1

The ratio between the axial column strain and bending strain at the global yield displacement is of significance. Shortly after the global yield displacement was exceeded, a plastic hinge formed at the base of the column. At the yield point,

however, the ratio of axial strain to bending strain in the column flanges was approximately 1:1. Since the axial strain condition indicated that the axial force was approximately 50 % of the fully plastic axial capacity of the section, the moment capacity as measured relative to the section's fully plastic moment capacity would have decreased to approximately 80 %, for the S75x8 section used. If the influence of shear in the section would be considered, in addition to the flexure and axial force interaction, the available moment capacity would be even further reduced. Designers must be aware of the consequences of this interaction between the axial and bending forces, and the interaction with the column shear (not studied) when sizing the column members. These results indicate that while the column remained elastic at this section at the global yield level, little reserve capacity was available prior to the formation of a plastic hinge.

4.2.3 Failure Mode

Termination of the test was governed by the imminent failure of the lateral bracing system. The beam supporting the ends of the bracing members was inadequately sized, and underwent distortion under the out of plane forces generated at high lateral deformations. At this point the pushover displacement was $7 \times \delta_y$. Figure 4.5 illustrates the overall extent of permanent damage in the SPSW1 specimen, after conclusion of the experiment.

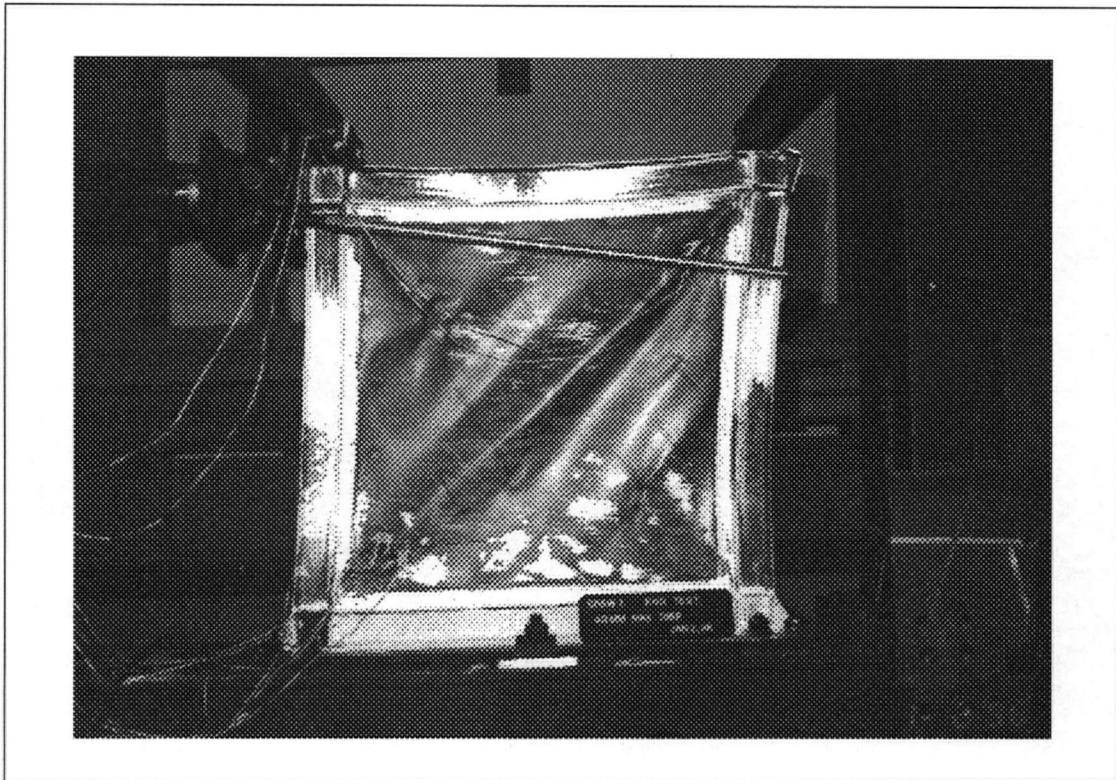


FIGURE 4.5: Global damage in SPSW1 after testing

Some cracking of the welds at the base of the south column and gusset plates was observed near the end of the test. The welding pattern used at this location was carefully observed in subsequent tests.

As described in Section 3.3, the loading system provided for force application under a compressive mode only. As a result, the top beam became badly distorted during the test, which can be attributed to the loading method, combined with the beam's low flexural stiffness which could not adequately anchor the tension field without large deformations. Patterns observed from whitewash flaking indicated that a plastic hinge had formed near the centre of the top beam. The pattern and curvature of the beam

indicated a torsional component to this structural damage. The beam-column joint regions remained relatively square and no yielding was observed in the connection panel zone.

It is important to note that the limited cyclic repetition at each load level may have prevented seismic related failure modes from becoming evident. This would include damage associated with frequent plate buckle reversals, such as plate tearing and folding reported by Timler and Kulak (1983). Fatigue related mechanisms would not be observed in this test due to limited testing cycles. There was no opportunity to assess the strength degradation between successive cycles at the same load level, which might otherwise have revealed damage which could not be readily observed.

4.2.4 Other Observations

One interesting observation during this test was the presence of audible plate popping noises, often described as an "oil can effect". These were typically heard as the applied force passed through the ± 30 kN range, which is a small fraction of the maximum applied load in each cycle. It is speculated that this coincided with the plate buckle reversing action, and was amplified by the large initial out of plane deformation of the infill plate. This effect was not readily observed in subsequent tests.

Further research needs to be conducted into the cause of these noises, and under what conditions they will occur. Otherwise, this could prove to be a cause for concern in

commercial building construction, if this effect was to occur under normal or extreme loading conditions. Occupants of the structure may not find these sounds reassuring.

4.3 SPSW2 Test

4.3.1 Load Deformation Characteristics

The key performance characteristic to be determined from the SPSW2 test was the relationship between storey shear and storey drift. In particular, data on the stability of this relationship under fully reversed cyclic loading at high displacement ductility levels was desired. Figure 4.6 illustrates the hysteretic behaviour of this relationship obtained from the SPSW2 test.

By examining an isolated cycle from this test in the post-yield region, several well defined segments of the hysteresis curve are evident. The basic form is similar to that described in Section 4.2.1, for the SPSW1 test. The overall stiffness immediately after yield was approximately 1/10 of the elastic value. The elastic stiffness was approximately 50 % higher than for SPSW1 (due to some design modifications, such as the double top beam), but the post-yield stiffness in the range immediately after global yield was approximately 600 % higher than SPSW1's corresponding value. The maximum storey shear resistance of the specimen was 260 kN, as compared to the global yield force level of 200 kN. This is a significantly higher post-yield strength

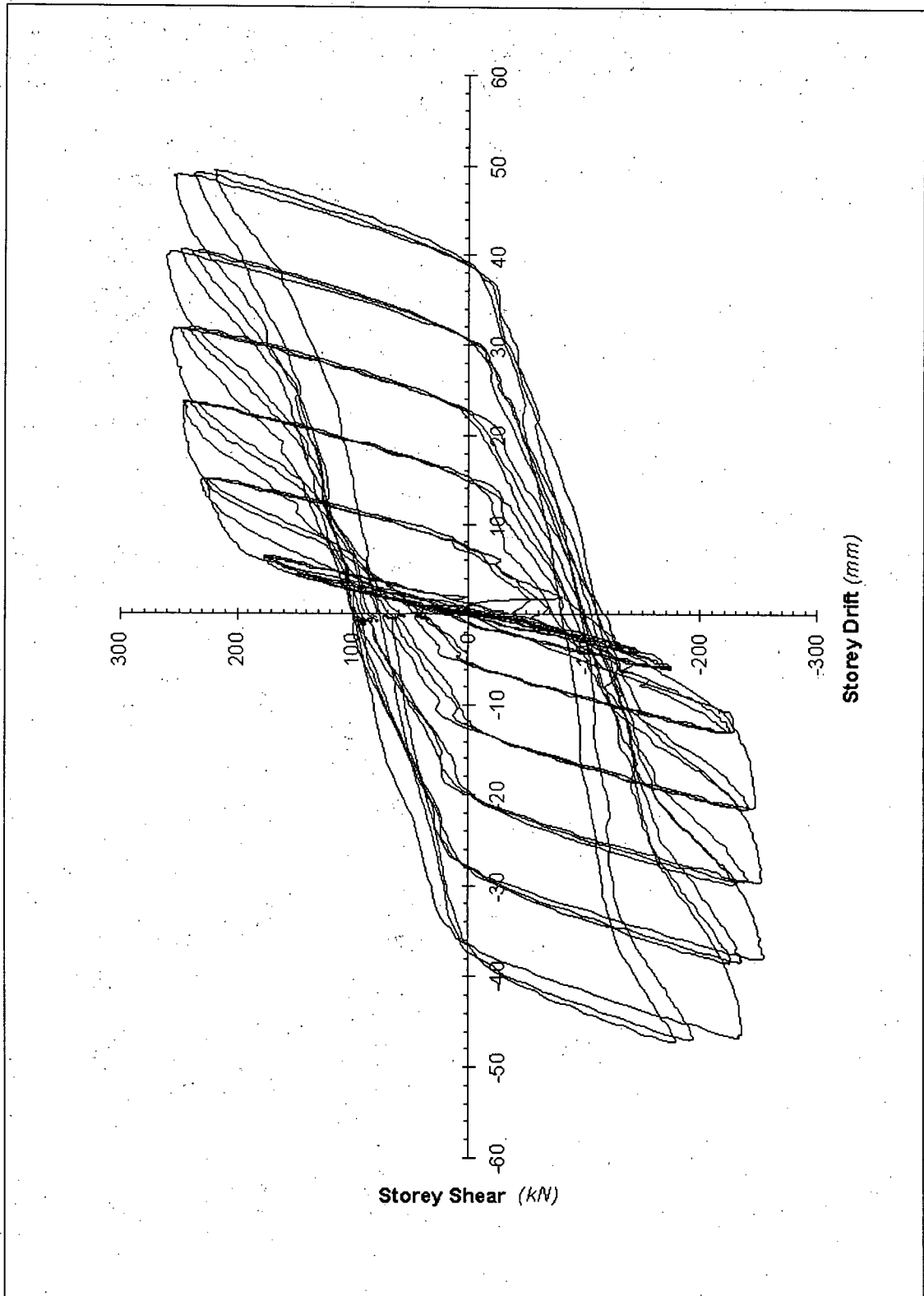


FIGURE 4.6: Force-deformation curve for SPSW2

increase than was observed in the SPSW1 test. This maximum value corresponds to a displacement level of $5 \times \delta_y$.

The overall cyclic loading achieved a maximum displacement of $6 \times \delta_y$, corresponding to a storey rotation angle of 0.056 radians. The test was terminated after the third cycle at this level, when a fracture was observed in the south column, propagating inwards through the outer flange and web. The crack appeared to have initiated at or near a weld location from the triangular column gussets (Figure 4.7).



FIGURE 4.7: Damage in the South column, SPSW2 specimen

The hysteretic behaviour was quite stable over successive cycles at the same load level, in terms of the stiffness properties. However, at higher displacement levels, a

significant load degradation was observed between the first and last cycles, with equal maximum displacement values. This is shown in Table 4.1, where the $5 \times \delta_y$ set of cycles showed a 9 % decrease in force at the same displacement, between the first and third cycles. The larger drop in the $6 \times \delta_y$ load level reflects the increased deterioration from the column fracture.

TABLE 4.1: Strength degradation over SPSW2 cyclic loading

Force Controlled Loading Regime						
LOAD LEVEL	Max Force Cycle 1 (kN)	Max Force Cycle 3 (kN)	Displ Cycle 1 (mm)	Displ Cycle 3 (mm)	Load Change (%)	Displacement Change (%)
A	24.8	24.8	0.63	0.63	0.00	0.00
B	70.8	70.8	1.94	1.81	0.00	-6.70
C	150.1	149.9	4.43	4.43	-0.13	0.00
D	176.4	176.4	6.14	6.4	0.00	4.23

Displacement Controlled Loading Regime						
LOAD LEVEL	Force Cycle 1 (kN)	Force Cycle 3 (kN)	Max Displ Cycle 1 (mm)	Max Displ Cycle 3 (mm)	Load Change (%)	Displacement Change (%)
E	223.5	223.1	15.12	15.12	-0.18	0.00
F	246.1	239.6	23.79	23.52	-2.64	-1.13
G	253.9	240.6	31.79	31.92	-5.24	0.41
H	258	234.1	40.32	40.46	-9.26	0.35
I	251.5	219.8	48.99	49.38	-12.60	0.80

NOTES: Displacements are "Cable Displacement" values.
Resolution of measurements are 0.35 and 0.13 for force and displacement respectively

The area bounded by the force deformation hysteresis loops is a measure of the energy dissipated by the structure through hysteretic damage. Energy dissipation values were calculated for each complete cycle, and are presented in Figure 4.8. This plot indicates that very little energy is dissipated through hysteretic means until the post-yield regime,

beginning with cycle E1. It also shows that over successive loading to higher displacement multiples, there is a stable relationship between the increase in displacement and energy dissipation. It can also be observed that the energy dissipation decreases between the first and third cycles at the same loading level, due to the force degradation noted above.

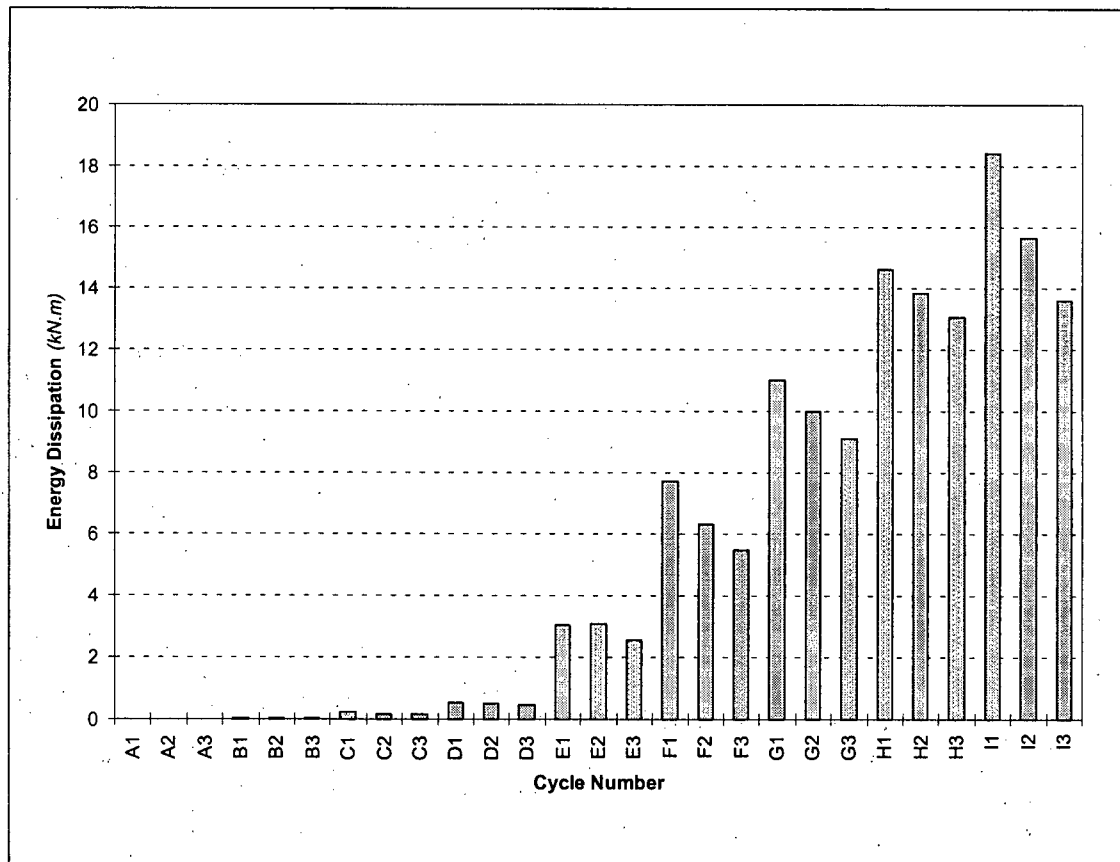


FIGURE 4.8: Hysteretic energy dissipation from SPSW2

4.3.2 Frame Behaviour

During the SPSW2 test, a significant amount of energy dissipation was observed to occur through shear yielding and the formation of plastic hinges in the column

members. Four distinct regions were identified, through visual inspection and observation of patterns in the whitewash. These were at the top of the columns, just below the beam-column joints, and at the bottom of the columns, above the point where the gussets terminated. Figure 4.9 shows the inelastic column deformation immediately below the south beam-column joint at the conclusion of the test.

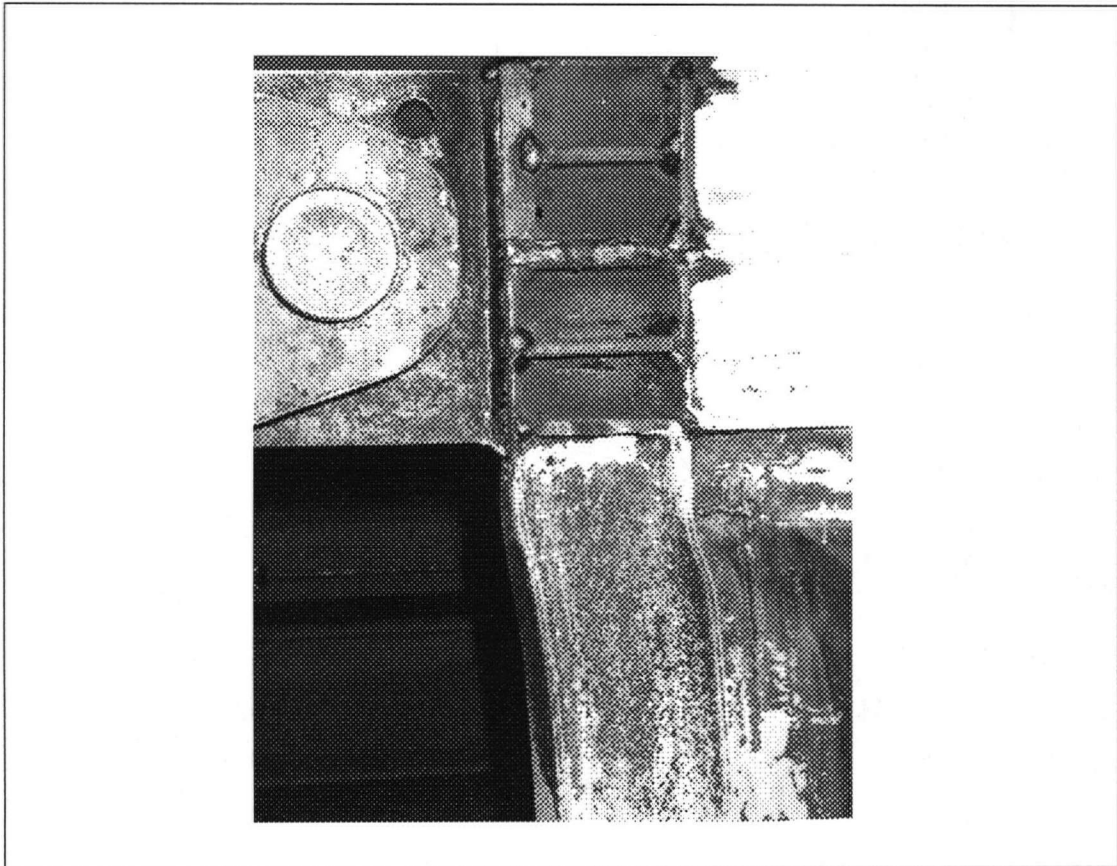


FIGURE 4.9: Inelastic column deformation on SPSW2 at the south, top joint at test completion.

Overall, the column members exhibited significant permanent deformation through the course of the test. In fact, at the end of the experiment, this deformation resulted in the panel taking on an “hourglass” shape, shown in Figure 4.10.

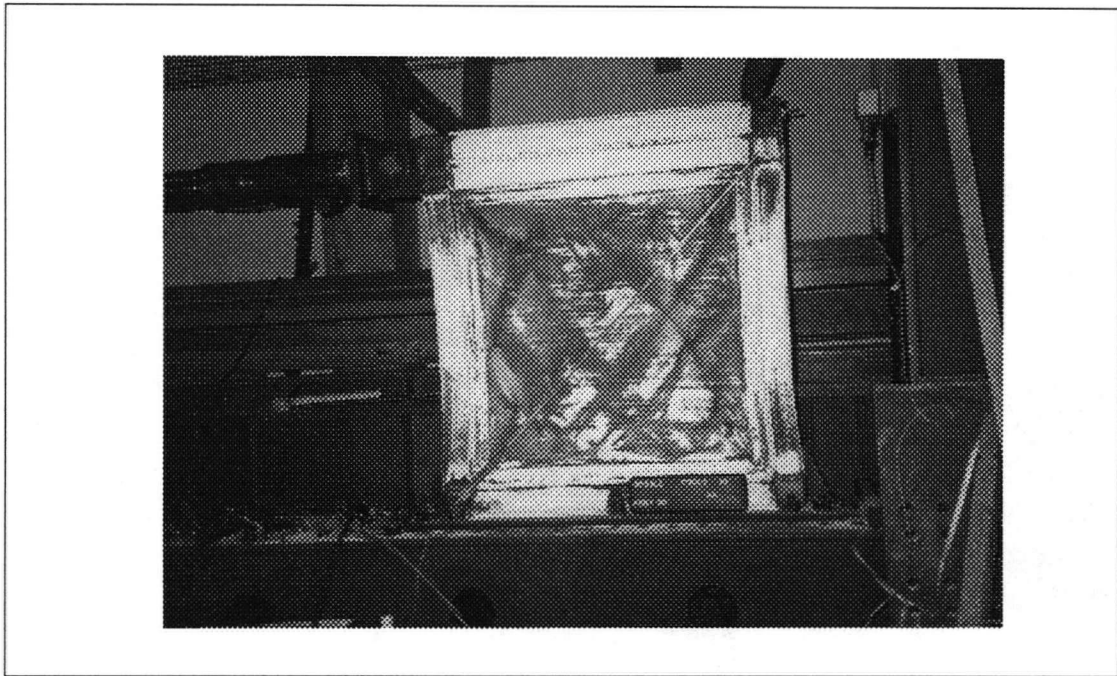


FIGURE 4.10: “Hourglass” shape resulting from deformation of the columns at completion of SPSW2 test.

4.3.3 Plate Behaviour

As the displacement level increased through subsequent cycles, a degree of plate “folding” was observed at the quarter points of the infill panel. These resulted when the plate buckles reoriented themselves due to load reversals, through the course of the loading history. At the displacement level of $4 \times \delta_y$, plate tears were observed at these locations. This type of plate folding and tearing has also been reported by other researchers (Timler and Kulak, 1983; Tromposch and Kulak, 1987).

Weld cracking was observed in the fillet welds joining the fish plate to the columns, in the top corners. The cracks were first observed after cycles at the displacement level of

$2 \times \delta_y$, and increased in size with further cycles. It is noted that due to the small dimensions of material involved, it would be difficult to ensure perfect welding in all locations. While this may have affected some of the local failure modes, and the load levels at which they appeared, the overall behaviour of the specimen and weld failure locations appeared consistent with tests conducted on larger scale specimens (Timler and Kulak, 1983; Tromposch and Kulak, 1987; Driver, 1997).

4.4 Comparison of SPSW1 and SPSW2

4.4.1 Frame Element Effects

As noted in Section 4.3.1, the elastic stiffness of the SPSW2 specimen was significantly higher than that of SPSW1. The addition of the stiffer double top beam provided better anchorage for the tension field, and permitted better activation of the infill plate shear resistance at smaller deformations. It also caused significant inelastic deformation at the top of the columns, and not in the top beam.

The SPSW2 specimen was constructed with column gussets that extended above the height of the base beam. From observations, the plastic hinges which formed at the bottom of the columns occurred above the gusset tips. In the case of the SPSW1 specimen, the column gussets terminated at the height of the bottom beam flange continuity stiffeners. Through observation of the deformed column shape, plastic hinges in that specimen formed immediately above this location. Based on these

observations, it is evident that the differences observed due to the local stiffening and strengthening would have altered the stress and strain distributions locally, in the various structural components.

4.4.2 Loading Histories

The two single storey specimens also differed in the load history sequence. Since the SPSW2 specimen was tested in a repetitive cyclic manner, different types of failure mechanisms might have become apparent. The weld cracking and plate tearing modes are two examples.

The strength degradation observed in the SPSW2 specimen over multiple cycles at the same load level, also indicates that different overall response characteristics may result, due to the difference in load application strategies. The accumulated damage from multiple cycles, reflected in the strength degradation, could impact the specimen's response at subsequent higher load levels. It is apparent from these load history dependent characteristics that a steel shear wall specimen loaded under multiple reversed cycles may exhibit different performance characteristics than one loaded monotonically.

4.4.3 Displacement Ductilities

It was noted earlier that the maximum displacement ductilities attained for the SPSW1 and SPSW2 specimens were $7 \times \delta_y$ and $6 \times \delta_y$, respectively. However, the maximum displacement of the SPSW1 specimen was approximately 50 % higher than that of the SPSW2 specimen, due to their differing elastic stiffnesses and yield strengths. Both specimens showed that considerable response capacity was available in the post-yield region. Termination of the experiments in both cases was due to local problems and test setup limitations, and not failure of the global structural system.

These results were compared against an accepted simplified measure of a structure's reserve capacity under extreme excitation. For this comparison, a schematic representation of a structural component capacity, suggested by FEMA-273 (Federal Emergency Management Agency, 1996), was selected. It represents the various phases of load-deformation response of a structure, including the deterioration in stiffness at very high deformation levels (Figure 4.11).

By comparing the load-deformation envelopes of the SPSW1 and SPSW2 specimens, it is apparent that the specimens, while damaged, have not reached their theoretical performance limits. Normalized "backbone curves" of the load-deformation relationships of the two specimens, using a method suggested by FEMA-273, have been included in Figure 4.12. The extreme response of the two specimens each fall within the

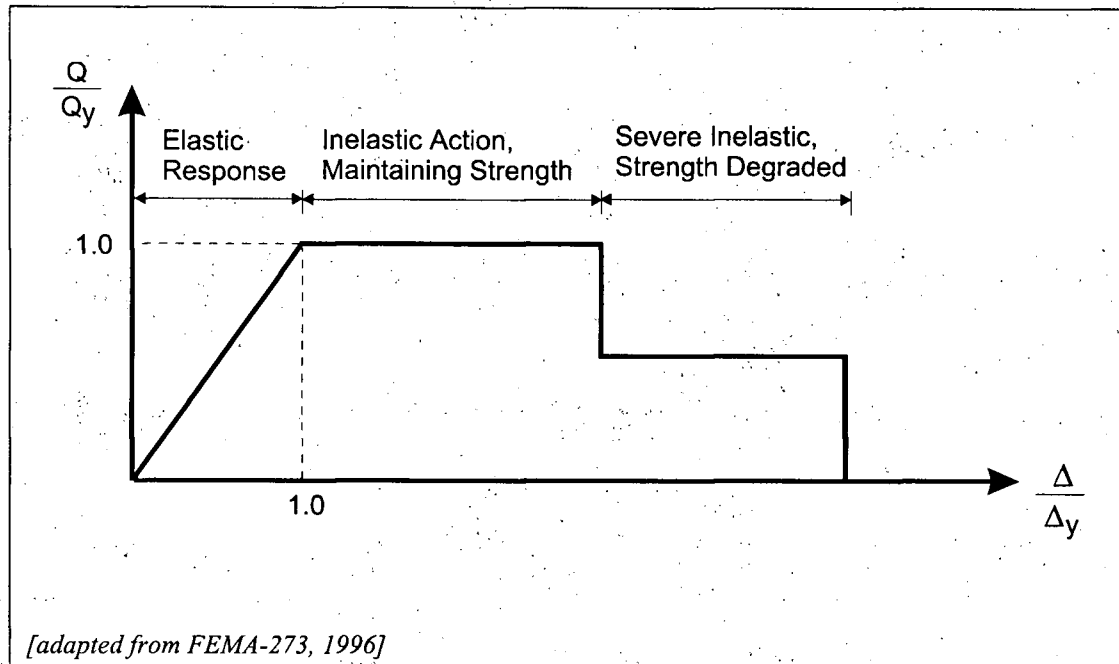


FIGURE 4.11: Representation of a ductile structure's load-deformation capacities

middle band of the capacity diagram, characterised by inelastic damage but with no significant loss in force resisting capacity. It is hypothesized that if the localized problems were corrected through strengthening, additional longitudinal deformation could be applied until the response of the specimens fell within the extreme right portion of Figure 4.11.

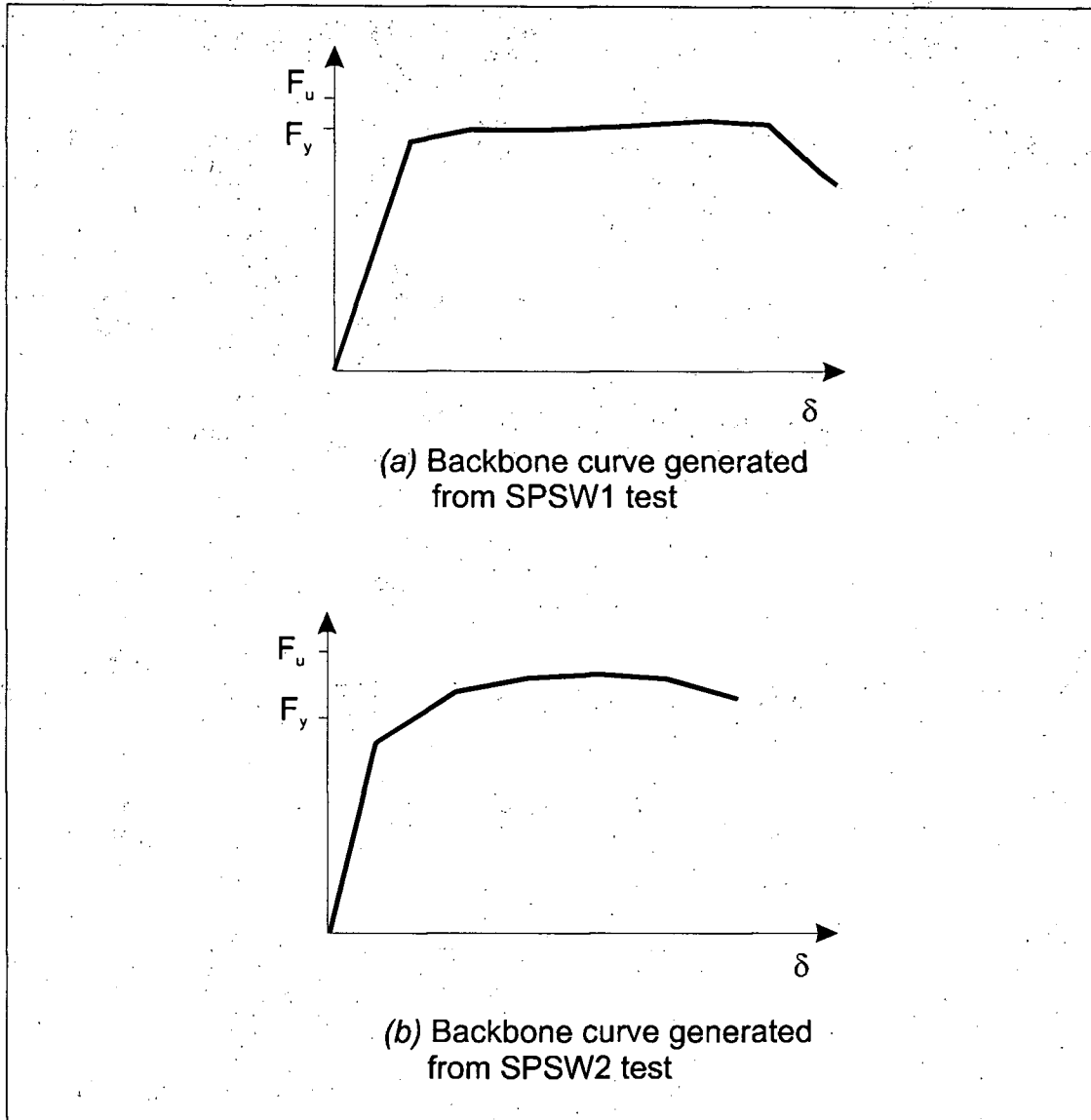


FIGURE 4.12: Normalized "backbone curves" up to test termination, for (a) SPSW1 and (b) SPSW2

CHAPTER 5

Multistorey Experimental Programme

5.1 Introduction

One four storey specimen was constructed and tested, to obtain data on the performance and behaviour of a multistorey steel plate shear wall under cyclic quasi-static loading conditions. Based on the preliminary results available from the earlier single-storey tests, appropriate procedures were used for its construction, instrumentation and testing.

A description of the test specimen, SPSW4, is provided in Section 5.2. Sections 5.3 and 5.4 contain descriptions of the loading and support systems used, respectively. The instrumentation and data acquisition employed during the experiments is described in Section 5.5. Finally, Section 5.6 summarizes the testing procedures.

5.2 Test Specimen

A four storey specimen was constructed and tested — referred to as SPSW4. The specimen was a 30 % scale model of an inner residential building core, with the specimen having floor-to-floor and column-to-column spacing of 900 mm. A photograph of the specimen and a dimensioned drawing are provided as Figures 5.1 and 5.2. The overall vertical dimension consisted of four storey panels, each with dimensions equal to those used in the SPSW1 test. The infill plate sizes for the lower

three storeys also remained constant. The top most infill panel was shorter, to accommodate a deep top beam within the overall dimension, so as to maintain a uniform floor to floor height.



FIGURE 5.1: Photograph of specimen SPSW4 within the test frame
(Tested specimen SPSW1 shown in foreground)

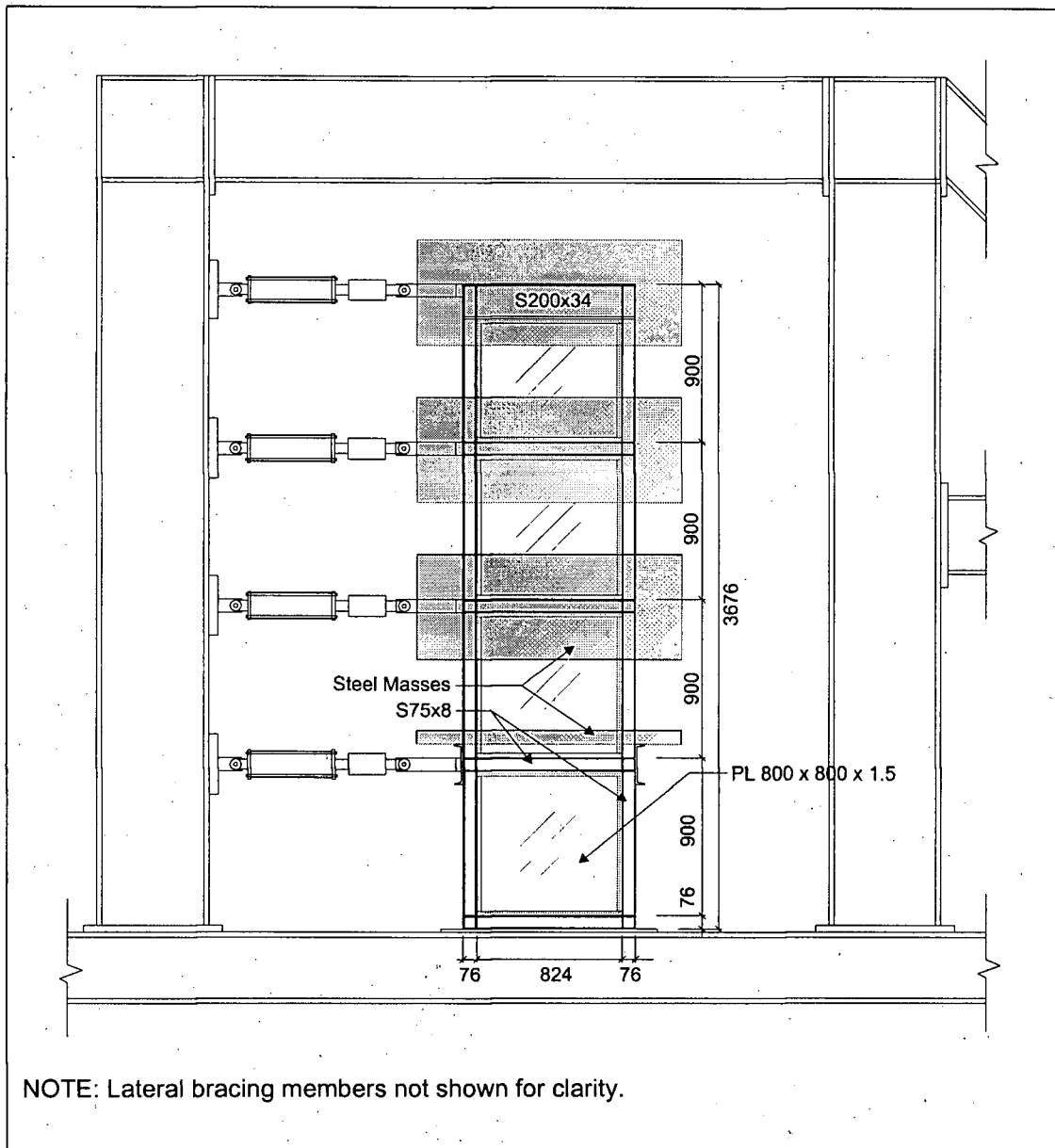


FIGURE 5.2: Specimen SPSW4

Frame members were constructed from S75x8 hot rolled steel sections. The deep top beam was constructed from a S200x34 section. The infill shear plates were constructed from 16 gauge (1.5 mm) thick hot rolled sheet steel. Beam-column joints were all fully

fixed, with flange continuity stiffeners added across the column webs. The column sections were continuous over the full height of the specimen. A fish plate detail was used to join the infill plate to the steel frame, as shown previously in Figure 3.2. A 20 mm x 200 mm base plate was attached to the bottom beam and around the column sections by continuous fillet welds. Gussets at the column base were used, as illustrated in Figure 5.3

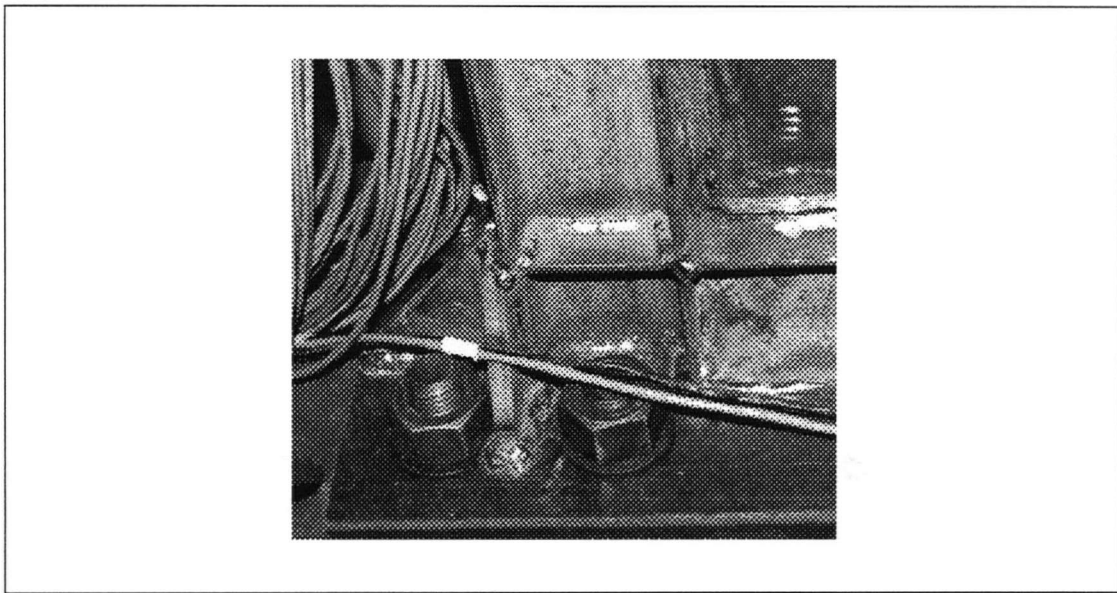


FIGURE 5.3: Gusset detail at base of SPSW4 specimen

All column sections were obtained from the same piece of steel. Similarly, the beam sections (except for the top beam) were all cut from another single length of steel. Tensile coupon tests were done of the respective steel components, and are discussed in Section 6.2. Three of the four infill panels were cut from the same piece of sheet steel. The second storey panel was obtained from a different piece. Coupon tests of the infill plate material are discussed in Section 6.2. In all cases, the infill plates were oriented

with the long direction from the original plate — the direction of rolling — oriented in the horizontal direction.

During fabrication, particular procedures were used to minimize the residual out of plane deformation in the infill plates due to weld distortion. These deflections were measured as less than 3 mm, at 9 locations on each panel. A residual twist remained in the specimen, however, which was easily eliminated through the lateral bracing system. Measurements of the specimen were obtained, when erected in an unbraced configuration, using a plumb bob. The top of the specimen was displaced laterally from the corresponding base location by up to 83 mm. This approximates to a twist of 2.8 degrees per metre of vertical rise.

A simulation of typical gravity loading was applied to the columns through the use of large steel plates. A weight of 13.3 kN was introduced at each storey level, by attaching masses using spacers and bolts, through the centre of each beam-column joint. The spacers helped to prevent interaction between the masses, frame members, and buckled infill plates. At the first floor level, the masses were supported by channels, welded to the outside of the column flanges over the floor beam height. The column web was stiffened at each joint to accommodate these concentrated forces, by welding 50 x 50 x 4 mm doubler plates to each side of the web. It is noted that this local strengthening would serve to effectively eliminate the possibility of a shear-type failure mechanism in the joint, which may need to be considered when designing a full-scale structure.

The addition of the dead load served a number of purposes. Primarily, it was used to reflect the loading required on a similar specimen, for shake table testing. The quantity of mass selected reflected the requirements for adequate shake table excitation, and a representative amount of scaled vertical load that would be collected by the columns in their assumed role. The influence of the column dead load could be significant since it reduces the tension uplift forces resulting from the applied overturning moment. However, it would also serve to decrease the capacity of the opposite compression column to resist the applied moments.

5.3 Loading System

A load application system was developed for the SPSW4 test, to apply loads to each of the four floor levels. All tests were conducted within a self-reacting test frame, significantly stiffer than the specimen. The hydraulic actuators and test frame are shown in Figure 5.1.

Four hydraulic actuators, with a rated capacity of 200 kN each, were used — one at each floor. Each actuator setup was pinned to rotate freely in the vertical direction at both the test frame connection and the loading tab joining the specimen. The actuators were set to apply the load at the mid-height level of each beam, or the top 75 mm in the case of the top beam.

The loading tabs consisted of 75 x 25 mm thick steel flat bar, welded over the full height of the floor beam (the top 75 mm in the case of the deep top beam). It was positioned on the column flange in the plane of the column web, and secured with a continuous perimeter fillet weld. A taper in the tab, to 7 mm thick, was provided at the specimen connection end. A pin joint was used to connect the tab to the actuator, leaving an effective length of tab of 330 mm.

The loading control for early cycles (A to F) was by an MTS 458.10 servo controller, and attached MTS sine-wave function generator. Different force levels were applied in each actuator, resembling the typical inverted triangular distribution for seismic loads. However, due to the complexity of force controlled loading of multiple actuators, connected through a stiff specimen, this approach was not feasible. Vibrations resulting from feedback instability in the control system were noted. Load levels applied during these cycles were significantly less than what would be required to cause inelastic damage in the specimen.

For the cycles of interest (G to M), loading control was accomplished through a SUN 0 - 1500 psi, 10 gpm manually operated pressure reducing valve. In this setup, the configuration of the hydraulic hoses provided for equal hydraulic pressures to be applied at each identical actuator. The force applied at each actuator would be essentially equal. However, variations could arise from factors including friction losses in the hydraulic hoses and tolerances in the actuator components. Consequently, the

instrumentation allowed for the measurement of the actual applied force at each actuator. Other researchers, including Driver (1997), have used equal applied forces at each floor with good results.

5.4 Lateral Support System

The lateral bracing system consisted of a series of steel-on-steel, 4 inch diameter rollers, acting between support members and the specimen. Bracing was provided at the fourth floor, second floor, and just below the first floor. At the first floor location, the rollers were bolted through the specimen columns, using spacers, and allowed to roll along stiff external bracing beams. At the other locations, the rollers were attached to the bracing members, and allowed to roll along the mass plates. The bracing system components are visible in Figure 5.1.

It was noted in Section 5.2 that the specimen had an initial degree of twist in an unbraced configuration, resulting from welding distortion. After the initial preliminary assembly of the specimen, mass plates, and bracing components, the bracing members were shimmed to remove the twist from the test specimen. Vertical alignment was confirmed with a plumb bob. While this would induce some additional stresses in the untested specimen, these were assumed to be negligible due to the inherent low torsional stiffness of the specimen.

The base plate of the specimen was fastened to the test frame using ten 25 mm diameter bolts, using a hand wrench. Four bolts were arranged around each column, with two bolts provided at the mid-length location. The contact surfaces between the base plate and test frame were cleaned prior to installation.

5.5 Instrumentation and Data Acquisition

The load deformation properties and the stresses induced in the various structural components were of primary interest in the experiment. The behaviour of the first storey frame and infill panel were of specific interest, due to the expected damage resulting from the greatest storey shear magnitude. The specimen was instrumented accordingly, with displacement and strain gauge sensors. Figure 5.4 illustrates the location of the instrumentation. Figure 5.5 provides an enlarged view of the strain gauge instrumentation applied to the first storey. Details of the devices are provided below.

Each hydraulic actuator was fitted with a load cell. The 1st to 3rd floors used 89 kN capacity load cells, with a recording resolution of 0.04 kN. A 222 kN load cell with 0.1 kN resolution was used on the 4th floor actuator. It is noted that the common channel between each of the three data acquisition computers was the 1st storey applied force. Each data acquisition system had a different resolution, with the lowest given above.

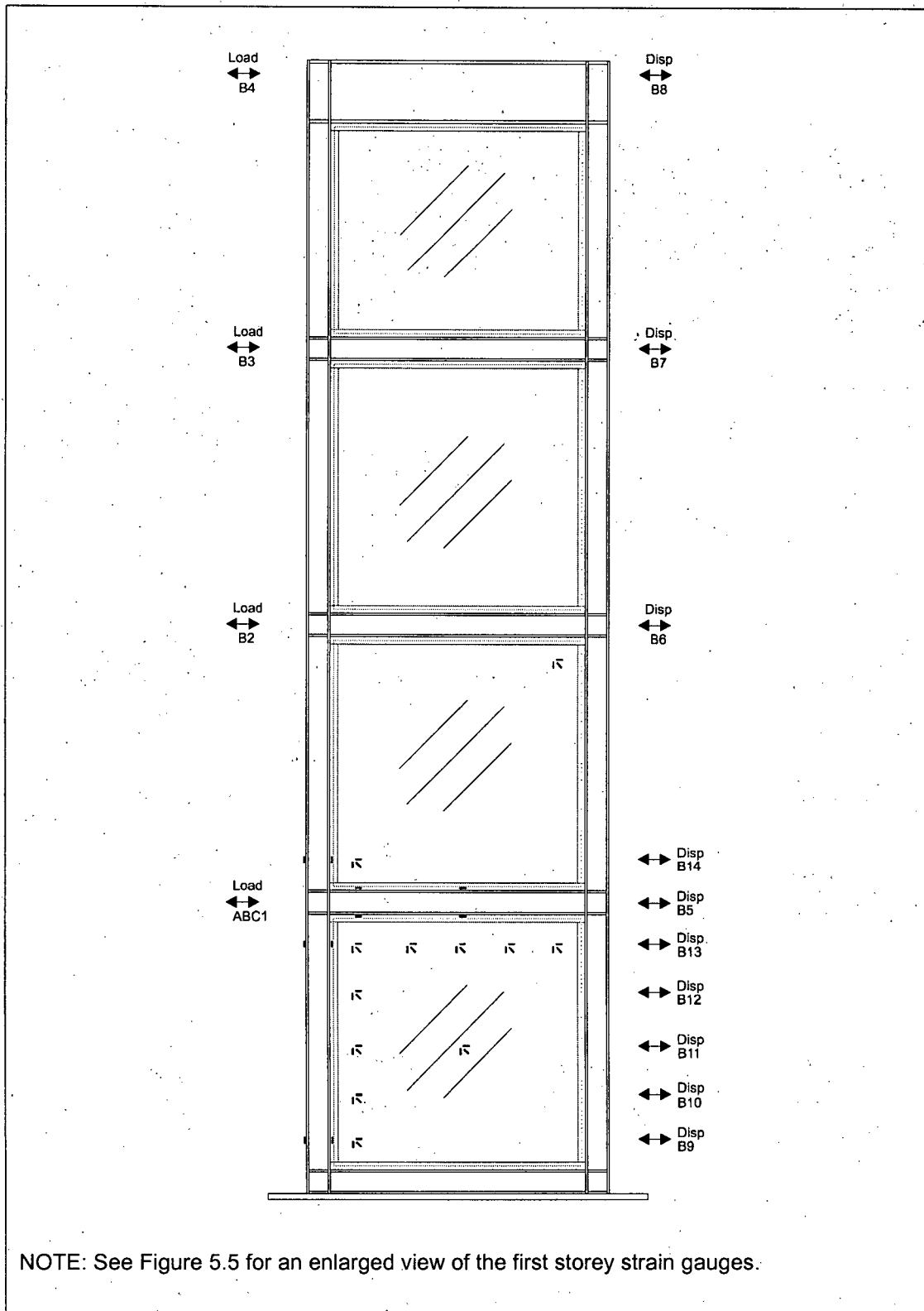


FIGURE 5.4: Instrumentation diagram for SPSW4

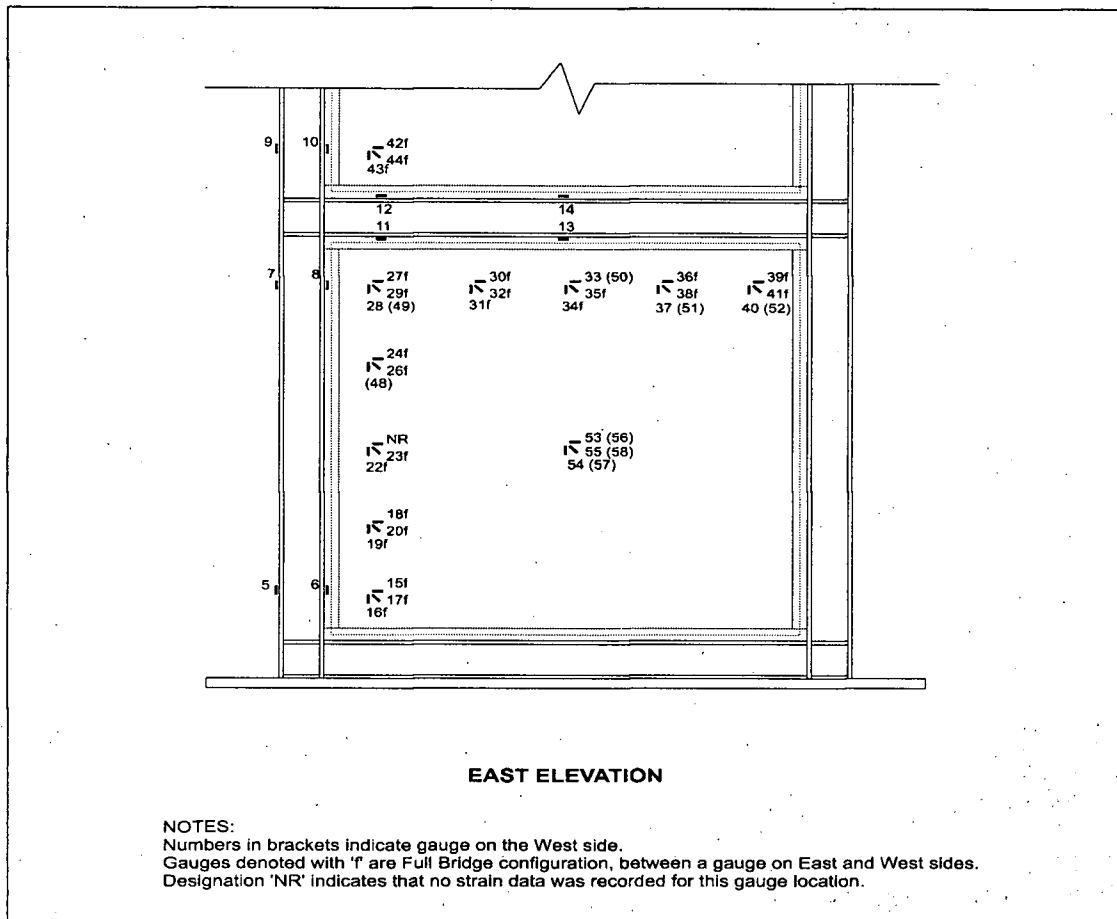


FIGURE 5.5: Strain gauge instrumentation on the first storey, SPSW4

Cable potentiometers were used on the North column at the mid-height of each floor beam (or 40 mm from the top for the 4th floor) to record storey longitudinal motions. Each device had a resolution of 0.12 mm. One additional cable potentiometer was installed above the first floor north column joint. Linear Variable Potentiometers (LVPs) were arrayed along the first floor North column, to measure the deformed profile of the column under applied loading. Each LVP had a resolution of 0.08 mm.

Uniaxial strain gauges were located on opposing flanges of the 1st and 2nd storey south column and 1st floor beam elements. Each gauge was capable of a resolution of 3 microstrain. Strain rosettes — using a 0-45-90 degree configuration — were arrayed on the first and second storey infill plates. Orientation of the strain rosettes is illustrated in Figure 5.6. Most gauges were installed in a full-bridge configuration, to record in-plane strains only. This has been identified on Figure 5.4. All gauges were attached using M-Bond 2000 adhesive, following the manufacturer's recommended surface preparation and installation procedures.

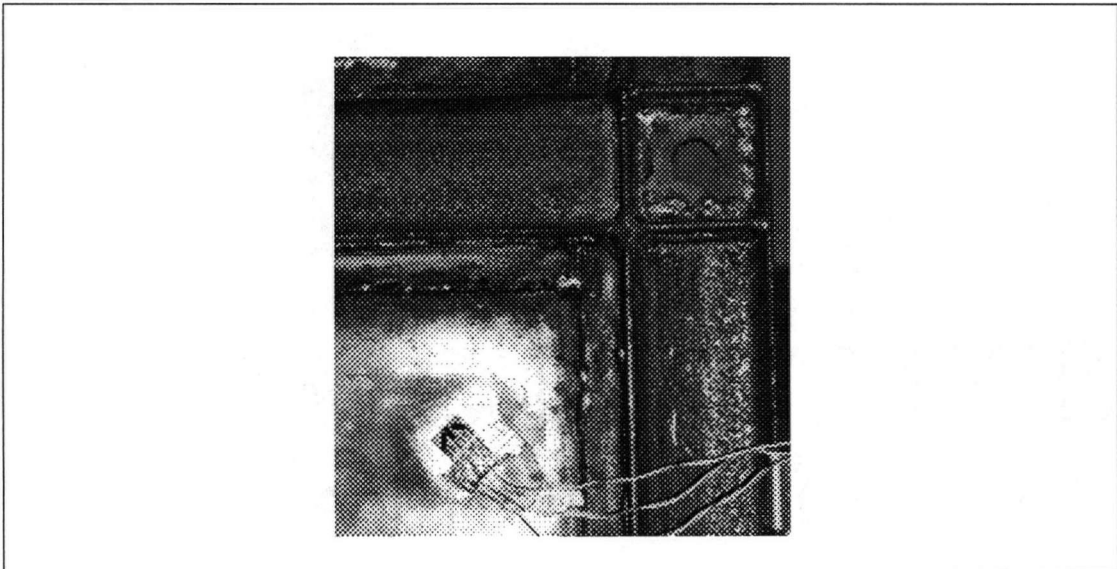


FIGURE 5.6: Photograph of typical strain rosette orientation

A total of 68 independent channels were monitored and recorded during the test. Due to the quantity and type of instrumentation employed, the data acquisition system consisted of three computer systems running simultaneously, using the 1st floor actuator force as a common channel.

The first system recorded strain gauge data from a number of the strain rosette locations. It consisted of a PC with analog-to-digital converters, connected to a custom built data controller which contains filters and amplifiers for all channels. The software package Labtech Notebook was used to sample and record the data, at a frequency of 2 Hz.

The second computer system employed a PC with analog-to-digital converters and Labtech Notebook software. This was used for recording all load cell and displacement measurements, which did not require amplification. No integral filtering was employed in the hardware. The software provided an on screen customized display of critical load and deflection readings in a graphical format. All data sampling was conducted at a rate of 2 Hz. The information presented by this computer was used for the experiment control.

Finally, the third system used an Optilog data acquisition system, which contains filters and amplifiers, and a manufacturer supplied software program on an attached PC for storage. This setup was used for all uniaxial strain gauges, and many of the strain rosettes. Data sampling was at a rate of 2 Hz.

5.6 Testing Procedures

The SPSW4 specimen was tested according to the guidelines presented in ATC-24 (Applied Technology Council, 1992). The methodology of ATC-24 has been described in Section 3.6.

In testing the specimen, cycles A1 to F3 were conducted using very low force levels (<50 kN total base shear). This allowed for confirmation of testing procedures, and verification of the data acquisition system. Some of the cycles contained applied loads at various storey shear ratios, with the load application controlled through a sine wave function generator. As noted above, however, it was determined that the complexity of force controlled loading of four independent actuators connected by a stiff specimen created substantial problems associated with feedback. For the cycles of interest (G1 to M1-), a loading system of equal storey loads, controlled by a manually adjusted valve, provided a more stable control system. Table 5.1 provides a complete record of all loading cycles on SPSW4, including relevant parameters. Plots of the force and displacement histories for SPSW4 for cycles G1 to M1- are presented in Figure 5.7. Each complete cycle (0-positive-negative-0) was approximately 5 minutes in duration.

TABLE 5.1: Load history for SPSW4

Load Level	Num. Cycles	Max Actuator Force at Floor #				Max Disp. at Floor 1 (mm)	Remarks
		1 (kN)	2 (kN)	3 (kN)	4 (kN)		
A	3	0	1	3	5	0.1	Pump shutdown due to feedback. Pump shutdown. Poor tracking. Poor tracking. Pump shutdown. Change to equal actuator loads. Change to manual valve control.
B	2	2	3	3	4	0.1	
C	4	2	4	3	3	0.2	
D	3	3	5	6	5	0.2	
E	4	8	12	14	16	2.1	
F	3	6	6	6	6	0.3	
G	3	6	6	6	6	1.2	
H	3	13	13	13	13	2.7	
I	3	20	20	20	21	4.3	
J	3	25	26	25	25	5.3	
K	3	32	32	32	31	7.1	
L	3	38	38	38	37	9.3	
M	0.75	44	44	43	45	14.8	

NOTES:

Values shown are for the peak excursion in first 'retract' cycle.

Poor tracking of the desired force distribution resulted from improper 'gain' settings, required to decrease the level of feedback in the servo system.

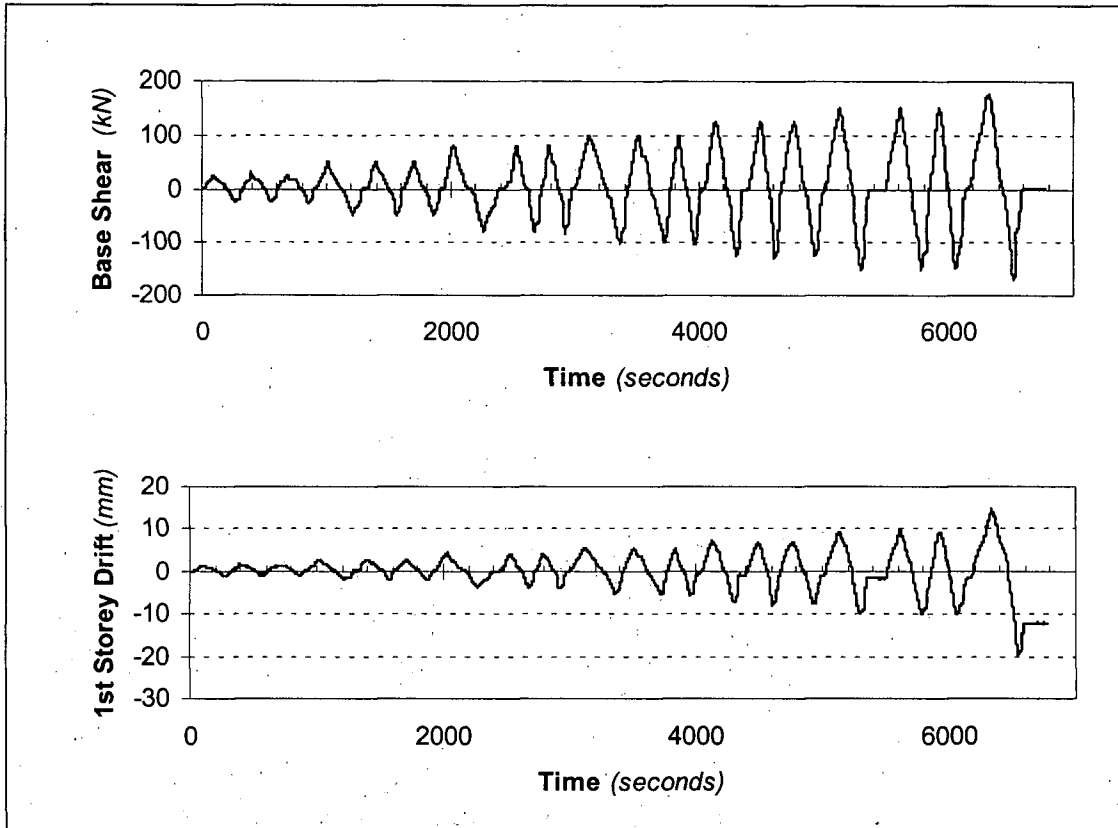


FIGURE 5.7: (a) Force and (b) displacement histories for SPSW4, cycles G1 to M1-

Chapter 6

Discussion of Multistorey Results

6.1 Summary of Test Results

The experimental results from the SPSW4 test provided data on the performance of multistorey steel plate shear walls. In particular, the results allowed for an examination of the validity of extrapolating single storey results to multistorey systems. While similar overall performance characteristics were observed, the results suggest that the practice of generalizing a multistorey steel shear wall as a number of single panels with stiff beams, each taken in isolation, will not adequately reflect all relevant performance characteristics. The influence of the higher overturning moment to storey shear ratio generated in a multistorey specimen can be significant.

Results of material testing, to establish the member properties, are presented in Section 6.2, including the frame and infill plate components. The overall failure mechanism of the SPSW4 specimen is presented in Section 6.3. Load-deformation relationships, and localized column deformations are described in Sections 6.4 and 6.5, respectively. The infill panel behaviour is discussed in Section 6.6. Strain gauge data is presented in Section 6.7. Finally, the results are compared, in general terms, to those from the single storey specimens in Section 6.9.

6.2 Material Tests

Ancillary tests were conducted on representative samples of the materials used in constructing the SPSW4 specimen. Tests included coupon tension testing of flange and web samples from the S75x8 members used for the columns and beams. Coupon tension tests were also conducted on samples of the infill plate and fish plate material, taken in orthogonal directions. Table 6.1 presents a summary of the test results, and compares them to the nominal design values. Full results of the ancillary testing programme are presented in Appendix A.

TABLE 6.1: Summary of material properties determined from coupon testing.

Element	σ_y (MPa)	σ_u (MPa)	Strain at ultimate (%)
Boundary Frame (S75x8)	380	550	10+
Infill Steel Plate	320	370	10+
Fish Plate	260	350	10+

NOTES:
Due to scatter in test results, Young's Modulus of Elasticity assumed as $E = 200$ Gpa, as suggested in Canadian Handbook for Steel Construction (Canadian Institute for Steel Construction, 1993)

The material properties for the S75x8 and infill plates both exhibited the desired hot-rolled steel properties, representative of what would be found in full sized steel elements of a commercial structure. They also showed effective material strengths much higher than used in the original specimen design, with the infill plate having a yield strength of approximately 320 MPa, corresponding to over 140 % of the nominal value assumed in the design. This is significant, since the specimen design originally allowed for the infill panel to yield prior to inelastic action in the columns. Since the actual infill panel would yield at a much higher force level, the component experiencing inelastic action first was altered from the infill panel to the columns. This was a less desirable inelastic response condition, as evidenced in part by the instability failure mode described in Section 6.3.

While good seismic design practices often impose limits on material overstrength factors to prevent undesired failure modes or yielding sequences, it was not practical to do so in this case, due to the required section dimensions and limited availability of materials.

6.3 Failure Mechanism

Cyclic loading was applied to the SPSW4 specimen up to a global yield level of approximately 175 kN base shear and 11 mm deformation at the 1st floor level. Prior to this cycle during which the point of "significant" yielding condition was reached, marginal yielding was noted from a gradual widening of the load-deformation

hysteresis curves and permanent longitudinal drift in the specimen. Prior to the start of Cycle M1+, the specimen had acquired a drift at the fourth floor level of 4 mm to the North, under no applied force.

During cycle M1+, the stiffness rapidly decreased after the global yield level was reached, such that an additional displacement of approximately 4 mm (to 15 mm total) was recorded at the first floor level. This resulted from a delay in the actuator response to the manually adjusted control valve, and the quick rate of stiffness reduction in the specimen. The load was reversed (M1-), proceeding towards the yield level in the opposite direction. It was not possible to control the actuator displacement when global buckling of the North (overturning compression) column occurred at the global yield force level. The major reason for the early failure of the specimen was the inability to conduct the test under displacement control. When yield levels are reached, a virtually flat (or even declining) load deformation relationship will not permit the required force control of the actuator displacements with only manual valve operation.

During subsequent removal of the specimen from the test frame, significant inelastic damage to the 1st storey column was observed resulting from the global lateral column buckling (Figure 6.1). In conjunction with the column buckling mode, the 1st storey infill panel also underwent inelastic buckling (Figure 6.2).

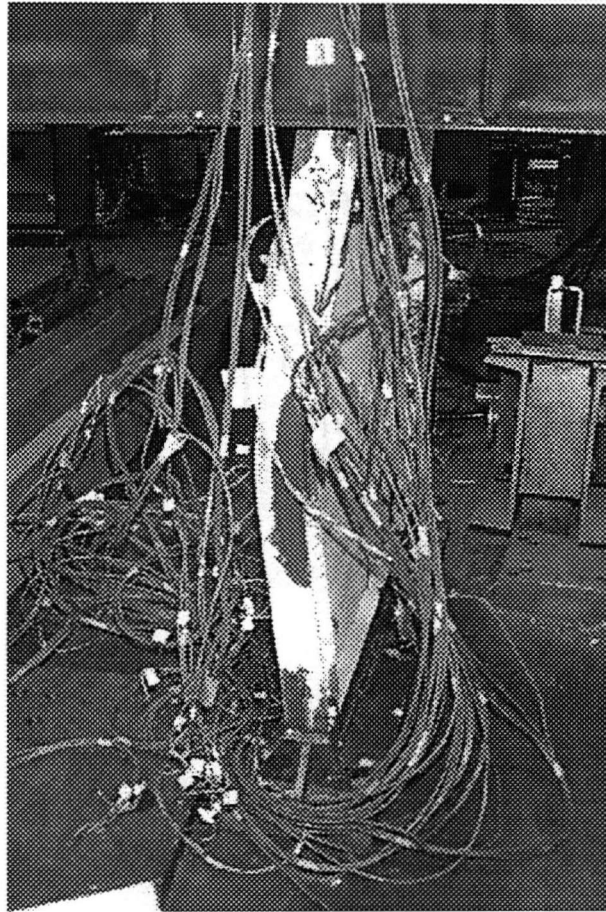


FIGURE 6.1: North column buckled shape

The global column buckling can be attributed to inadequate lateral stiffness of the column section, which is a result of the design limitations discussed earlier in Section 3.2. In addition, while the bracing system was considered adequate to prevent elastic buckling, the influence of the yielded column under axial and orthogonal flexural loads

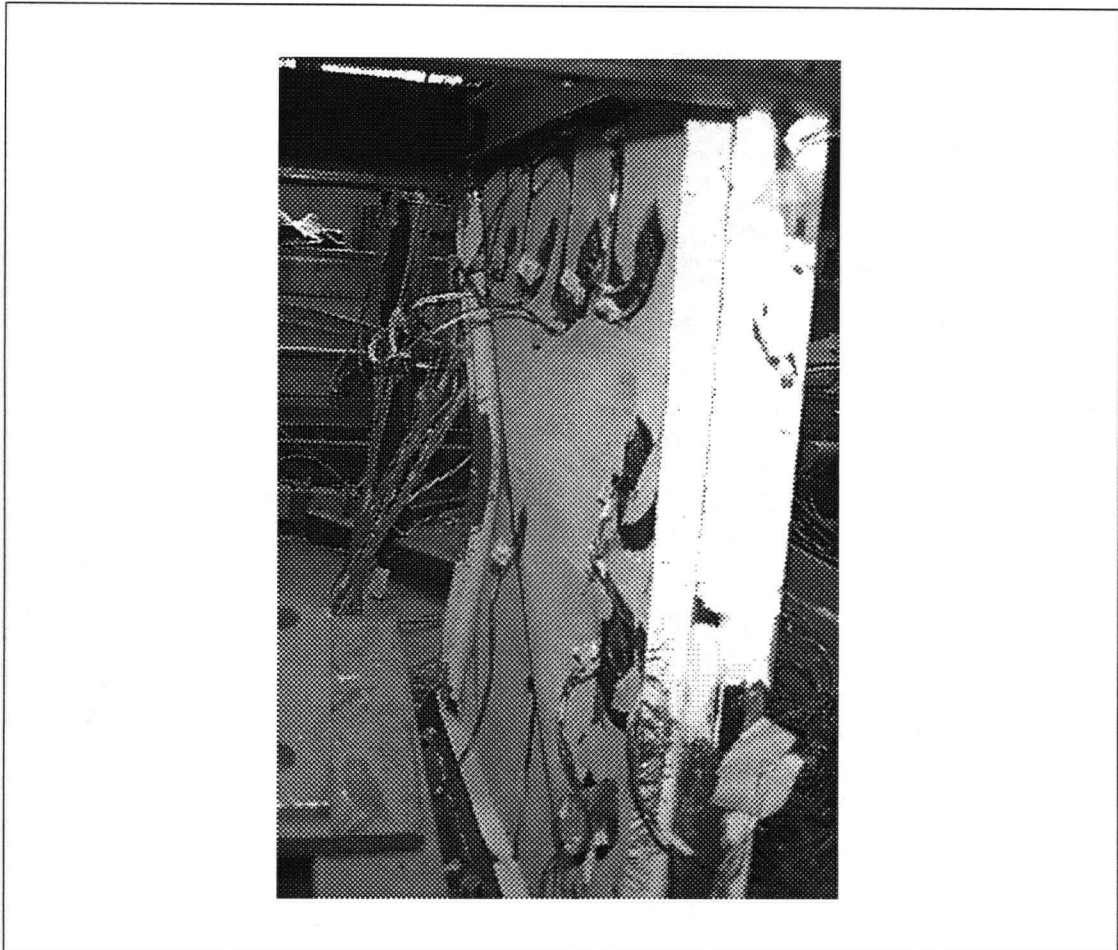


FIGURE 6.2: Inelastic buckling of the 1st storey infill panel

on the critical global buckling load could not be readily assessed. The bracing system may also not have possessed sufficient rigidity to ensure the degree of restraint required. Variations between the actual load paths generated and those predicted by the simplified analytical model used to establish bracing requirements may have compounded these problems.

While it was not possible to test the SPSW4 specimen under the large inelastic incursions that would be expected for severe seismic loading, valuable data was

collected on the performance of multistorey steel plate shear walls under less severe cyclic conditions. Performance characteristics derived from this test are applicable to lower intensity cyclic loading, such as wind or low and moderate magnitude earthquakes. Current numerical analysis techniques were also verified in the structure's elastic region.

6.4 Load-Deformation Characteristics

One of the key performance characteristics to be determined from the SPSW4 test was the relationship between the storey shear and storey drift. In particular, data indicating these relationships for various storey levels was desired. Figure 6.3 illustrates the hysteretic behaviour of this relationship obtained from the SPSW4 test, at the first floor level. The corresponding relationships for each of the four storeys are presented in Figure 6.4. The different relative stiffnesses of the stories are evident, resulting from the influence of column axial forces generated by the overturning moment.

These load-deformation relationships show stable hysteresis patterns for each storey. Some widening of the hysteresis is evident at higher load levels, in particular for displacements in the North direction. When the curves are compared for storey shear vs. storey drift in Figure 6.4, it becomes evident that the hysteresis loops are much fuller at lower storey levels.

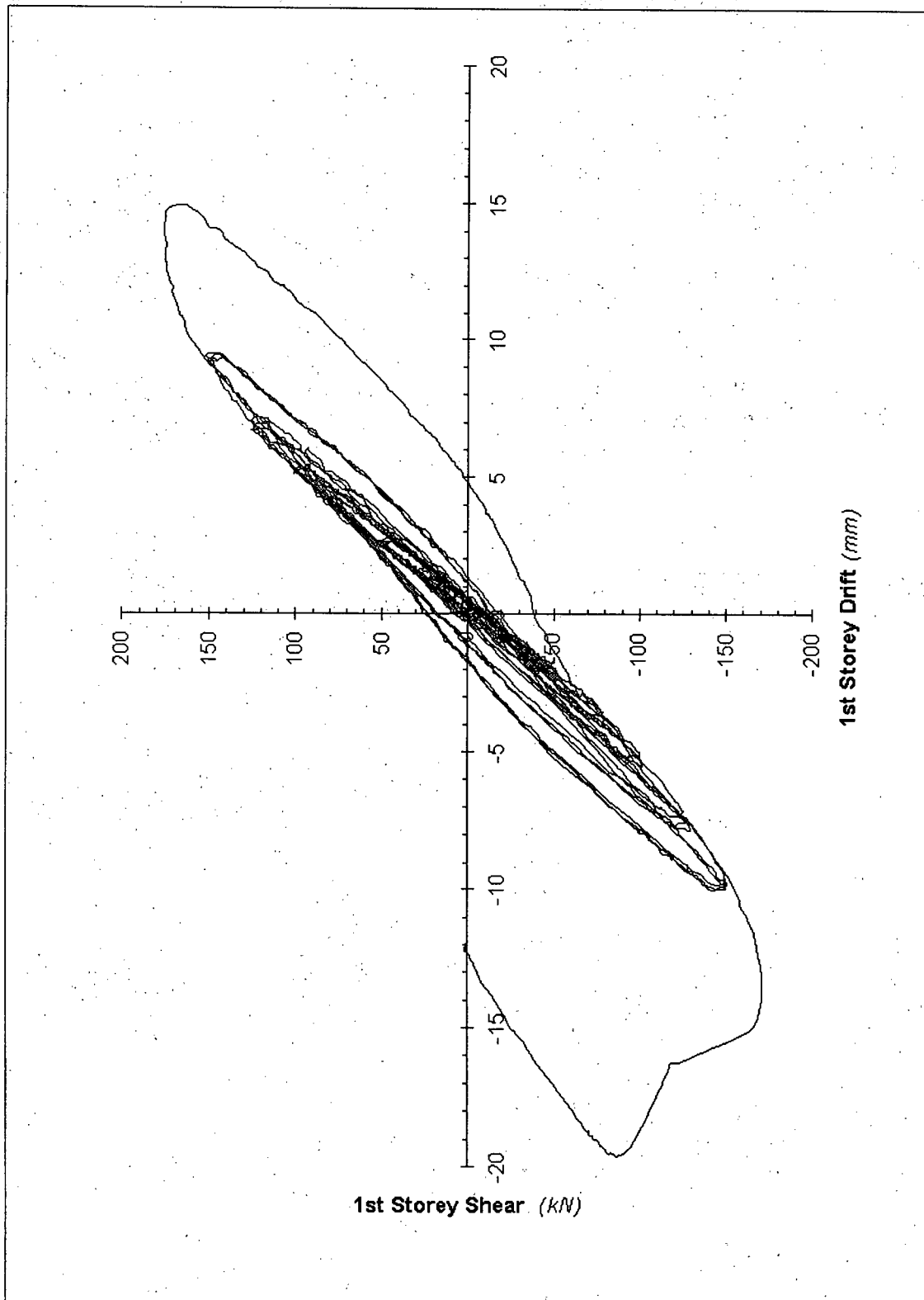


FIGURE 6.3: Force-deformation curve for the 1st floor, SPSW4.

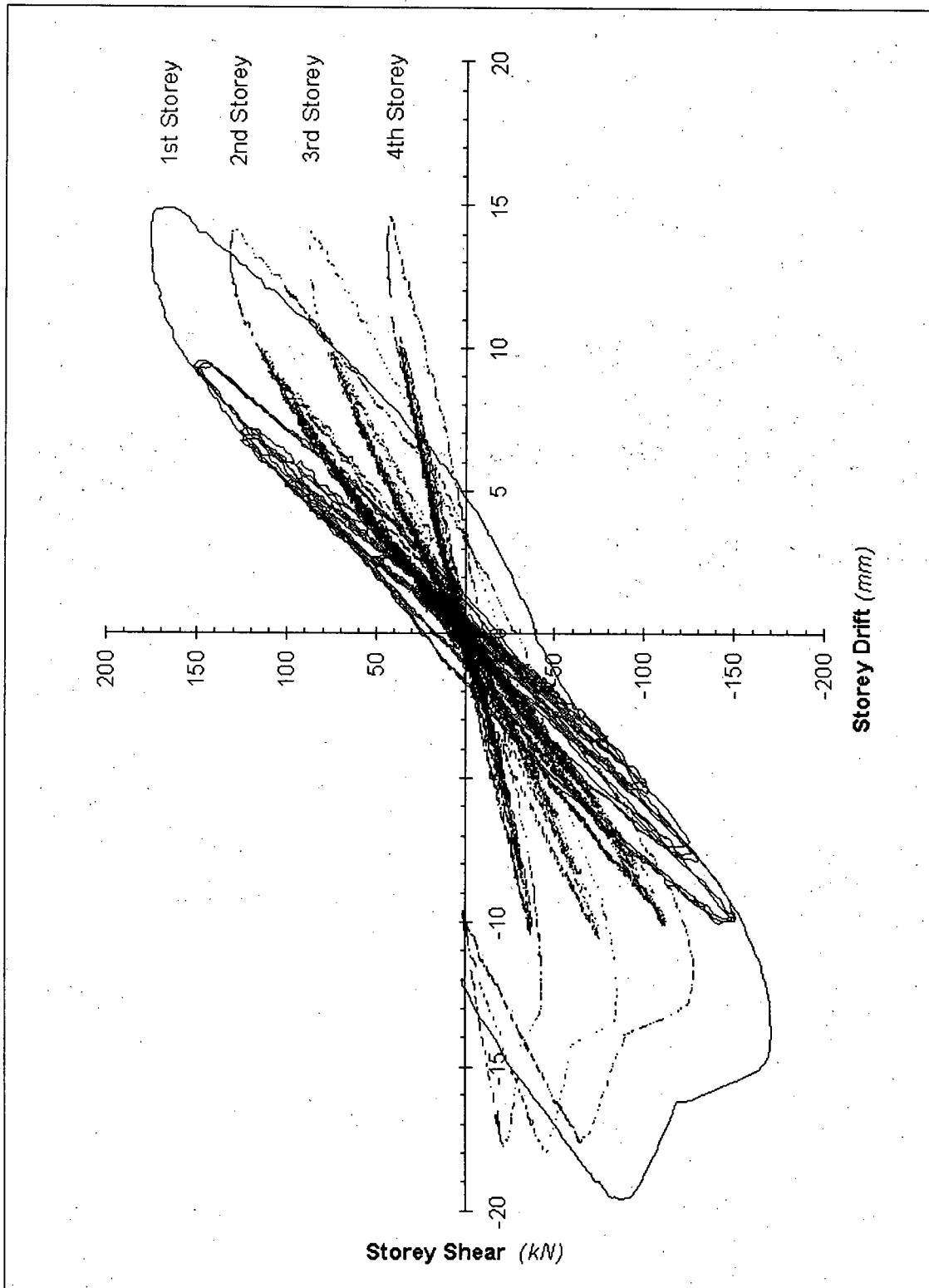


FIGURE 6.4: Storey shear — storey drift relationships for SPSW4

A measure of the relative energy dissipation for each load level under cyclic conditions was obtained by computing the area contained within the storey shear vs. storey drift curves for each storey. Simpson's Rule was used for this operation, with results presented in Table 6.2. As was observed in the single storey specimens, very little energy is dissipated in the low force level "elastic" cycles. When the M load level — the failure cycle — is omitted, 64 % of all energy dissipation occurred during the L load level. From the energy dissipation results, it is also evident that the largest proportion of energy dissipated through hysteretic action occurs in the 1st storey (56 % of the total, omitting cycle M). The second storey accounts for a little under half of this amount. These values reflect the permanent deformations and localized yielding occurring at higher applied load levels, and resultant force locations. They also confirm that the inelastic deformation mode of this multistorey steel plate shear wall can be characterised as a "soft-storey" behaviour.

6.5 Local Column Deformation

During the SPSW4 test, displacement instrumentation was arrayed along the 1st storey column and at each floor level. The data recorded served to quantify localized deformations in the first storey North column, and determine the overall deformed column profile. This helped in assessing the mechanism of column pull-in due to the infill panel tension field that had been observed in the earlier single storey experiments. Figure 6.5 illustrates the North column profile obtained under various base shear conditions in Cycle L1.

TABLE 6.2: Energy dissipation for the SPSW4 specimen

Load Level	Dissipated energy* by storey (kN.m)				TOTAL	%	% Excluding M
	1st	2nd	3rd	4th			
G	0.054	-0.008	-0.006	0.009	0.049	0.4	1.1
H	0.120	-0.004	-0.002	0.016	0.129	1.1	2.8
I	0.250	0.020	0.025	0.032	0.327	2.8	7.0
J	0.120	0.068	0.046	0.047	0.281	2.4	6.0
K	0.392	0.220	0.162	0.112	0.885	7.6	19.1
L	1.680	0.582	0.459	0.253	2.974	25.7	64.0
M	3.157	1.868	1.250	0.656	6.931	59.9	—
TOTAL	5.772	2.745	1.933	1.126	11.577	100.0	100.0
%	49.9	23.7	16.7	9.7			
Excluding M							
TOTAL	2.616	0.877	0.683	0.470			
%	56.3	18.9	14.7	10.1			

* Area bounded by storey shear - storey drift hysteresis curves (kN.m)

It can be observed that the columns are displaced inwards by up to 4 mm from a straight line joining the base and first storey beam-column joints, under an applied base shear of 150 kN (i.e. North column under overturning tension forces). When the applied base shear is reversed and the North column is subjected to overturning compression, a similar trend of the column pulling inwards from the line joining beam-column joints is observed, but to a lesser degree .

6.6 Infill Panel Behaviour

Throughout the course of the load history, up to the column and panel buckling failure, no significant localized damage was detected in any of the infill panels. In fact, until

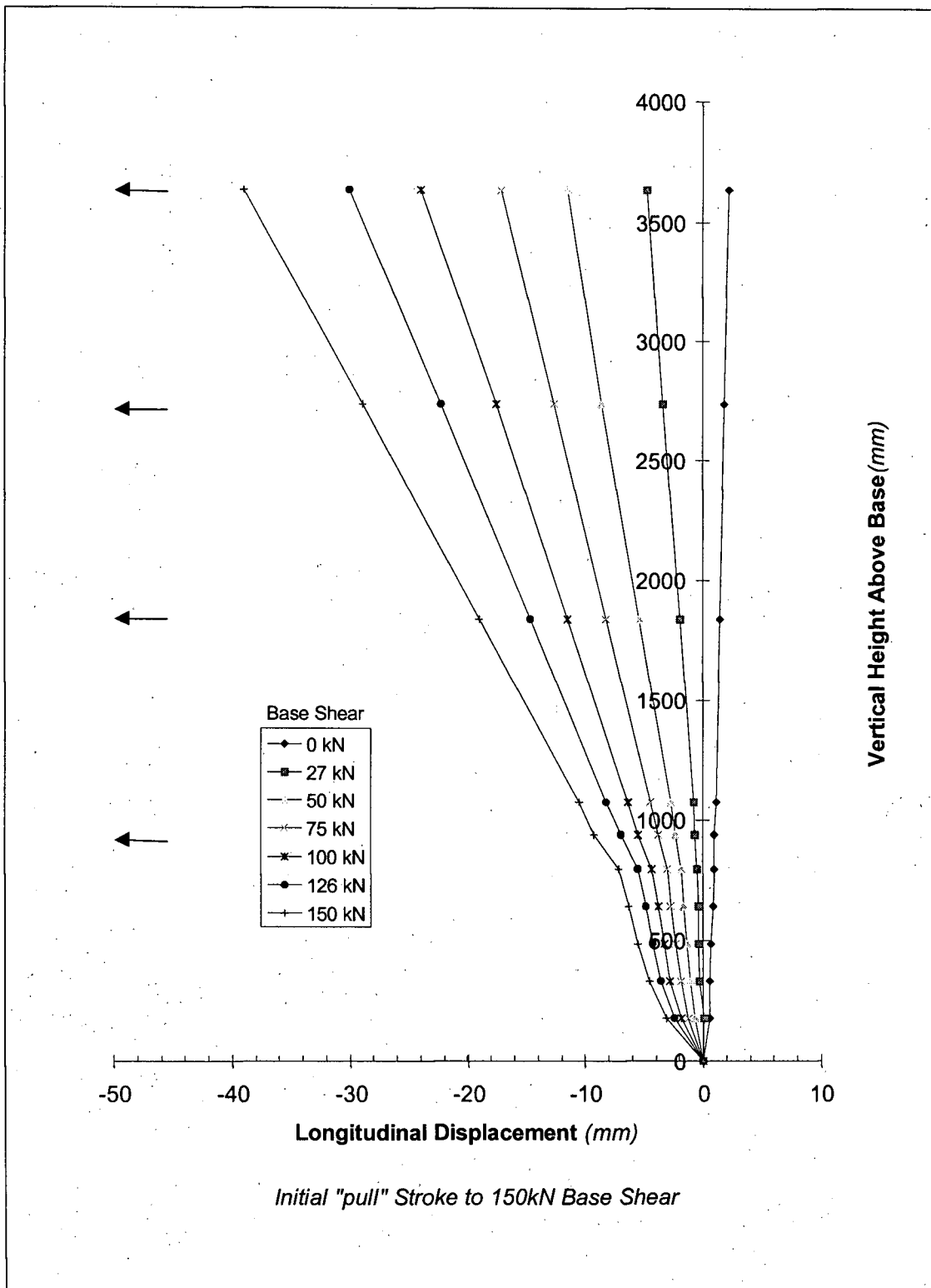


FIGURE 6.5: Displaced North column profile, cycle L1+

load level K, infill panel buckling in the first storey panel was not detectable by casual observation. Even under load level L, the amplitude of the panel buckles remained less than 15 mm. No visible buckling of the other three storey panels was evident. No plate popping sounds were detected due to realignment of the infill plate buckles under load reversal.

6.7 Strain Gauge Analysis

6.7.1 Infill Panel Strain Distribution

The strain rosettes affixed to the first and second storey panels provided data related to the strain distributions across the respective elements. In particular, they allowed for an assessment of the direction and magnitude of principal strains at various locations on the infill panels. A comparison of these values was performed with the predicted angle of inclination of the activated tension field, and the negligible compressive resistance assumption, described in current simplified numerical analysis techniques. Background on these methods is presented in Chapter 7.

The magnitudes of the principal strains were observed to increase with an increase in the applied storey displacement. This is illustrated in Figure 6.6. Figure 6.7 provides a “snapshot” of the principal strain conditions under cycle L1+, at an applied base shear level of 150 kN. It can be observed that most of the principal strain values are less than 50 % of the nominal steel yield strain value. Significant compressive strains can also be

observed in the infill panels, in particular at the beam-column joints undergoing a “closing” type action.

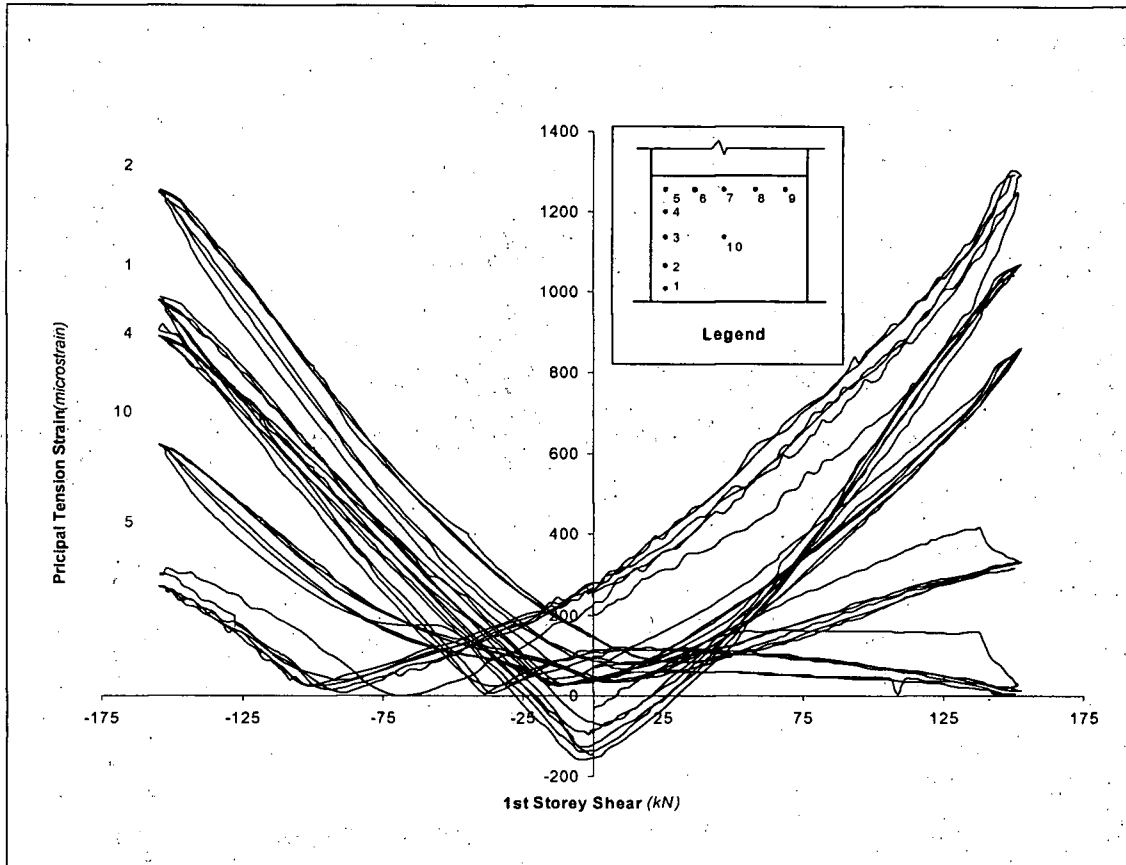


FIGURE 6.6: Magnitude of principle tension strains and applied base shear relationship, cycle L

The principal tension strains occurred at angles of inclination from the vertical of 35 to 40 degrees, for most of the strain rosettes. This is in line with the predicted angle of inclination of approximately 37 degrees, using the tension field strip model suggested in CAN/CSA S16.1-M94 (Canadian Standards Association, 1994). However, an interesting observation is that while the angle of inclination for the rosettes mounted

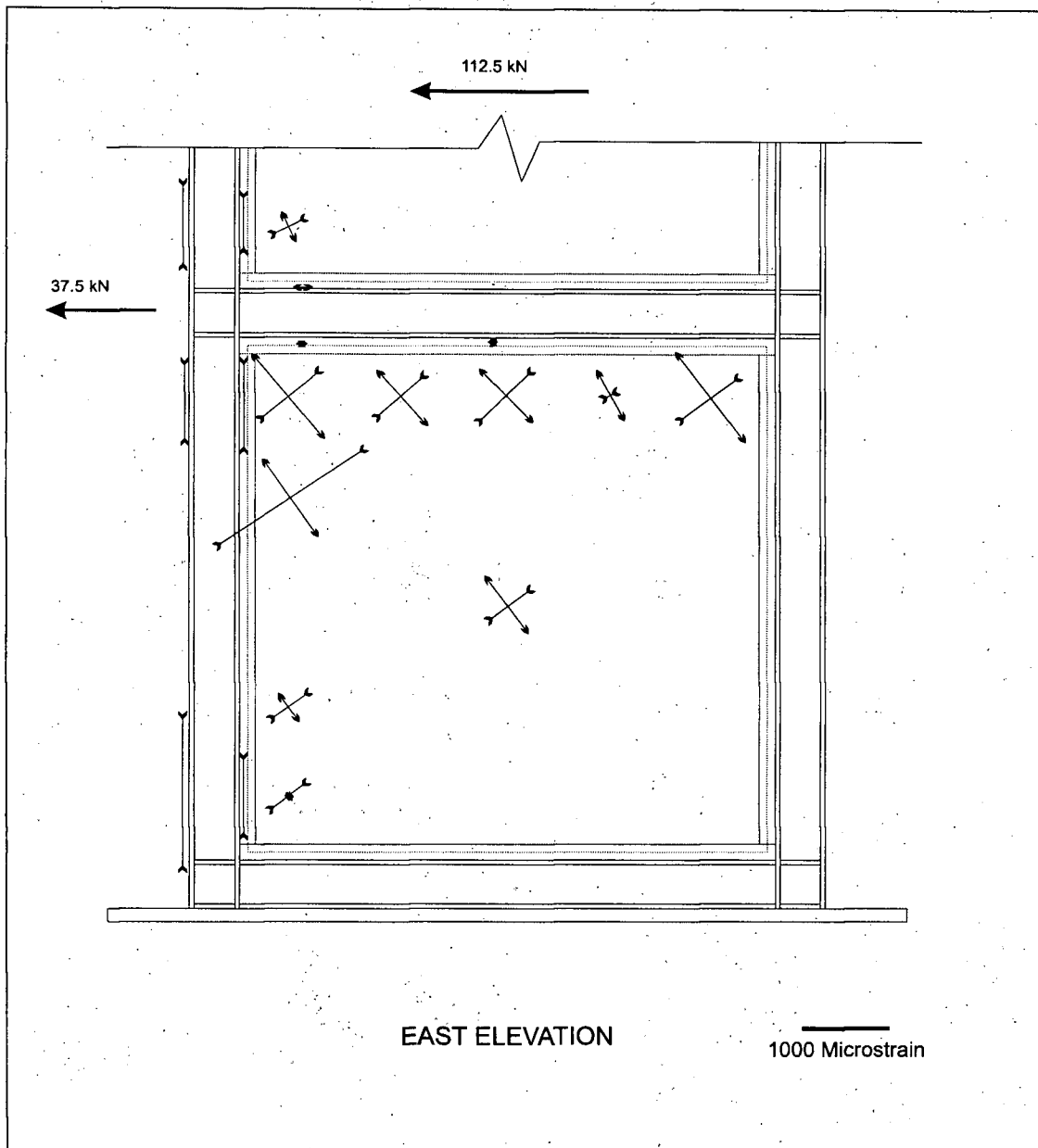


FIGURE 6.7: Schematic of principle strains under 150 kN base shear

near the boundary frame reversed quickly between approximately +37 and -37 degrees, as the specimen passed through a zero displacement position, the rosette mounted at the centre of the 1st storey panel indicated a more gradual change (Figure 6.8). A steeper

angle of inclination (i.e. smaller angle) resulted in a lower proportion of the internal

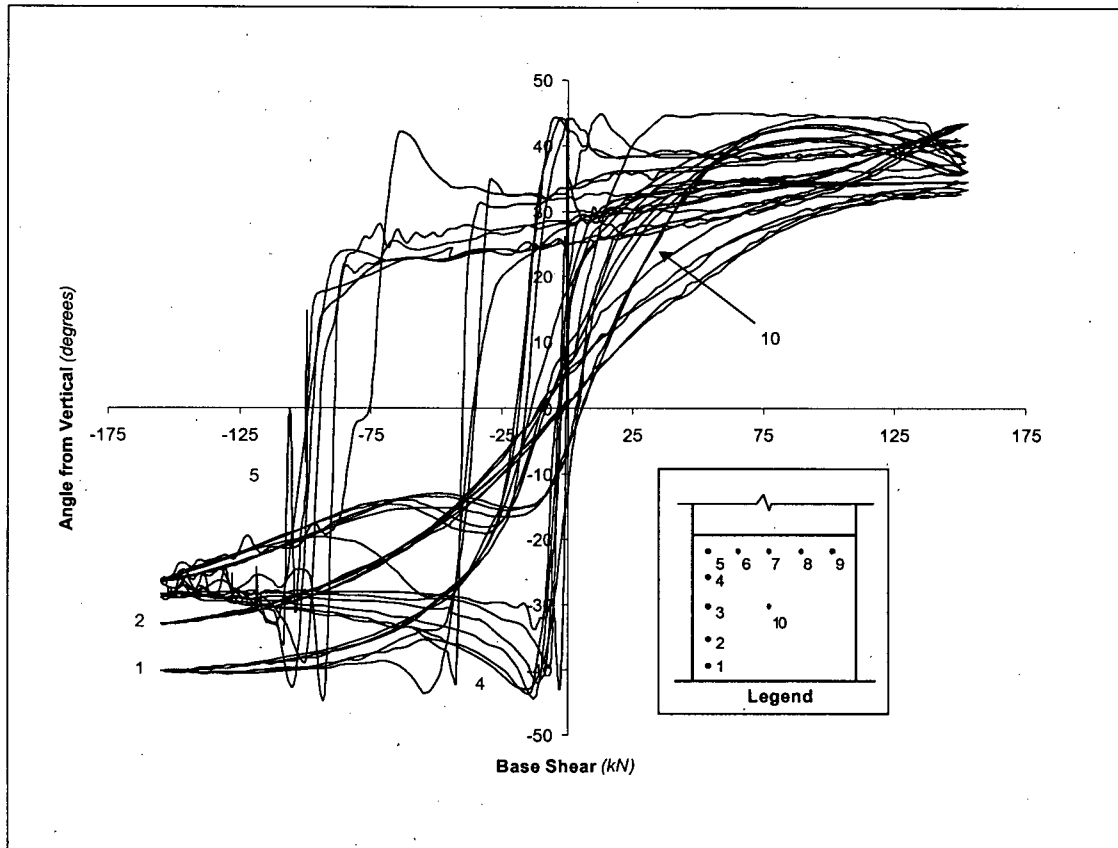


FIGURE 6.8: Angle of inclination—base shear relationship

force generated by the tension field resisting the longitudinal deformation. This behaviour leads to a lower *net* stiffness of the specimen, than is predicted by the numerical models which assume a constant angle of inclination.

6.7.2 Frame Element Strains

An investigation was conducted into the relationship between the base shear applied to the specimen and the resulting strains in the first floor beam. The axial beam strains, given by the average strain over the section, showed a relationship with the base shear

having two distinct regions: under net applied tension; and net applied compression in the actuators (Figure 6.9). For the region when the actuators were retracting (net beam tension), the slope of the axial strain to base shear relationship is lower than for the actuator extension region. This indicates that under actuator retraction — a “pull” mode — a larger proportion of the load path to the actuator is through the infill plate and/or column shear. For actuator extension — a “push” mode — more of the load is transferred away from the actuator through the beam. In both cases, the relative strains at the South location (closer to the actuator) are higher, indicating that there is a distribution of tension field anchorage forces over the length of the beam. Since strain gauges were only installed near the South beam-column joint and the mid-length of the beam, insufficient instrumentation locations were available to further define this relationship. For instance, from the beam strain data available, it is unknown whether the load transfer between the beam and the tension field occurs at a constant or varied relationship over the length of the beam. Some rigid floor action, preventing the 1st floor beam from deforming axially, would be present due to the mass plates. However, while this may have reduced the axial strains produced, the masses were mounted on channels with some flexibility and thus would not alter the underlying axial strain relationship observed.

Evaluation of the bending strains in the 1st floor beam reveal that there is a degree of flexure in this member. Bending strains, defined by the difference in strain between the top and bottom flanges, revealed higher flexure near the columns than at mid span. The

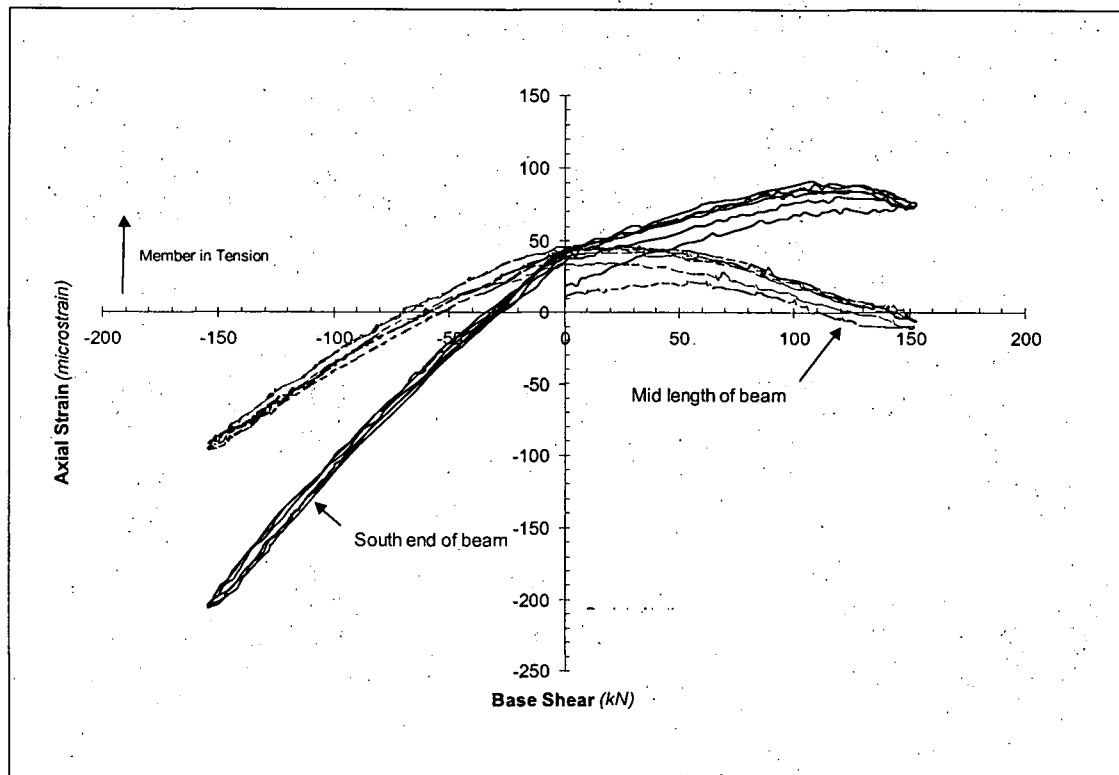


FIGURE 6.9: Axial strains in first floor beam, load level L

results for load level L are presented in Figure 6.10. The magnitude of these strains are very small, suggesting that the flexure generated in the beam is small. This supports the use of a flexurally rigid beam assumption in simplified numerical models, when an internal panel is modelled in isolation.

Strain gauges mounted on the south column provided information on the axial and flexural forces introduced in the column under lateral loads. The axial strain vs. base shear curve, Figure 6.11, indicates that a near linear relationship exists during load level L. This relationship is maintained for load application in both the actuator retract and extend modes. The small difference in axial column strains recorded near the top and

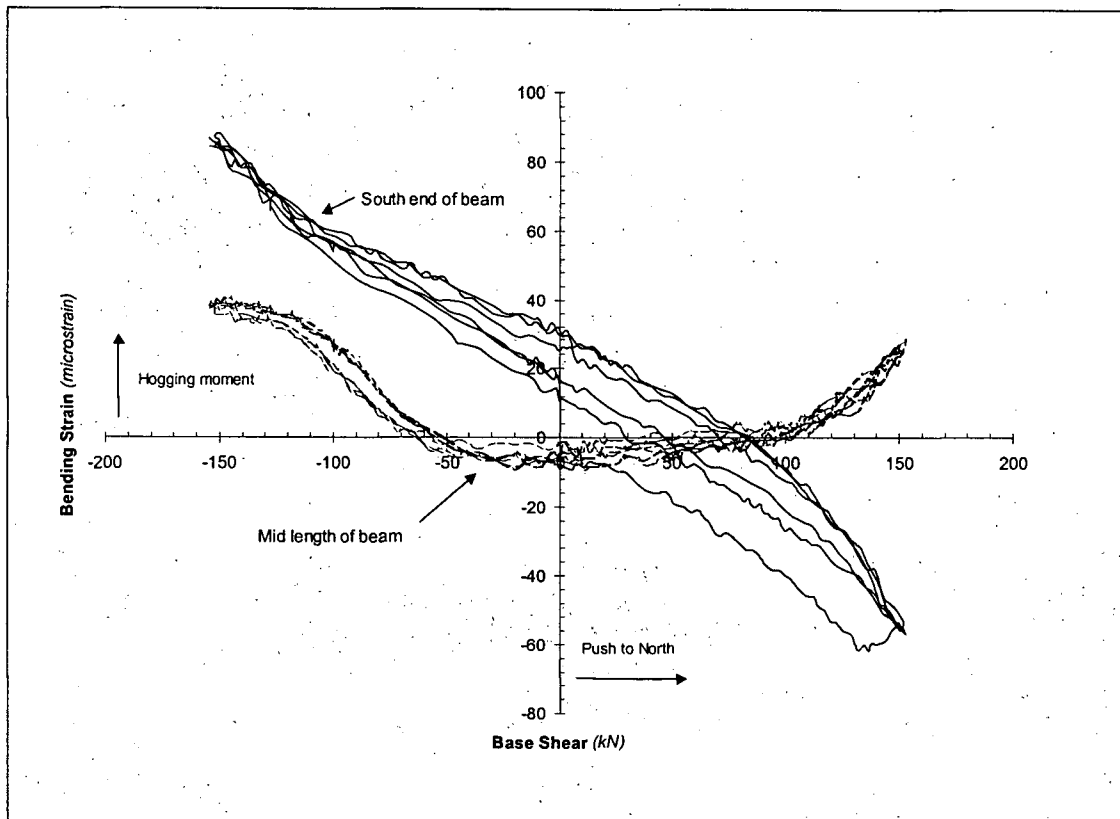


FIGURE 6.10: Bending strains in first floor beam, load level L

bottom flanges of the first floor beam suggest that little load is transferred to the column through beam shear. The larger difference in axial strain between gauges mounted at the top and bottom of the first storey column indicate that the vertical component of the infill panel's in-plane forces are being anchored in the column. Anchorage of both in-plane tension and in-plane compression forces is indicated, since a similar relationship is observed for loading in both directions.

The bending strains measured in the lower portion of the south column also reveal the relationship between the frame action and the applied base shear (Figure 6.12). The

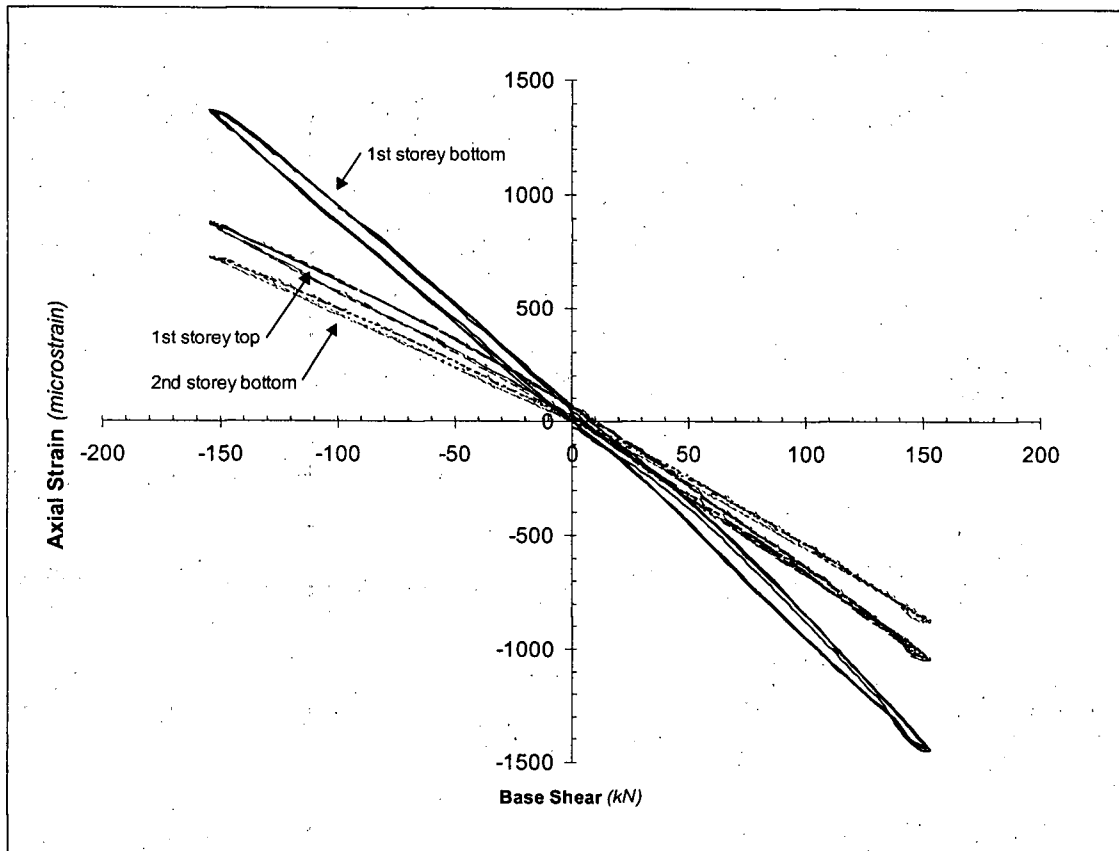


FIGURE 6.11: Axial column strain—base shear curve, load level L

bending strains at the base of the first storey columns indicate substantial column flexure. The enlarged hysteresis loop at the zero base shear location indicates some local yielding present in the column. The instrumentation attached near the 1st floor beam-column joint indicates very little flexural response in the column members at the joint. This compares with that observed in the beam bending strain analysis near this joint, as described above. This suggests that a localized area at the joint remains rigid, in part due to the presence of the infill plate, and potentially does not require the use of a moment resting beam-column connection to achieve similar overall behaviour

characteristics. Further study is required through full scale connection testing and numerical modelling, to validate this hypothesis.

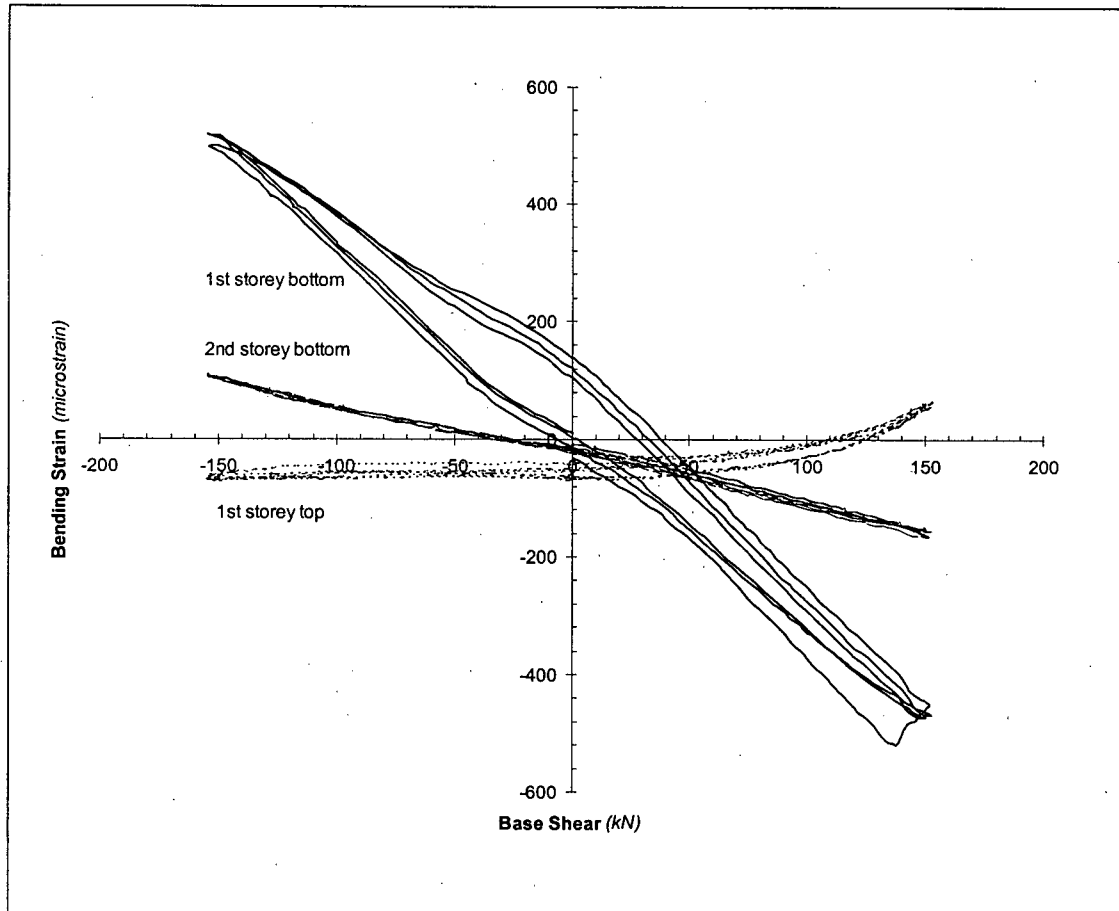


FIGURE 6.12: Column bending strains, load level L

6.8 Vibration Testing

A number of experimental tests were conducted on the SPSW4 specimen to determine its dynamic response. These tests included using impact and ambient excitation techniques. Response of the specimen was recorded using force-balance accelerometers, located at the beam-column joints. The specimen was tested in unbraced, undamaged but braced, and damaged conditions.

By analysing the response of the specimen to various forms of excitation, an attempt was made to capture the relevant steel plate shear wall characteristics. Damage was detected through a shift in the natural frequencies. Results of this experimental work have been presented in Rezai *et al.* (1997), and other publications pending.

6.9 Comparison with Single Storey Results

Overall, the SPSW4 specimen exhibited similar behavioural characteristics as the single storey specimens, prior to global yielding. Linear force-deformation properties were obtained, with similar hysteretic energy dissipation properties.

The most significant differences in performance characteristics from the single storey specimens were the low longitudinal stiffness and yield strength of the 4-storey frame. This is evident in Figure 6.13, showing plots of the storey force-deformation envelopes of the three specimens. It is evident that the longitudinal stiffness of the multistorey frame (SPSW4) is less than that of the single storey specimen with the stiff top beam (SPSW2), and closer to the stiffness of the flexible SPSW1 specimen. This comparison indicates that approximating an internal panel (from SPSW4) simply as one with infinitely rigid beams (like SPSW2), taken in isolation, does not truly reflect the stiffness characteristics of the multistorey specimen. Neglecting the actual net force distribution on the internal panel and considering applied lateral loads only will produce very different results for the panel in isolation case, as compared to the full shear wall frame. In particular, the overturning moment to base shear ratio has a significant effect

on the storey stiffness properties. Strain gauge results, presented in Section 6.7.2, showed that little flexural action is present in the intermediate floor beams, validating the stiff beam approximation for a panel taken in isolation. However, the above results show that an internal panel of a multistorey shear wall frame has different initial elastic stiffness and yield strength properties than a simple isolated panel test would suggest.

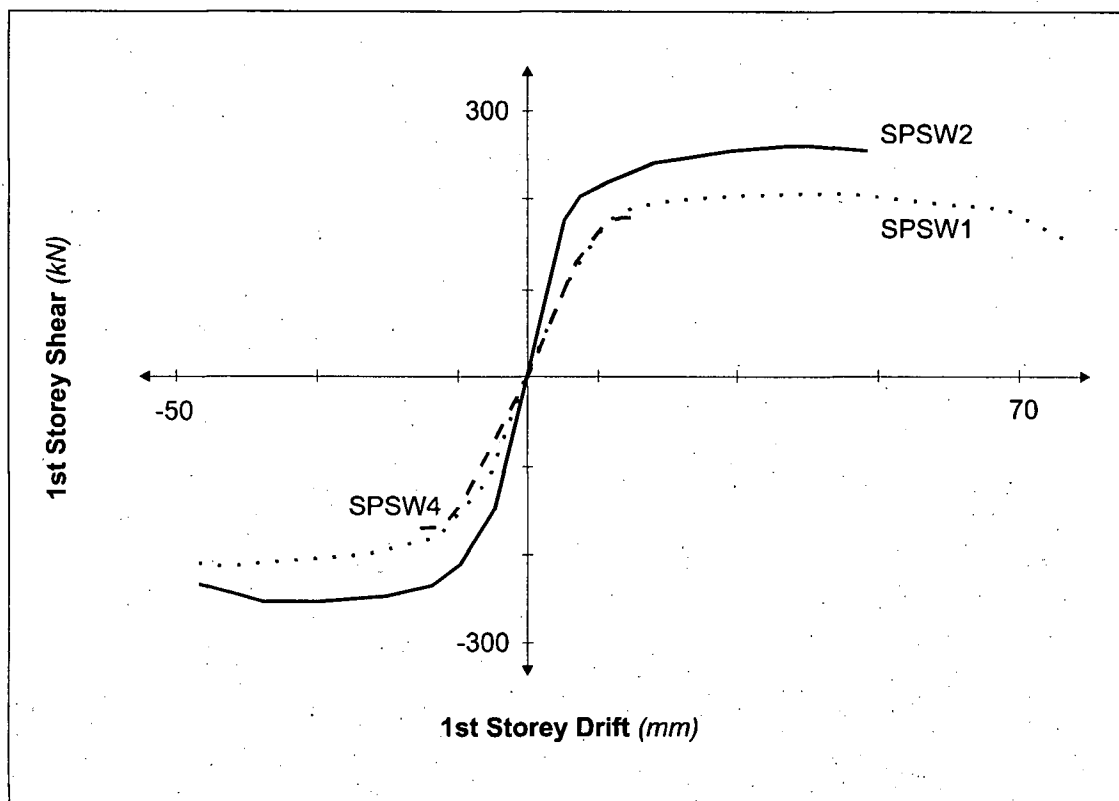


FIGURE 6.13: Comparison of longitudinal load-deformation envelopes

The increased axial forces and moments at the base of the columns in the SPSW4 specimen, resulting from the high overturning moment of the applied load, combine to produce columns with lower effective stiffness. Second order effects amplify the

structure's deformations, particularly in the SPSW4 case which had large vertical gravity loads, resulting in a more flexible structure. The gradual change in the angle of inclination of the infill panels' principal strains, with increasing horizontal load, also creates a lower net effective storey stiffness. It is noted that no instrumentation was provided on the SPSW2 specimen to record the infill panel strains, but results from numerical modelling presented in Chapter 8 suggest that this gradual angle change was not present or not significant for that specimen.

The effect on the post-yield strength of the SPSW4 specimen due to the overturning moment was also significant. Large magnitude axial and moment forces resulted in the columns from the overturning moment generated. The interaction between these forces and those generated due to the tension field action developed through the infill plates caused the column sections to yield at lower base shear levels. Since the infill panel strains were shown to be substantially below their theoretical yield values, the post-yield properties of the specimen were very dependent on the post-yield characteristics of the columns. The strength interaction between axial, moment and shear in the columns is significant. The high overturning moment to base shear ratio in the SPSW4 specimen affected the applied horizontal load level at which structural components, principally the columns, exhibited inelastic behaviour. In contrast, the inelastic action of the SPSW2 specimen was dominated initially by the deformation in the infill panel.

CHAPTER 7

Analytical Modelling of the Test Specimens

7.1 Introduction

Steel plate shear walls with thin, unstiffened plates, are inherently complex redundant systems. While a finite element technique incorporating shell elements is well suited to analysing these systems, the complexity involved exceeds that desired by most designers. Geometric and material nonlinearity parameters are required to accurately model the characteristics of the buckled infill plate, and the behaviour of the yielded boundary frame and infill panels. Simplified analytical techniques have thus been developed by researchers, to describe the performance of steel plate shear walls with analysis tools found in most design offices. Numerical modelling in this research programme was conducted using these simplified techniques, to assess their validity as applied to single and multistorey steel shear wall frames.

Modelling of the force-deformation response envelopes was performed using a tension field strip model, originally presented for unstiffened steel plate shear walls by Thorburn *et al.* (1983). This technique relies on the replacement of the buckled infill plate with pin-ended truss members, to simulate the resistance provided by the activated tension field. The modelling technique is described in Section 7.2. A nonlinear frame analysis program, CANNY-E (Canny Consultants, 1996), was used for these studies. Details of the software and related material models are presented in Section 7.3.

Modelling was conducted for both monotonic and reverse cyclic loading, discussed in Section 7.5 and Section 7.6 respectively. Model specific configurations and parameters studied are discussed therein. Finally, a discussion of computational demands of the numerical models and significant problems or limitations encountered in performing the numerical analysis is provided as Section 7.7.

7.2 Simplified Tension Field Strip Model

A simplified technique for analysing the load-deformation properties of an unstiffened steel plate shear wall has been developed by various researchers. It mathematically represents the tension field developed in a buckled thin plate, by discretizing the resultant force distribution into a series of tension ties. For this representation, all compressive resistance of the infill plate is ignored, since the plate is assumed to buckle immediately under any applied load. Deformation results can be obtained for both the elastic and post-yield responses, by considering the respective material properties of the constituent members. This method has been adopted as part of Appendix M of the latest Canadian design code for steel construction, CAN/CSA S16.1-M94 (Canadian Standards Association, 1994). This form of analysis can be conducted using commercial plane frame analysis software, available in most design offices. Second order effects should be included in the calculations.

Replacing the infill plates for a simplified analysis requires the introduction of pin-ended tension members, with equivalent properties to the tension field developed. Two

main parameters are required for this substitution: the angle of inclination of the tension ties, α , and the cross-sectional area of each tie, A_s .

Thorburn *et al.* (1983) established an expression for the angle of inclination of the strips, using least-work principles. This followed earlier work on tension field theory by Wagner (1929) and Basler (1961). Timler and Kulak (1983), expanded this solution to account for the work performed through column flexure. Their expression is given by the equation (some symbols altered from the original work):

$$\tan^4 \alpha = \frac{\frac{2}{tL} + \frac{1}{A_c}}{\frac{2}{tL} + \frac{2h_s}{A_b L} + \frac{h_s^4}{180I_c L^2}} \quad (7.1)$$

where the variables are as defined in the List of Symbols. A schematic representation of this relationship is provided in Figure 7.1.

The other critical parameter in the tension field strip model is the cross-sectional area for each tie. An appropriate representation is needed, to arrive at a system of equivalent stiffness. The area of each strip, A_s , is determined from the infill plate thickness and the spacing of strips used.

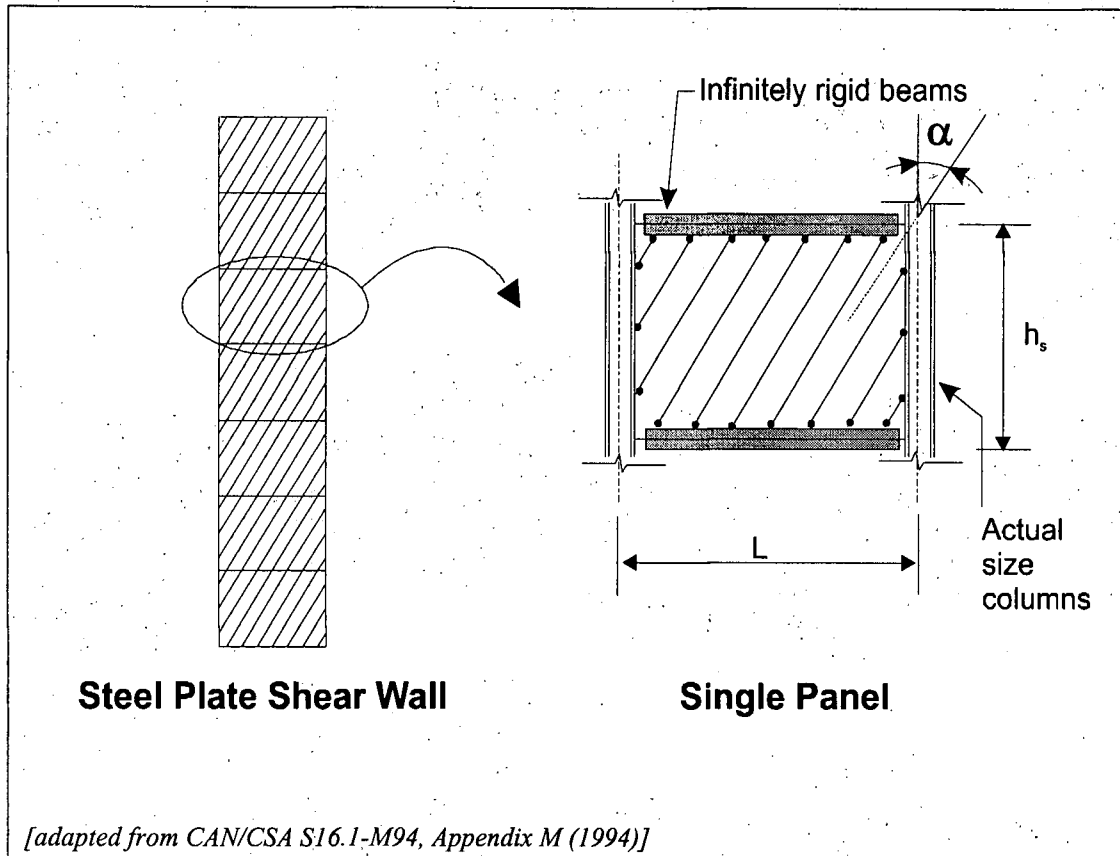


FIGURE 7.1: Schematic used in deriving the tension field strip model

It has been suggested that a minimum of 10 strips be used per panel for this simplified modelling technique (Tromposch and Kulak, 1987; Canadian Standards Association, 1994). However, this guideline is subject to the engineer's judgement. Depending on factors such as the panel aspect ratio, and boundary member stiffnesses, discretizing the plate into too few strips may produce unrealistic results in terms of the moment and shear envelopes for the frame members. Each strip applies concentrated loading where it joins the frame member, so a greater number of strips will come closer to the reality

of a continuous plate with a distributed loading to the frame. Sensitivity studies by Elgaaly *et al.* (1993) indicated that as little as 1 to 3 strips per panel were required in their models, when the infill panel was sized to yield well before the columns. Driver (1997) has reported that little difference is observed in the overall force-deformation characteristics of numerically modelled specimens when more than 10 strips are used. All analysis contained herein was conducted with 15 strips per panel, unless otherwise indicated.

Results from physical testing of symmetric single storey steel plate shear wall specimens by Timler and Kulak (1983) and Tromposch and Kulak (1987), were reported to correlate well with the simplified analysis results. Recently, Driver (1997) reported that good correlation was achieved between the physical testing of a four-storey, 50 % scale steel plate shear wall specimen and numerical predictions of the force-deformation response envelopes developed using this technique. Elgaaly *et al.* (1993), also reported good correlations between physical testing of three-storey specimens and this modelling technique, although elastic stiffness values were often predicted above the experimentally obtained performance.

7.3 CANNY-E Software

The analytical modelling in this study was conducted using a three-dimensional structural analysis computer program called CANNY-E (Canny Consultants, 1996), capable of inelastic nonlinear computation. The software allowed for the introduction

of varied yield parameters for each component, as well as post-yield strain hardening. Multi-spring elements were available to model the interaction between the axial and flexural capacities of the columns. Loading options available in CANNY-E included force control, displacement control, and dynamic time-history records. The October 1996 version of the software and reference documents were used throughout the numerical modelling programme.

By allowing the input of nonlinear material properties, much of the repetitive tasks associated with inelastic analysis were removed from the user. There was no need to manually update the structure properties as members yielded or plastic hinges formed. Driver (1997) provided a good description of the analysis process that would have been required for steel plate shear wall analysis if a typical elastic frame analysis package was to have been used, which could not accommodate material nonlinearity.

7.4 Common Model Parameters

For all numerical modelling of the specimens tested — SPSW1, SPSW2, and SPSW4 — common geometric and material parameters were used. This allowed for direct comparisons between models, and between specimens. Variations to these parameters are indicated where applicable. All numerical modelling included second order P- Δ effects.

The geometric location of each element was established along member centrelines, such as the mid-depth of the columns. The exception to this was for SPSW4, where the top beam was modelled at a height 37 mm below the top flange, to create four storey panels of equal aspect ratio. All members were modelled with theoretical geometric properties, such as the moment of inertia, as obtained from the Handbook for Steel Construction (Canadian Institute of Steel Construction, 1993). The plate thickness was modelled using an approximated average value obtained from coupon testing. These properties are summarized in Table 7.1. Full moment connections were assumed at all beam-column joints, except where indicated. A rigid floor assumption was used at all beam locations, providing in-plane axial stiffness, but not affecting the flexural characteristics. The presence of the fish plate detail, which would create a localized section of thicker infill panel was ignored for the purpose of numerical modelling.

The tension only strip members were modelled using a uniaxial CANNY Sophisticated Bilinear/Trilinear model. This permitted definition of the yield force level, as well as post-yield stiffness parameters. Additional parameters accounted for stiffness degradation, strength degradation and pinching action. A simplified hysteresis model for this type of element is schematically represented in Figure 7.2.

The flexural properties of the beam elements were also modelled using the CANNY Sophisticated Bilinear/Trilinear model, adapted to specify yield moment values. The axial stiffness of the beams was represented using a linear-elastic model. However,

TABLE 7.1: Summary of geometric and material properties

	Nominal Design Value	Actual Value
S 75x8		
A	1070 mm ²	—
I _{xx}	1.04 x 10 ⁶ mm ⁴	—
E	200 GPa	—
σ _y	300 MPa	380 Mpa
σ _u	—	550 Mpa
K _{py}	—	0.0465*K _e
S 200x34		
A	4370 mm ²	—
I _{xx}	27.0 x 10 ⁶ mm ⁴	—
E	200 GPa	—
σ _y	300 MPa	380 MPa
σ _u	—	550 MPa
K _{py}	—	0.0465*K _e
Infill Plate		
t	1.57 mm	1.5 mm
E	200 GPa	—
σ _y	225 MPa	320 MPa
σ _u	—	370 MPa
K _{py}	—	0.0015*K _e

since a rigid floor assumption was implemented at each beam level as noted above, no internal axial beam deformation would result.

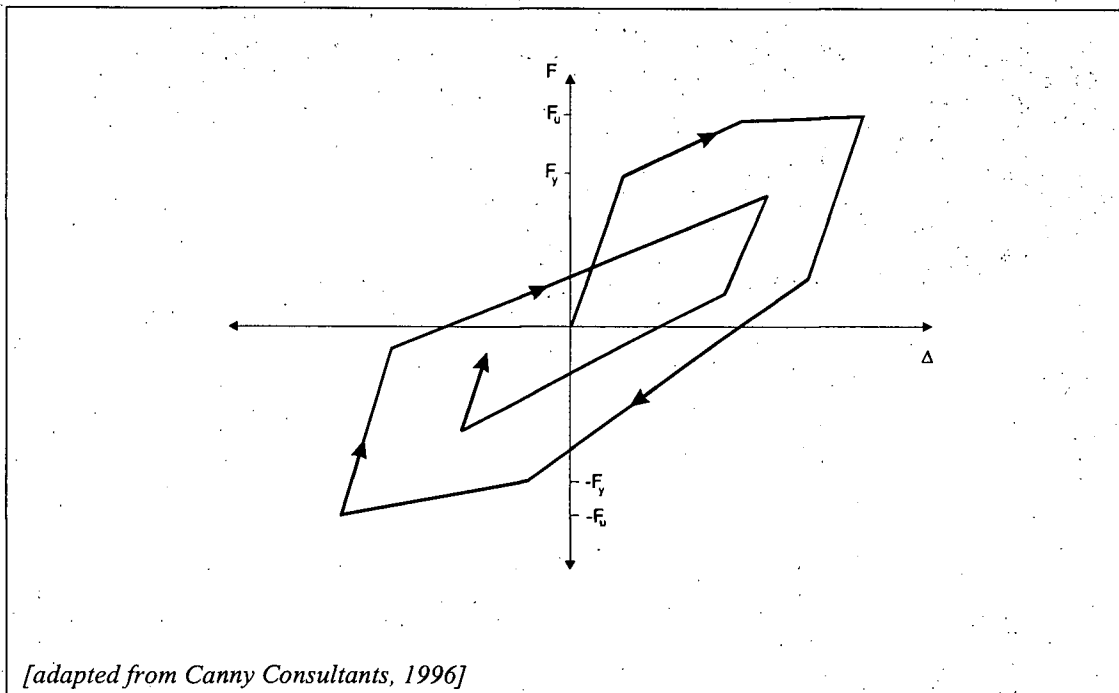


FIGURE 7.2: Hysteresis curve for CANNY Sophisticated Bilinear/Trilinear Model

Column members were modelled using a linear-elastic model for shear. The interaction between the axial and flexural characteristics of the column were represented by using a multi-spring model, consisting of a total of 10 flange steel springs and 10 web steel springs. This model is illustrated in Figure 7.3 and Figure 7.4. A plastic hinge length of 20 % of the column depth was assumed, corresponding to the maximum value the software permitted. Interaction between the column shear, and the axial/flexural multi-spring model could not be implemented with this software.

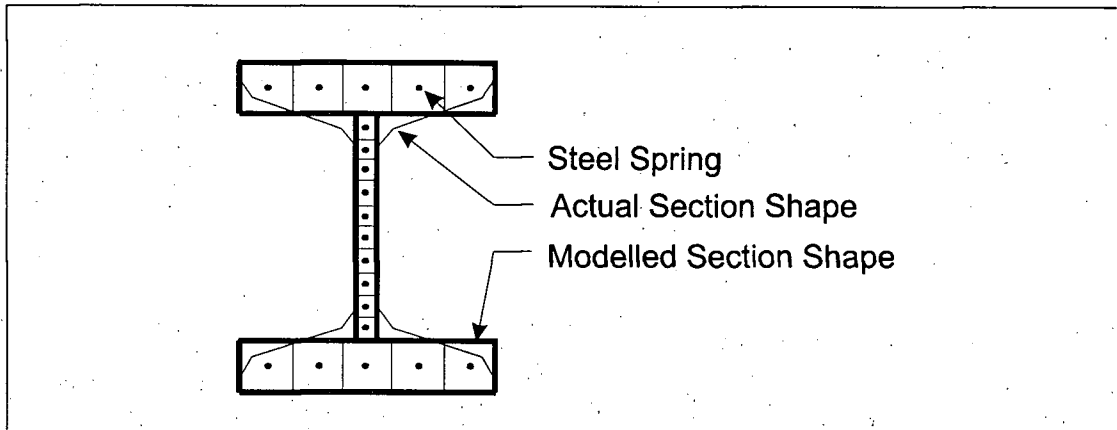


FIGURE 7.3: Multi-spring column model

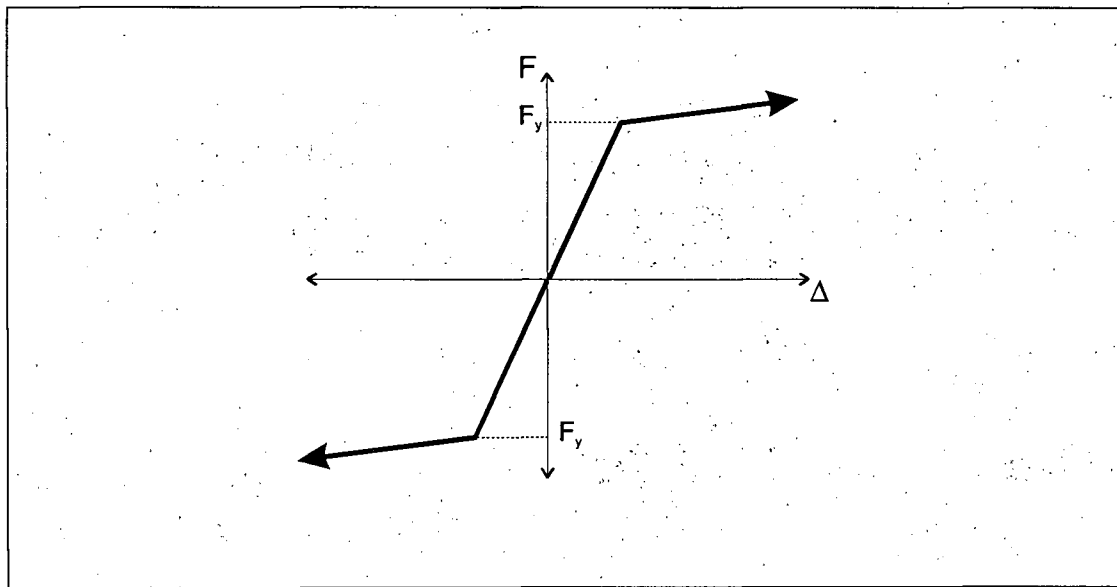


FIGURE 7.4: Column steel spring hysteresis model

7.5 Modelling of Monotonic Loading

Various models were developed to represent each of the three test specimens. Properties were defined, as described above, and appropriate loading introduced to match the test conditions. Schematic representations of the model configurations, for

the single storey and multistorey specimens, are presented in Figure 7.5 and Figure 7.6, respectively.

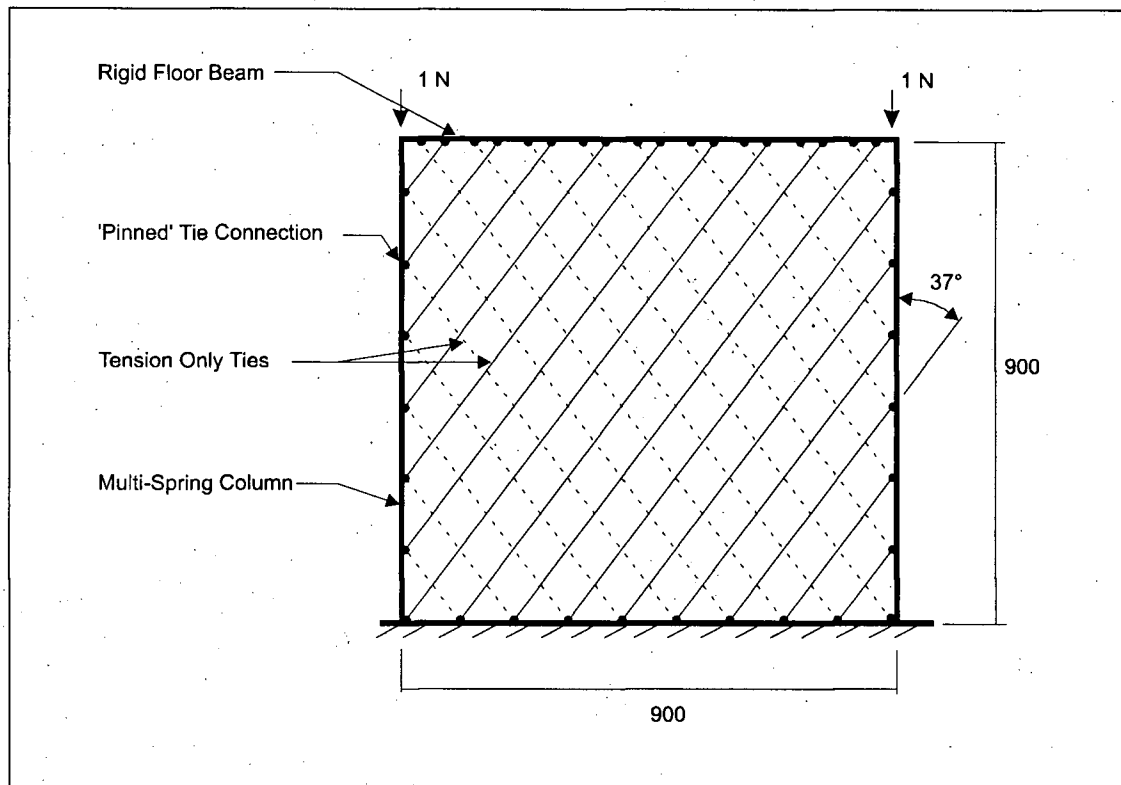


FIGURE 7.5: Schematic for single storey numerical models

Loading of the models was accomplished through force control, at increasing base shear levels. With this loading system, the net base shear was successively scaled at each iteration by a user specified increment. The software utilized the mass incorporated in the model (as a weight term) to distribute the lateral forces. In the case of the single storey specimens, nominal weights of 1 N were applied at each of the top beam-column joints. Weights of 6800 N were applied at each of the beam-column

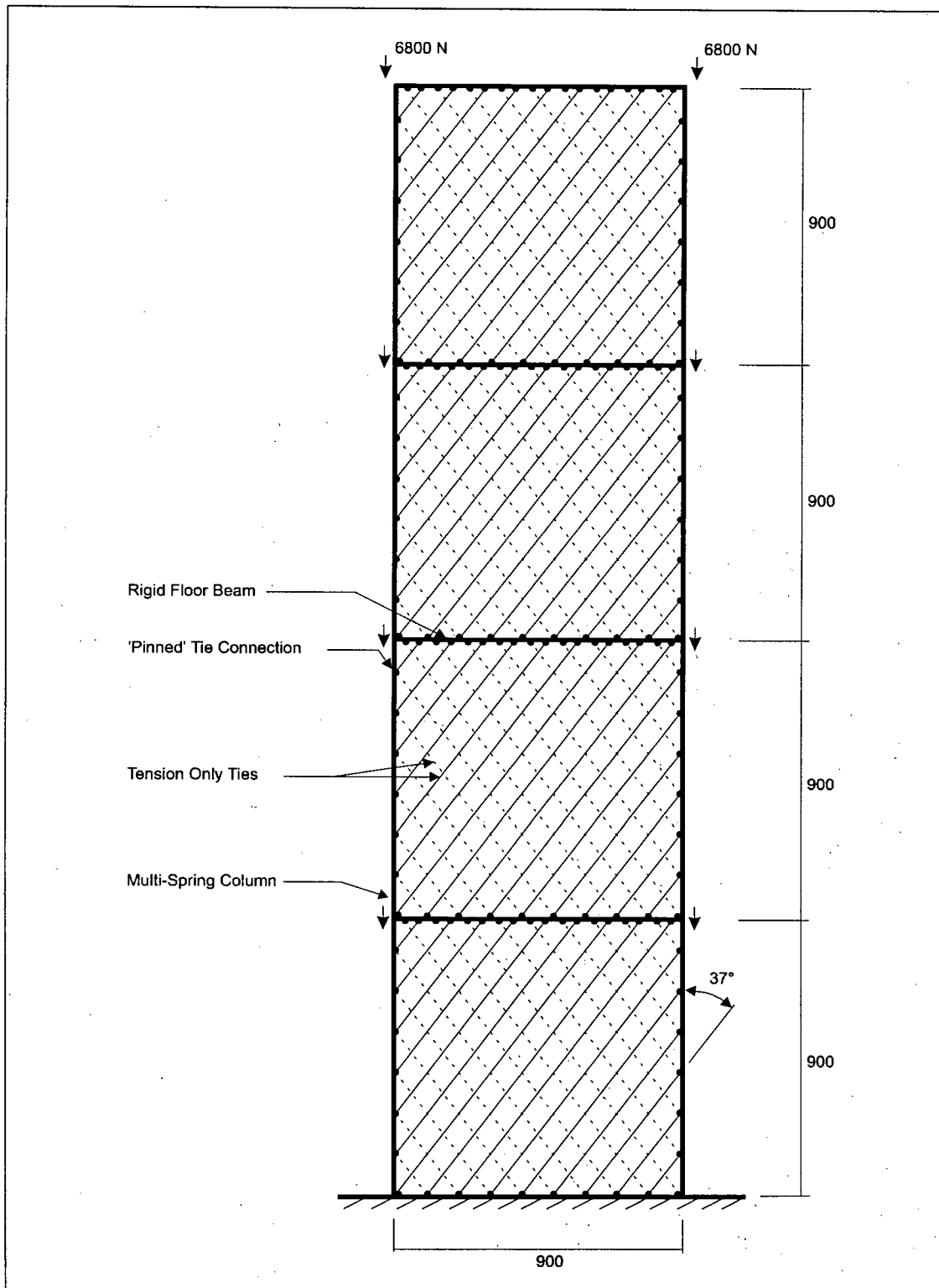


FIGURE 7.6: Schematic for 4 storey numerical models, $\alpha = 37^\circ$

joints for the SPSW4 specimen. The software did not include the self weight of the structure.

7.6 Modelling of Reverse Cyclic Loading

The structural models developed for monotonic pushover loading, as described in Section 7.5, were enhanced to allow for study under reverse cyclic loading. Additional infill panel strips were introduced, oriented at the appropriate angle for loading in the opposite direction. Each strip used in representing the infill steel plates was provided with tension-only characteristics, such that only relevant strips would be activated under a given loading direction. Schematic representations of the model configurations, for the single storey and multistorey specimens, are presented in Figure 7.5 and Figure 7.6, respectively.

Loading control for these models consisted of both force control at base shear multiples, and displacement control. Under the force control loading segment, the base shear acting on the specimen was incremented over successive iterations, in a manner described in Section 7.5. During displacement controlled loading, the target displacement at a control location — the first floor beam — resulting from an increased base shear level was incremented over successive iterations. Loading histories were selected to match those employed during experimental testing, including force controlled loading cycles to the experimental yield force level, followed by displacement controlled loading cycles.

7.7 Discussion of Computational Demands and Limitations

Computation demands of each model varied widely. The requirements of models subjected to monotonic loading were modest in terms of processing time, number of iterations, and the coarseness of the loading increment specified. However, the cyclic models in the post yield region proved to be highly unstable if large load increment values were specified, resulting in long computer runs. This was determined to be caused in part by the low post-yield stiffnesses present, particularly for the SPSW4 specimen, and the iterative solution technique employed by the software.

A summary of significant computational aspects for the models reported in Chapter 8 are provided in Table 7.2. All computation was conducted on an IBM-type personal computer with a Pentium 133 MHz processor, 32 Mb of random access memory and running under the Windows 95 operating system.

In all cases, the nominal section properties and experimentally obtained material strengths described in Table 7.1 were used in the modelling. No attempt was made in any of the models to improve the correlation with the results from physical testing through a manipulation of input parameters. Every effort was made to use standard modelling practices, without unwarranted assumptions or simplifications.

TABLE 7.2: Computational aspects of numerical modelling using CANNY-E software

Model	# of Iterations	Processor Time (seconds)	Binary Output File Size (Mb)
SPSW1 Monotonic	107	2	0.2
SPSW2 Monotonic	144	2	0.2
SPSW2 Cyclic (1 Cycle / Load Level)	8945	94	13.6
SPSW2 Cyclic (3 Cycles / Load Level)	10003	107	15.2
SPSW4 Monotonic ($\alpha = 37$)	1594	162	6.3
SPSW4 Monotonic ($\alpha = 22$)	4105	203	11.7
SPSW4 Cyclic	1747	157	6.9

NOTE:
Actual analysis run time was typically 3 to 10 times the program reported processor time.

Driver (1997) proposed various alterations to the basic tension field strip model. These included using compression struts in the corner to account for the stiffness provided by the locally unbuckled infill panel. Vertical tension strips adjacent to the columns were also proposed, to account for an effective width of the infill panel acting with the column in resisting vertical forces resulting from overturning moments. In both cases, however, these modifications would have resulted in a longitudinally stiffer numerical model. As discussed in the following chapter, the models were already as stiff or stiffer than the results obtained from physical testing. Therefore, these model variations were not implemented for the specimens involved in this study.

CHAPTER 8

Results of Analytical Modelling

8.1 Introduction

The analytical modelling portion of the research programme proved useful in interpreting the performance characteristics observed during the experimental phase. Numerical models, based on simplified tension field techniques, allowed for validation of code recommended analytical procedures relative to the actual performance.

The numerical modelling of the single storey test specimens, SPSW1 and SPSW2, provided mixed results in terms of correlation with the recorded behaviour. This is described in Section 8.2. Models of the SPSW4 specimen, using code recommended techniques, were good at predicting post yield strength levels, but were less accurate at predicting the specimen's stiffness in the elastic response region. This is discussed in Section 8.3. Finally, a number of parametric studies, described in Section 8.4, were conducted to assess some of the sensitivities of the models.

8.2 Single Storey SPSWs

8.2.1 Monotonic Loading of Single Storey Specimens

Numerical models of the single storey test specimens — SPSW1 and SPSW2 — were created, and subjected to monotonic pushover loading. Mixed results were obtained for

the correlation between the monotonic load-deformation curves and the envelopes obtained from quasi-static cyclic testing of the physical specimens.

The SPSW1 numerical model was found to be significantly stiffer than the corresponding experimental results in the elastic region. This is illustrated in Figure 8.1. The yield force level generated was approximately 10 % above that observed from physical testing. These inaccuracies are consistent with the less than exact physical characteristics of the specimen, as compared to the inherent numerical model assumptions.

Since the top beam of the SPSW1 specimen was observed to be quite flexible, deforming under the tension field generated in the infill panel, the actual angle of inclination of the tension field would be altered from that predicted by the model parameters. In fact, as was described in Section 4.2.2, the actual angle of inclination is suspected of changing over the loading history. As shown through the parametric studies discussed in Section 8.4.2, a model with a smaller α value — using struts closer to vertical — would result in a structure with lower longitudinal elastic stiffness.

The initial out of plane deformation of the infill plate for specimen SPSW1 also contributed to the lower than predicted longitudinal elastic stiffness. The plate deformation would allow some longitudinal drift in the frame prior to fully activating the tension field.

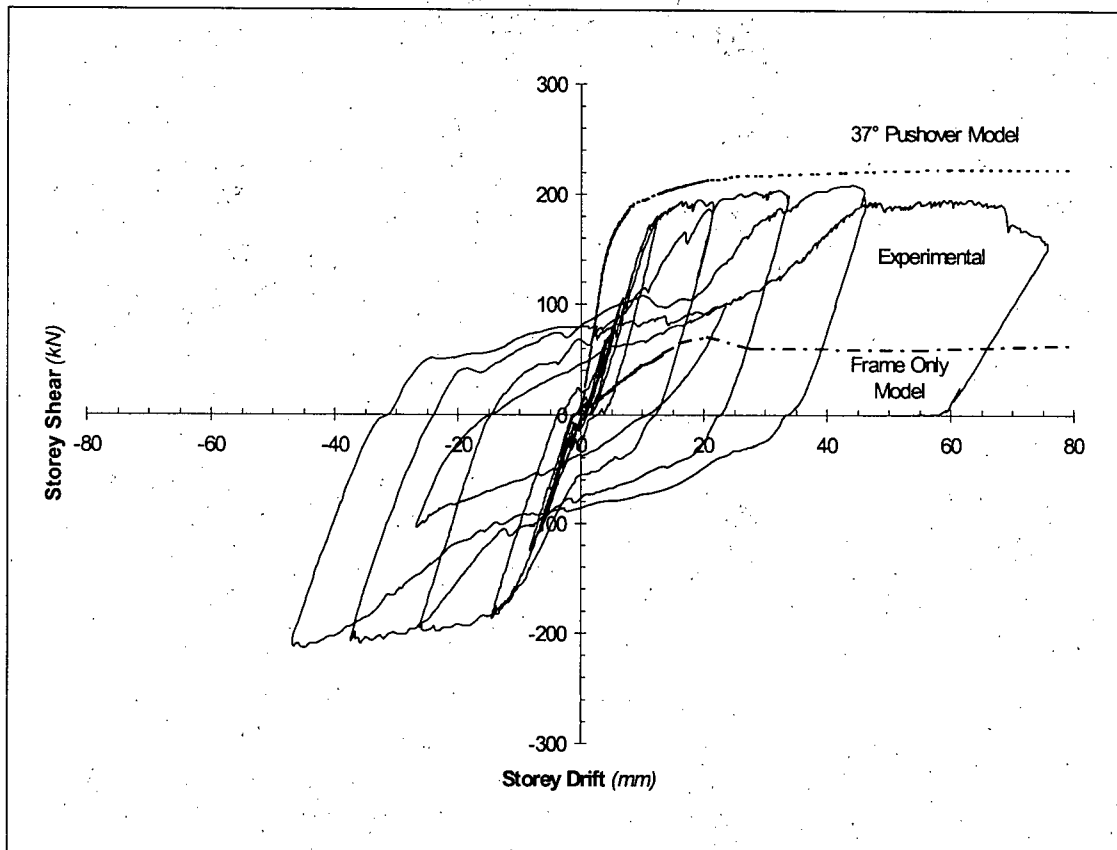


FIGURE 8.1: Monotonic load-deformation curve from numerical modelling of SPSW1

The overprediction of the post-yield strength results in part from the observed plastic deformation in the top flexible beam. The true top beam properties and loading system could not be accurately reflected in the numerical model, where the beam remained elastic and straight in plan. The deformations observed in the experiment would have altered the load paths, with forces redistributed to stiffer less damaged sections. Inaccuracies in the modelled angle of inclination contributed, to some extent, to the overpredicted post-yield strength level. In addition, the incremental damage associated

with cyclic loading in the experiment would result in an envelope below that predicted from monotonic results.

The load-deformation results obtained from the SPSW2 model are presented in Figure 8.2, along with the envelope obtained from testing. A “backbone curve” has also been generated, based on a method suggested by FEMA-273 (Federal Emergency Management Agency, 1996). These results show a good correlation between both the elastic stiffness and the post yield behaviour of the specimen. The pushover envelope closely resembles the backbone curve, apart from the lack of strength degradation, which could not be simulated in the numerical model due to software limitations.

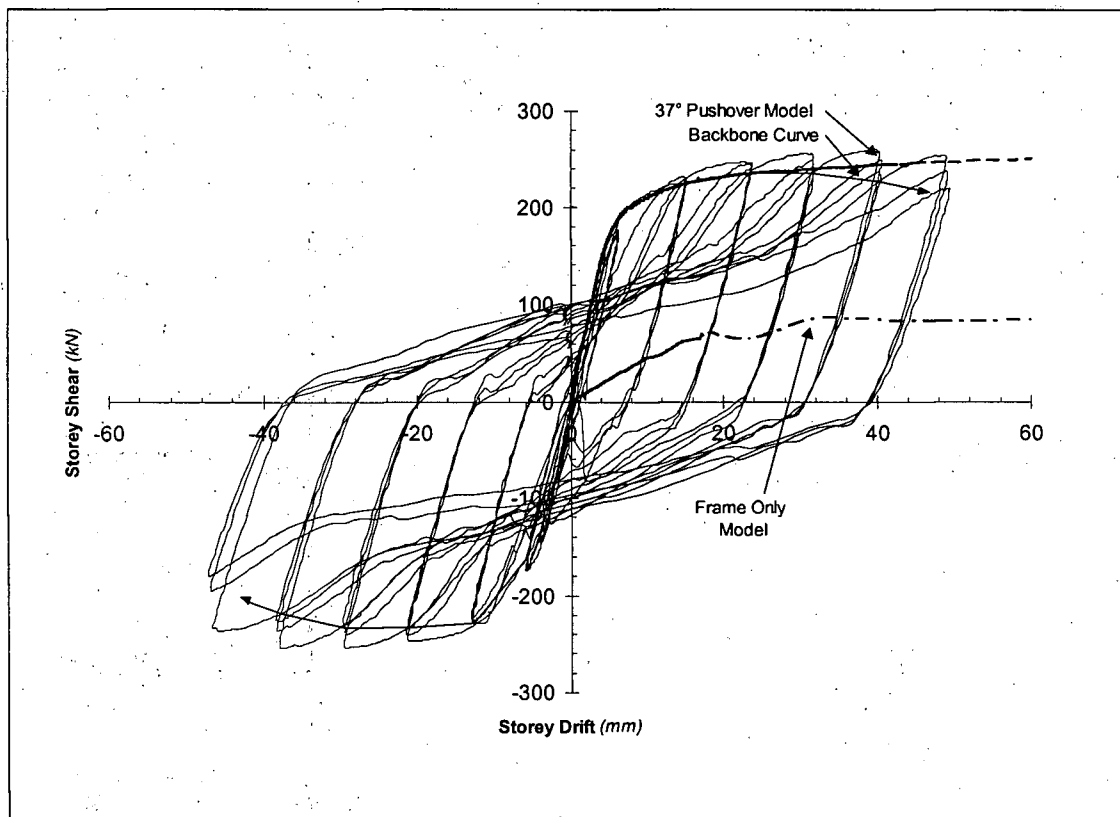


FIGURE 8.2: Monotonic load-deformation curve for numerical modelling of SPSW2

The good correlation between the SPSW2 specimen and model results from the similarity between the specimen design and the inherent model assumptions. A very stiff double top beam prevented any significant beam curvature, thus providing good anchorage for the tension field. The as built infill panel assembly was taut, ensuring adequate initial stiffness in the test specimen.

Numerical models were also generated to allow for comparison between the respective steel plate shear wall properties and the corresponding moment frame with the infill panels removed. These have been included in Figure 8.1 and Figure 8.2 respectively. For the specimen with the flexible top beam (SPSW1), the elastic stiffness numerically calculated for the system with infill plates is nearly 20 times that of the bare frame. The same comparison with the experimental results provides a system 10 times stiffer. The fully plastic response of the model with infill plates occurred at 30 % of the corresponding bare frame displacement. It is noted that the numerical models include strain hardening but no strength degradation at high strains, due to software limitations.

8.2.2 Reverse Cyclic Loading of Single Storey Specimens

From the single storey specimens, only the SPSW2 structure was numerically modelled under cyclic loading conditions. The inaccuracies in the SPSW1 numerical models, from monotonic modelling results, prevented further analytical study of that specimen.

The SPSW2 model was subjected to reverse cyclic loading histories comparable to, but not exactly matching, that of the experimental specimen. All loading magnitudes were based on the experimental specimen, even though the global yield may have occurred at slightly different displacement levels in the numerical model. Each model was loaded to the maximum $6 \times \delta_y$ achieved in the experiments, although the numerical models had not failed at this level. Models generated included using 1 cycle at each load level, and 3 cycles at each load level as was the case in the experiment. These are provided as Figure 8.3 and Figure 8.4 respectively.

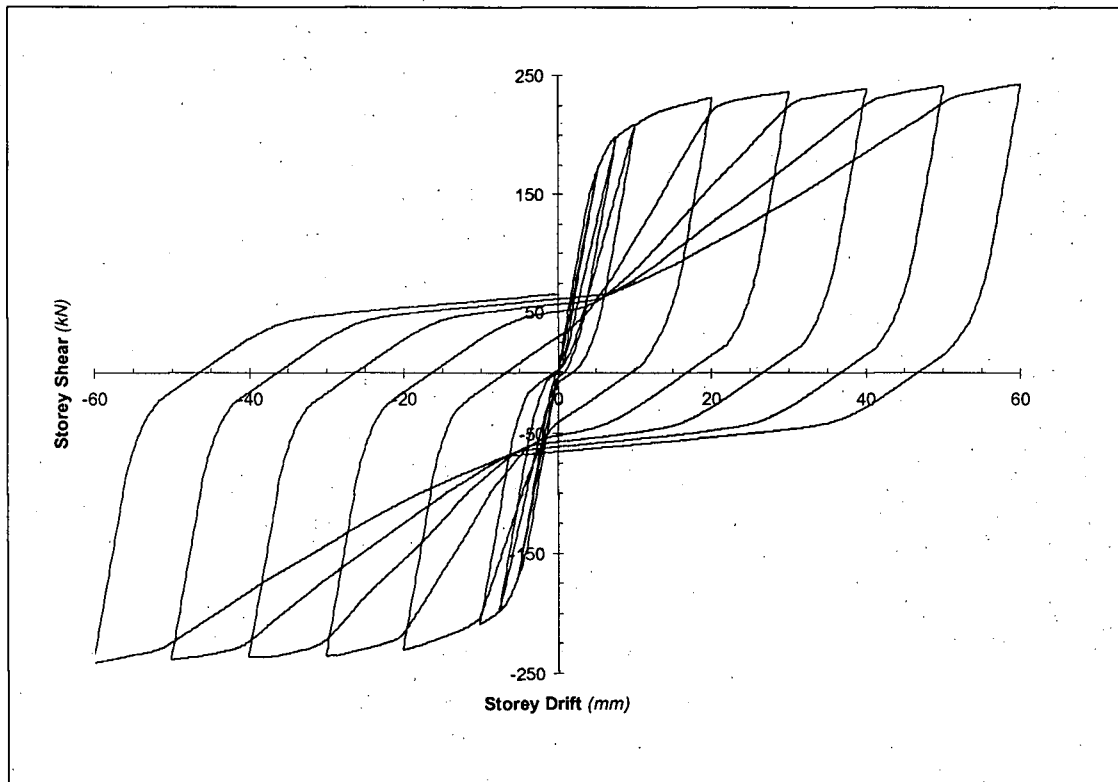


FIGURE 8.3: SPSW2 cyclic model, 1 cycle at each load level

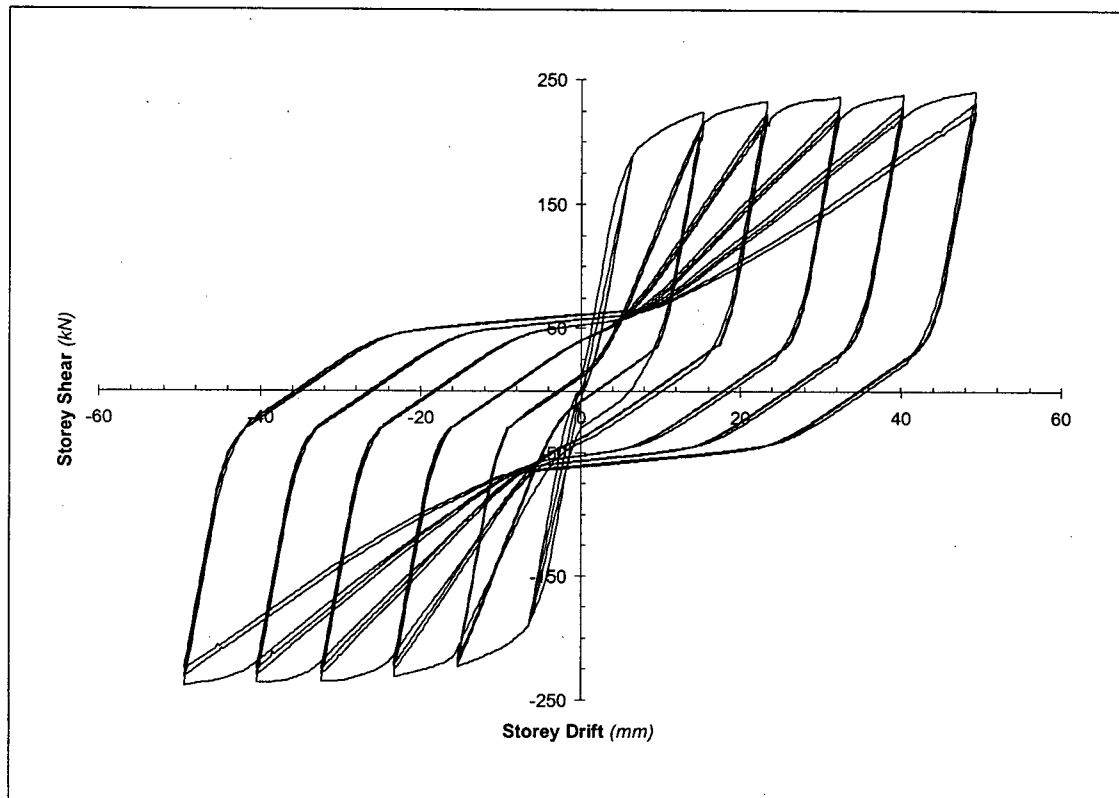


FIGURE 8.4: SPSW2 cyclic model, 3 cycles at each load level

The cyclic models of specimen SPSW2 were able to capture the pinched nature of the force-deformation hysteresis curves. Distinct segments of longitudinal stiffness properties are evident, including the regions of reloading, extreme envelope, unloading, and reorientation of plate forces, as were noted for the experimental results discussed in Section 4.2.1. The cyclic model with multiple cycles at each load level exhibited some strength degradation between successive cycles at the same load level, as was observed for the physical specimen.

While the overall behaviour of the cyclic models matched that of the physical specimen, a number of localized differences were apparent. These differences can

largely be attributed to the numerical modelling simplifications. During the loading region of the force-deformation relationship, a linear stiffness is apparent in the numerical model, unlike the curved relationship from testing. This is related to modelling of the infill plate as discretized struts, which do not consider the geometric nonlinearity of the plate, or the two-dimensional interaction of the in-plane plate forces. In the unloading region, an additional intermediate stiffness region is present in the model, with a slope less than or equal to that from the loading region discussed above. This represents the reduced stiffness caused by inelastic elongation of some of the discrete infill tension struts. After this region, the segment of low stiffness as the model passes through the zero displacement position is much softer than in the physical specimen. Since the model relies on discrete infill struts, some of which have inelastically elongated, the stiffness in this region is governed largely by the resistance of the plastic flexural hinges in the columns, especially for the increasing load levels where more of the infill elements would have yielded in tension. In the physical model, plate buckle reversals occur in this region, but the continuous nature of the infill panel provides redundancy and alternate load paths, to maintain a higher stiffness level.

8.3 Four Storey SPSW

8.3.1 Monotonic Loading

A number of monotonic pushover models were created for the four-storey SPSW4 specimen. No single model was able to accurately describe the stiffness and strength relationships obtained from experimental testing.

The code recommended procedure, employing an angle of inclination calculated with Equation 7.1, produced a load-deformation relationship nearly twice as stiff as the experimental specimen in the elastic region. As a result, the global yield displacement level was approximately one half of the experimental value. However, a good correlation resulted between the post yield strength levels predicted through numerical modelling and the results of physical testing. A comparison between the force-deformation envelope from modelling and the results from physical testing is provided in Figure 8.5.

An additional numerical model was developed using an alternate derivation of the angle of inclination, α , for a system with flexible columns, as presented in Thorburn *et al.* (1983). This derivation for α assumes that a partial tension field is developed, anchored between beams only, and not to the columns. However, tension ties were included in the model over the full infill plate, anchored to the beams and columns as appropriate. The angle of inclination was evaluated to be 22 degrees. The results of this partial tension field model provided a reasonable approximation to the elastic stiffness of the specimen, as shown in Figure 8.5.

In Section 6.7.1, the results from strain gauges affixed to the first storey infill panel were presented. From that discussion, it becomes evident why the two models are good at describing the SPSW4 specimen's force-deformation relationships over the respective elastic and inelastic regions.

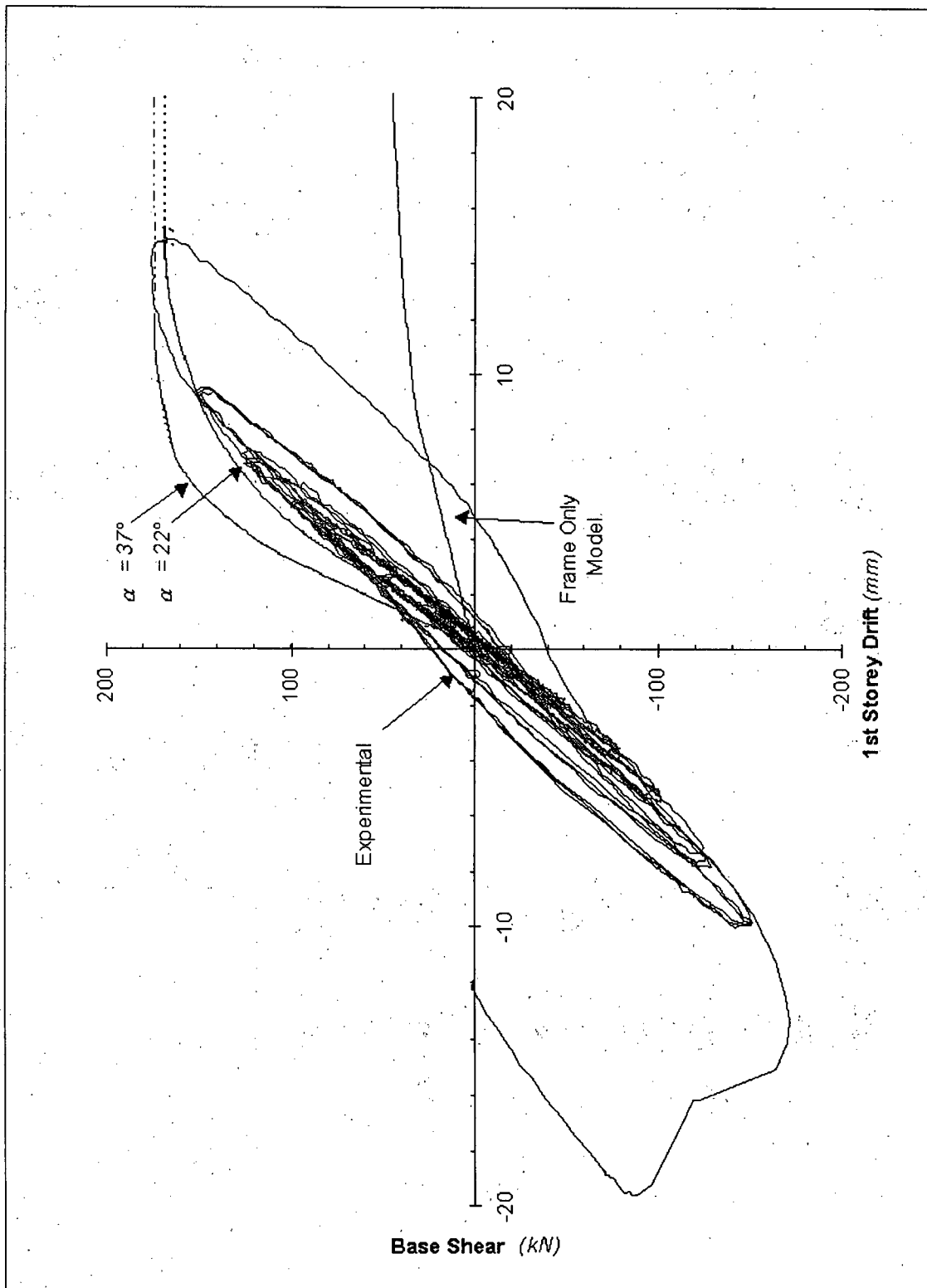


FIGURE 8.5: Monotonic load-deformation curve from numerical modelling of SPSW4

In the initial elastic region, the principal strains at the centre of the first storey infill panel were observed to change gradually between approximately 37 and -37 degrees as the cyclic loading proceeded. This produced a condition of a net effective angle of inclination near to the 22 degrees used in the flexible column model. Figure 8.2 shows that the model slightly overpredicts the stiffness at very low displacements when the angle was less than 22 degrees, and underpredicts the stiffness at higher displacements when the angle was greater than 22 degrees. This confirms the "effective angle" hypothesis.

Near the global yield level, the angle of inclination calculated from physical testing is close to the 37 degrees predicted from the tension field model given by Equation 7.1. Under these larger deformations, the tension field has fully activated, satisfying the assumptions used in deriving the equation to a greater extent. As a result this numerical model provided a good correlation to the post-yield strength.

8.3.2 Reverse Cyclic Loading

A numerical model was generated to investigate its ability to describe the load-deformation characteristics of the SPSW4 specimen. This model relied on the tension field approximation with an angle of inclination of 37 degrees from the vertical, as calculated from Equation 7.1. While it was noted from monotonic loading that this model would prove to be overly stiff in the elastic range, it provided a good correlation with the post-yield level. The intent was to generate a model which could be used to

extrapolate the test results, which ended when the global yield level was reached, into the post-yield region. The cyclic four-storey model could then be compared with the results obtained from the cyclic single storey model, and any significant differences in the performance noted.

The numerical model was subjected to one cycle at each load level, to decrease the computational requirements. In the elastic region, force controlled loading was used to match the load history to that of the physical test. Beyond global yielding, displacement control was used to displacements of 10, 20, and 30 mm. One cycle was used at each load level. No further loading into the inelastic region was conducted, due to computational and storage demands necessitated by the model, detailed previously in Table 7.2. In addition, the actual displacement results generated by the software were significantly larger than the input displacement control levels. Both of these problems were in part compounded by the very low global post-yield stiffness along the load-deformation envelope, which necessitated very small displacement increments for each iteration. This suggested that the solution technique employed by the software was not entirely suitable for this type of model. The load-deformation curve for the 1st storey is presented as Figure 8.6.

The overall cyclic behaviour of the model was similar to that generated for the single storey specimens. However, a few distinct differences were apparent. During the loading region of the hysteresis loop, the slope was more curvilinear. In addition, the

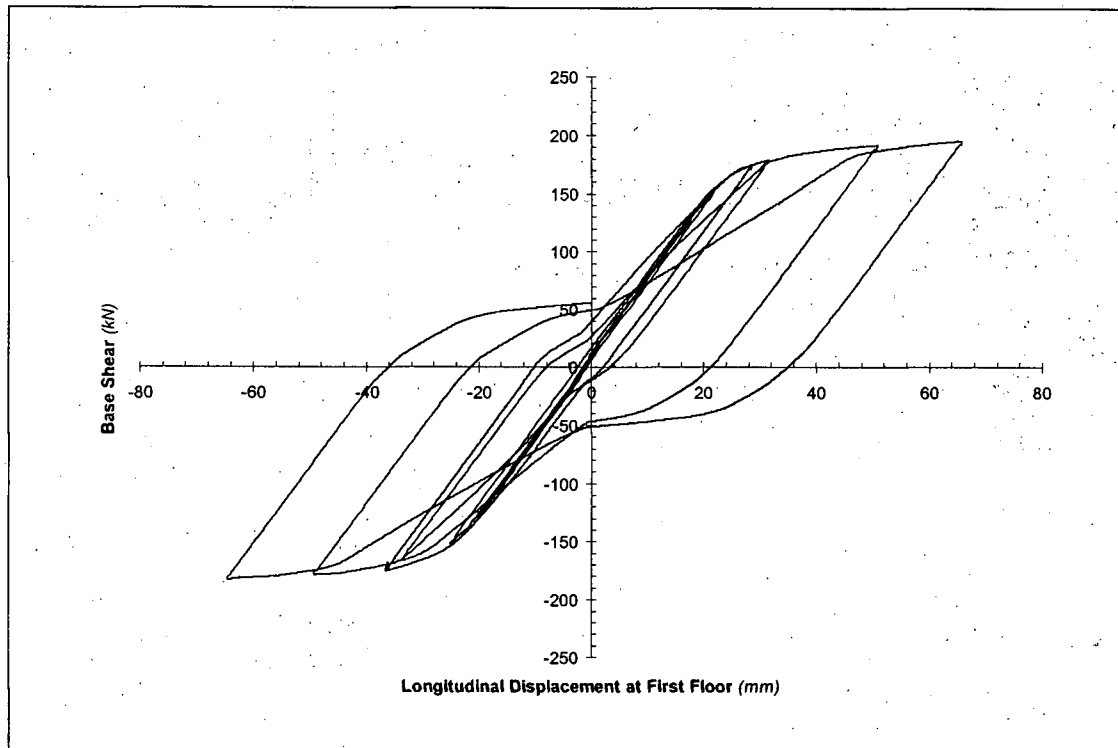


FIGURE 8.6: Cyclic force-deformation curve of the 1st storey, from numerical modelling of SPSW4

unloading segment did not exhibit the additional intermediate stiffness detected in the single storey model. This results from the fact that the multistorey model did not experience infill plate yielding at the same low global displacement levels as the single storey model.

Further testing of a multistorey steel plate shear wall at high displacement ductility multiples needs to be completed to verify this model's predictions. Driver (1997) reported good correlation between a multi storey experimental specimen and a corresponding numerical model using this technique. However, the aspect ratio

selected for the SPSW4 specimen generated proportionately very different column forces than Driver's work, including initial yield in the columns, due to the high overturning moment to base shear ratio and narrow bay width. It remains to be proven whether this modelling technique will accurately predict large deformation behaviour in a steel plate shear wall system in which the columns are allowed to yield well before inelastic deformations are generated in the infill panel.

8.4 Parametric Studies

A number of parametric studies were completed using the above SPSW2 monotonic model, to assess the sensitivity of the reported results to changes in model parameters. This model was selected since it provided the best correlation to its corresponding physical specimen in both the elastic and inelastic regions. The monotonic loading model was used to minimize computational demands. The SPSW2 specimen also provided a system in which both boundary frame and infill panel yielding contributed to the inelastic response of the system, with the infill panel governing the initial yield state.

8.4.1 Thickness of the Infill Plate

Based on the monotonic loading model for specimen SPSW2, a series of numerical modelling was conducted to assess the influence of the infill plate thickness on the calculated performance. The control value was based on the model described in Section 8.2, having an infill plate thickness of 1.5 mm, and strength parameters as

described in Section 6.2. This model was reported in Section 8.2.1 to provide a good correlation with the load-deformation envelope generated from experimental testing.

With all other model parameters remaining constant, the plate thickness was varied in a range from 80% to 120% of the control value. This variation required modifications to the cross-sectional area of each tension field strip, A_s , and an adjustment to the force parameters in the hysteresis models. For example, the yield force of the strip, defined by $\sigma_{ys} \times A_s$, was adjusted accordingly.

The results of this parametric study show that the initial elastic stiffness of the steel plate shear wall is not overly sensitive to the thickness of the infill plate. This is illustrated in Table 8.1. However, it also shows that the post-yield capacity is dependent on the infill plate thickness. The *percentage* of the respective global yield force at which the load-deformation curve diverges from a linear elastic relationship does not appear to be affected. The models suggest that in the elastic range of the shear wall, the infill plate provides sufficient stiffening to the perimeter frame to cause a given load-deformation characteristic. The axial stiffness of the tension strips themselves do not have a significant effect on the overall elastic behaviour. In the post-yield region, some of the strips will yield under large longitudinal frame deformations, thus influencing the overall load-deformation envelope. Parametric studies on a wider panel aspect ratio wall by Anjam (1997) achieved similar sensitivity results.

TABLE 8.1: Sensitivity to infill plate thickness

Plate Thickness (mm)	Plate Thickness (% Nominal)	Elastic Tangent Stiffness (kN/mm)	Global Yield Strength (kN)
1.20	80	34	202
1.35	90	36	214
1.50	100	38	226
1.65	110	39	236
1.80	120	41	246

While a good correlation was achieved using assumed component geometries with actual material strength properties, the consequences of these sensitivities may be significant in some design situations. Since the overall elastic stiffness was not significantly influenced by the plate thickness, steel shear walls designed to operate in this region will not be detrimentally affected by minor fluctuations in thickness or plate strength parameters. However, in structures which rely on a predictable inelastic response, such as those designed with large seismic force reduction factors, the designer will need to exercise an added level of care when predicting the overall structure's performance. Capacity design procedures require that appropriate material overstrength and understrength factors be established for the infill panels, as well as bounding values for the plate thickness. Further study needs to be completed to establish the appropriate design tolerances and specifications required, to allow for an economical use of steel plate shear walls in this type of application.

It is noted that the maximum plate thickness implemented in this parametric study was not thick enough to alter the governing initial yield mode from the infill panel to the columns. It was also thin enough relative to the bay dimensions to be considered a “thin” plate with characteristic buckling properties.

8.4.2 Angle of Inclination

Based on the monotonic loading model for specimen SPSW2, a series of numerical modelling was conducted to assess the influence of the angle of inclination parameter, α , on the calculated performance. The control value was based on the model described in Section 8.2, having an angle of inclination from the vertical of 37 degrees. This model was reported in Section 8.2.1 to provide a good correlation to the load-deformation envelope and backbone curve recorded during experimental testing.

A range of models were constructed by establishing a fixed number of evenly spaced nodes across the top and bottom beams of the frame. Tension field strips were modelled to join these nodes, at various angles in the different models. In combination with altering the angle, the cross-sectional area of each strip, A_s , and associated parameters were adjusted to reflect the new configuration. A different number of infill strips was used for each model, as indicated, in order to achieve uniform strip spacing. The infill plate thickness was maintained at 1.5 mm for all models.

The results, presented in Table 8.2, show that as the angle of inclination α of the infill strips was decreased so that the strips were more vertical, the longitudinal elastic stiffness of the specimen decreased. In addition, as the angle was decreased, the yield strength of the specimen decreased. These two trends occur since the longitudinal properties of the specimens with steeper vertical strips depend more heavily on the contribution of the frame, and less on elongation of the plate in the direction of the tension field. It is noted that these properties are not substantially affected when α is in the 37 degree range suggested by the design code. However, the properties change rapidly at smaller angles.

TABLE 8.2: Sensitivity of longitudinal properties to the angle of inclination

Angle of Inclination α (degrees)	Number of Strips in Model	Number of Strips Joining Beam to Beam	Elastic Tangent Stiffness (kN/mm)	Global Yield Strength (kN)
42	16	2	41	232
38	15	3	38	228
34	14	4	33	222
29	13	5	27	215
24	12	6	20	185

CHAPTER 9

Conclusions and Recommendations

9.1 Summary of Findings

From the results of the physical experimentation and numerical modelling, it is evident that a steel plate shear wall system will provide good energy absorption and displacement ductility capacity. The load-deformation hysteretic behaviour is stable and S-shaped. Higher levels of energy were dissipated under higher magnitude displacement excursions. The majority of energy dissipated in the multistorey specimen was in the first storey, demonstrating the potential “soft storey” nature of this system. Performance characteristics obtained in this study generally resembled those reported by other researchers, including high elastic stiffnesses, and post yield stiffnesses at smaller positive magnitudes. Each specimen studied relied on tension fields activated in the infill panels, with the infill panels significantly increasing the stiffnesses as compared to the equivalent bare frame systems.

9.1.1 System Performance

The governing conditions requiring termination of each of the three experiments were not global system performance related. The SPSW1 specimen had an insufficient external bracing system, and some locally damaged welds. The SPSW2 specimen had a local column failure due to high tensile stresses, with a tension crack developing from a

weld location. The multistorey SPSW4 specimen had an insufficient lateral bracing system which permitted a global column buckling mode once the column had experienced inelastic action. In each case, the overall design of the specimens contributed to these local failure mechanisms. The design of the specimens was influenced by various constraints including availability of materials, maximum specimen dimensions, and the desired global yield strength for a similar specimen to be tested dynamically on a shaking table. However, the global system performance characteristics recorded up to the occurrence of local problems provides sufficient data to establish representative behavioural traits in this range. Maximum displacement ductilities of $7 \times \delta_y$, $6 \times \delta_y$ and $1.5 \times \delta_y$ were attained for the respective specimens. It was shown that the extent of the force-deformation relationship obtained for each specimen up to termination of testing corresponded to a state of inelastic damage while maintaining force resistance. It is noted that past research into the extreme post-yield performance of steel plate shear walls by other researchers has been hindered by similar local problems. In some cases local failures occurred within the expected operational range of a structure. Actual commercial designs incorporating steel plate shear walls must address these local issues.

Inelastic response in the specimens resulted from infill panel yielding (SPSW1, SPSW2), plate tearing (SPSW2), weld fractures (SPSW1, SPSW2) and the formation of plastic hinges in the boundary frame (top beam — SPSW1; bottom of columns — SPSW1, SPSW2, SPSW4; top of columns — SPSW2). Significant shear deformation

was also observed in the columns of SPSW2. Since overall structural stability and performance is affected by column deformation and the axial-shear-moment force interaction, it is recommended that an infill panel failure mode be established in the design as governing the steel plate shear wall response. For this reason, it is also recommended that minimum and maximum strength limits, confirmed through material testing, be established for all infill steel panels.

9.1.2 Overturning Moment to Base Shear Ratio

The influence of the overturning moment to storey shear ratio is significant in the overall behaviour of the system. An increased overturning moment in the multistorey specimen resulted in high axial and flexural column forces and affected the overall stiffness of the specimen. Local variations in the hysteretic behaviour of the first storey panel (from numerical modelling) due to these high forces were noted, as compared to the behaviour of the single storey SPSW2 specimen. The increased axial column forces in the multistorey specimen altered the plastic deformation characteristics of the system by allowing the columns to yield prior to achieving inelastic axial action in the infill panels. An examination of the strain levels in various components confirmed these findings.

9.1.3 Angle of Inclination

The angle of inclination of the principal in-plane strains of the infill plates was stable at the plate perimeter. At the centre of the infill plate, however, the angle of inclination of

the tension field was observed to vary in the multistorey specimen. In-plane strains were not measured at this location in the single storey specimens.

9.1.4 Boundary Frame Response

Strain recordings on the multistorey specimen verified that little flexural action occurred in the first floor interior beam of the steel plate shear wall. Little flexural action was also recorded near a first floor beam-column joint, in both the column and beam elements. This suggested that a localized area around each joint remained stiff, due in part to the full perimeter infill panel attachment, regardless of the degree of beam-column joint fixity.

Significant “pull-in” of the columns, caused by the tension field as it was transferred from the infill plates, was observed in the SPSW2 and SPSW4 specimens. In the SPSW2 specimen, the column inwards deformation resulted in the formation of plastic hinges at the top and bottom of each column. For the multistorey specimen, the global deflected column shape resembled a shear mode for the first storey, and a mode between shear and flexure for the upper stories.

The importance of a flexurally stiff member at the top and bottom of a steel shear wall stack was demonstrated by the poorer performance of the SPSW1 specimen. Insufficient stiffness permitted the formation of a plastic hinge in the horizontal

member, preventing proper anchorage of the tension field. A decrease in out of plane stability, due in part to the plastic hinge, was also reported.

9.1.5 Numerical Modelling

Numerical modelling, using an accepted simplified tension field strip model technique was conducted. In all cases, the numerical models were reasonably accurate at predicting the post-yield strengths and stiffnesses of the respective specimens. However, the elastic stiffness was significantly overpredicted for the SPSW1 and SPSW4 specimens. A better approximation of the elastic stiffness of the multistorey SPSW4 specimen was achieved by using an angle of inclination much steeper than that calculated by verified formulations.

Load-deformation hysteresis characteristics resembling those from physical testing were generated using this simplified tension strip modelling technique, with tension only infill strips oriented in symmetric longitudinal directions. Strength degradation between successive cycles was simulated through the inelastic material models that were implemented.

Parametric studies using the SPSW2 monotonic numerical model, which had a governing inelastic mechanism dominated by the infill panel, showed that the elastic stiffness was insensitive to the thickness of the infill panel. The elastic stiffness was moderately affected by the angle of inclination of the infill strips in the range of 37 to

42 degrees, with a larger effect occurring as the angle was reduced further below this range. The yield strength of the system was significantly affected by the infill panel thickness. The yield strength was also affected by the angle of inclination, but only moderately in the angle range that would typically prevail for geometric dimensions and structural sections used in most building construction.

9.2 Recommendations for Further Study

Through the findings of this research program, a number of additional areas related to steel plate shear wall performance were identified as needing investigation, through further experimental and analytical studies. The additional information generated through the suggested research will aid in refining the established design guidelines, and serve to quantify the effects of some potential interactions and tolerances which have not been considered to date by the research community.

It was noted that in the SPSW1 specimen, a large initial out of plane deformation was present in the infill panel. This may have contributed somewhat to a lower elastic stiffness of the specimen, as well as to the audible noises detected during plate buckle reversals. Additional parametric studies need to be conducted, both numerically and experimentally, to determine the true effect of the plate imperfections. The influence on full scale steel shear wall assemblies is of primary concern. Guidelines as to acceptable tolerances for construction should be developed. Additional potential sources of the

audible plate popping noises, and appropriate methods to eliminate or control these sounds, must be addressed.

Xue and Lu (1994b) developed empirical equations for various behavioural characteristics of steel shear walls in which the infill panels were attached to the girders only. Similar parametric studies should be conducted for infill panels with full perimeter attachment, in order to investigate whether the characteristics of steel shear walls of this type can be generalized in a similar manner. If so, it would appear to be an easier method for designers to use in completing preliminary steel shear wall sizing for a structure than the current tension field strip model or finite element techniques.

All steel shear wall research to date has focused on applying loading, whether vertical or horizontal, at the beam-column connection nodes. Additional research is required to investigate the effect of applying imposed rotations or moments at these locations, to simulate the effect of eccentrically applied loads and external member attachment using partial or full fixity connections. The effect of loading at intermediate column or beam locations should also be studied. The influence of these types of loading on the applicability of the current simplified modelling techniques would be of primary concern. They would also help to establish the feasibility of creating a coupled steel plate shear wall system, when a building's layout would make it impossible to use a single full bay with an adequate aspect ratio.

Current research to date has considered steel plate shear walls to be two-dimensional planar structures, when in reality they are incorporated into three-dimensional buildings. A steel plate shear wall is typically very strong in its plane, but weak in transverse and torsional directions. Experimental and numerical investigations are required to establish the influence of deformations in the transverse or torsional modes on the performance in the primary longitudinal direction. For instance, the introduction of a twist in the steel shear wall due to eccentric loading may serve to alter the stiffness characteristics of the system. Rational guidelines and tolerances need to be developed. The applicability and sensitivity of current simplified modelling techniques are of primary concern.

Most steel plate shear wall research has been focused on panel width to height aspect ratios greater than 1.0. This study utilized specimens with panel aspect ratios of 1.0. Appropriate limiting values for the aspect ratio should be established, under which the behavioural properties established through past and current research efforts can be assumed to apply.

The research needs identified will serve to validate and expand the knowledge base of steel plate shear wall performance. Only through an improved understanding of the behaviour of this system will it begin to receive widespread adoption in the design community.

9.3 Rational Design Guidelines

From the results of this research program, it is recognized that the current design guidelines contained in the Canadian steel design code (Canadian Standards Association, 1994) may be inadequate. While they provide a good starting point for steel plate shear wall design, analytical work by the design community based solely on these guidelines may not reflect the true performance realized from the built structure.

A simplified method is provided in this standard to model the infill panels as discrete tension strips. While good predictions were achieved for the yield strength of each specimen, this research has shown that using this method may result in a significant overprediction of the structure's elastic stiffness under certain conditions. This could have consequences for calculations ranging from drift limitations to determining the fundamental frequencies of the structure for use in seismic design. These recommended modelling techniques must be improved, through extensive parametric studies, with the results validated through large scale experimental testing.

Any guidelines should include the limitations for their use. In the case of these design methods, such restrictions may include limits on the permissible panel aspect ratios, and limits on the relative strengths and stiffnesses of the infill panel and boundary frame members. Additional information must be presented to the designer to allow for the sound application of engineering judgement in the design process.

Any changes to the design guidelines must not obscure the actual failure mechanism and sequence of localized inelastic action. It was recommended in Section 9.2 that Xue and Lu's (1994b) approach to developing empirical design formulae be investigated for full perimeter steel shear walls. However, since that method would potentially hide the yield mechanism from the designer, it is recommended that any approach along those lines be used for preliminary design only.

Significant column deformation can occur due to "pull-in" when the full perimeter of the infill panel is affixed to the boundary frame. There is also a complex combined stress interaction in the columns from axial, shear and flexural forces. Inelastic action in the columns will further weaken the overall structural strength and stability. It is recommended that the design codes *require* that the principal yield mechanism and elastic deformation sequence is through infill panel yielding. Capacity design approaches, including the use of material overstrength factors, should be utilised to guarantee this mechanism. Maximum column deformation limits for elastic and inelastic response should be established.

It has been demonstrated that significant axial and flexural forces generated in the steel plate shear wall columns will affect both the stiffness and yield strength of the structure. For this reason, it is essential that all simultaneously acting forces, including those caused by lateral and vertical loading, be applied to the shear wall during analysis. It is

also noted that the actual load paths and force distribution through a steel plate shear wall make the force decomposition at the shear panel level difficult.

Clause M2.1 of CAN/CSA S16.1-M94 (Canadian Standards Association, 1994) states that:

"The design forces and moments for the members and connections for a shear wall may be determined by analyzing the wall, a panel at a time, using a plane frame computer program provided that:

(a) pin-ended connections are used to attach the end of beams to columns; and

(b) the magnitudes of vertical components of the tension fields do not vary by more than 25 percent between adjacent stories."

It is recommended that this clause be removed, and replaced with a clause requiring that all steel plate shear walls be analysed in their entirety under all conditions. The current single panel approach is applicable to preliminary sizing only.

In addition, it is recognized that steel plate shear walls in their present suggested implementation, with full perimeter infill panel attachment, may result in a "soft-storey" type of structure under inelastic conditions. Significant redundancy is provided, but only through alternate load paths in the element (i.e. the infill panel) which has already experienced inelastic action. Inelastic action in the columns will introduce additional strength and stability issues into the design process. Therefore, it is

recommended that extreme inelastic response of the columns should not be considered when assessing the displacement ductility capacity of a steel plate shear wall system.

The current design guidelines provide a good starting point for the engineering community to use in designing steel plate shear walls for steel building construction. Analytical and experimental testing confirms, to some degree, the theoretical basis under which the guidelines were established. However, the results of this study revealed several areas for concern. These need to be addressed, modified and documented so that all limitations associated with the suggested analytical design approach are presented to the designer. With further improvements to the codified design requirements, steel plate shear walls show good promise as lateral load resisting systems for structures, including those in areas of high seismic risk.

REFERENCES

1. Anjam, R., 1997. *Steel plate shear wall design study*. University of British Columbia, Vancouver, BC.
2. Anon., 1989. *An eight-storey steel frame in 15 weeks; design incomplete at tender stage*. Steel Construction (South African Institute of Steel Construction), 13(5): 5.
3. Applied Technology Council, 1992. *ATC-24: Guidelines for cyclic seismic testing of components of steel structures*. Redwood City, CA.
4. ASTM, 1994. *E 8M-94a, Standard test methods for tension testing of metallic materials [metric]*. Vol. 03.01, American Society for Testing and Materials, Philadelphia, PA.
5. Basler, K., 1961. Strength of plate girders in shear. ASCE Journal of the Structural Division, 87(ST7):151-180.
6. Caccese, V., Elgaaly, M. and Chen, R., 1993. *Experimental study of thin steel-plate shear walls under cyclic load*. ASCE Journal of Structural Engineering, 119(2), pp. 573-587.
7. Caccese, V., Elgaaly, M. and Chen, R., 1994. *Closure to the discussion of experimental study of thin steel-plate shear walls under cyclic load*. ASCE Journal of Structural Engineering, 87(ST7).
8. Canadian Standards Association, 1994. *CAN/CSA-S16.1-M94, Limit states design of steel structures*. Rexdale, ON.
9. Canadian Institute of Steel Construction, 1993. *Handbook of steel construction, fifth edition*. Willowdale, ON.
10. Canny Consultants Pte. Ltd., 1996. *CANNY-E Users' manual, Win-95 version (October)*. Singapore.
11. Derecho, A.T., Iqbal, M., Fintel, M., and Corley, W.G. 1980. *Loading history for use in quasi-static simulated earthquake loading tests*. ACI Publication SP63, Reinforced Concrete Structures Subjected to Wind and Earthquake Forces. American Concrete Institute, pp. 329-356.
12. Driver, R.G., 1997. *Seismic behaviour of steel plate shear walls*. Ph.D. Dissertation, Department of Civil and Environmental Engineering, University of Alberta, Edmonton, AB.
13. Elgaaly, M., Caccese, V., and Du, C., 1993. *Postbuckling behaviour of steel-plate shear walls under cyclic loads*. ASCE Journal of Structural Engineering, 119(2).

14. Elgaaly, M., Caccese, V., and Du, C., 1994. *Closure to discussion of postbuckling behaviour of steel-plate shear walls under cyclic loads*. ASCE Journal of Structural Engineering, 120(7).
15. Federal Emergency Management Agency, 1996. *FEMA-273: Guidelines for seismic rehabilitation of buildings*. Washington, DC.
16. Kennedy, D.J.L., Kulak, G.L. and Driver, R.G., 1994. *Discussion of Postbuckling behaviour of Steel-Plate Shear Walls Under Cyclic Loads by Elgaaly, M., Caccese, V., and Du, C.* ASCE Journal of Structural Engineering, 120(7), pp. 2250-2251.
17. Kulak, G.L., Kennedy, D.J.L. and Driver, R., 1994. *Discussion of Experimental Study of Thin Steel-Plate Shear Walls Under Cyclic Load by Caccese, V., Elgaaly, M. and Chen, R.* ASCE Journal of Structural Engineering, 120(10).
18. National Research Council of Canada, 1995. *National Building Code of Canada*. Ottawa, ON.
19. Popov, E.P., 1990. *Engineering Mechanics of Solids*. Prentice Hall, Englewood Cliffs, New Jersey.
20. Rezaei, M., 1997. *Seismic behaviour of steel plate shear walls by shake table testing*. Ph.D. Dissertation to be submitted to the Department of Civil Engineering, University of British Columbia.
21. Rezaei, M., Ventura, C.E., Prion, H.G.L. and Lubell, A.S, 1997. *Dynamic properties of steel plate shear wall frame by impact testing*. Proceedings of XV International Modal Analysis Conference, Orlando, FL.
22. Roberts, T.M. and Sabouri-Ghomi, S. 1991. *Hysteretic characteristics of unstiffened plate shear panels*. Thin Walled Structures, 12: 145-162.
23. Roberts, T.M. and Sabouri-Ghomi, S. 1992. *Hysteretic characteristics of unstiffened perforated steel plate shear panels*. Thin Walled Structures, 14: 139-151.
24. Sabouri-Ghomi, S. and Roberts, T.M, 1992. *Nonlinear dynamic analysis of steel plate shear walls including shear and bending deformations*. Engineering Structures, 14(5): 309-317.
25. Sugii, K. and Yamada, M., 1996. *Steel panel shear walls, with and without concrete covering*. Paper Number 403, Proceedings of 11th World Conference on Earthquake Engineering, Mexico.
26. Thorburn, L.J., Kulak, G.L., and Montgomery, C.J. 1983. *Analysis of steel plate shear walls*. Structural Engineering Report No. 107, Department of Civil Engineering, University of Alberta, Edmonton, AB.
27. Timler, P.A. and Kulak, G.L. 1983. *Experimental study of steel plate shear walls*. Structural Engineering Report No. 114, Department of Civil Engineering, University of Alberta, Edmonton, AB.

28. Timler, P., Ventura, C.E., Prion, H. and Anjam, R., 1997. *Experimental and analytical studies of steel plate shear walls as applied to the design of tall buildings*, Proceedings of 4th Conference on Tall Buildings in Seismic Regions, Los Angeles, CA.
29. Tromposch, E.W. and Kulak, G.L., 1987. *Cyclic and static behaviour of thin panel steel plate shear walls*. Structural Engineering Report No. 145, Department of Civil Engineering, University of Alberta, Edmonton, AB.
30. Troy, R.G. and Richard, R.M., 1979. *Steel plate shear walls resist lateral load, cut costs*. Civil Engineering — ASCE, February.
31. Wagner, H. (1931). *Flat sheet metal girders with very thin webs, Part I - General theories and assumptions*. Technical memo No. 604, National Advisory Committee for Aeronautics, Washington, DC.
32. Xue, M. and Lu, Le-Wu, 1994a. *Interaction of steel plate shear panels with surrounding frame members*. Proceedings of the Structural Stability Research Council Annual Technical Session, Bethlehem, PA, pp. 339-354.
33. Xue, M. and Lu, Le-Wu, 1994b. *Monotonic and cyclic behaviour of infilled steel shear panels*. Proceedings of the 17th Czech and Slovak International Conference on Steel Structures and Bridges, Bratislava, Slovakia.
34. Yamada, M., 1992. *Steel panel encased R.C. composite shear walls*. Proceedings of the ASCE Engineering Foundation Conference on Composite Construction in Steel and Concrete II, pp. 899-912.

APPENDIX A

Material Properties Testing

A.1 Frame Member Properties

Tests were conducted to determine the stress-strain relationships of the critical frame members used in the SPSW4 test. One coupon was taken from a flange mid-width and web mid-height of each section received from the supplier, and tested according to the standard coupon dimensions presented in ASTM E 8M - 94a (ASTM, 1994). A summary of the results are presented in Table A1. Figure A1 shows a typical stress strain curve obtained for a 'flange' coupon.

TABLE A1: Summary of boundary frame coupon test results

Specimen	σ_y (MPa)	σ_u (MPa)	Strain at ultimate (%)
A Flange	393	579	15
A Web	424	587	15
B Flange	382	555	13
B Web	413	568	16
TYPICAL	380	550	10+

NOTES:
S200x34 section assumed to have identical material properties.

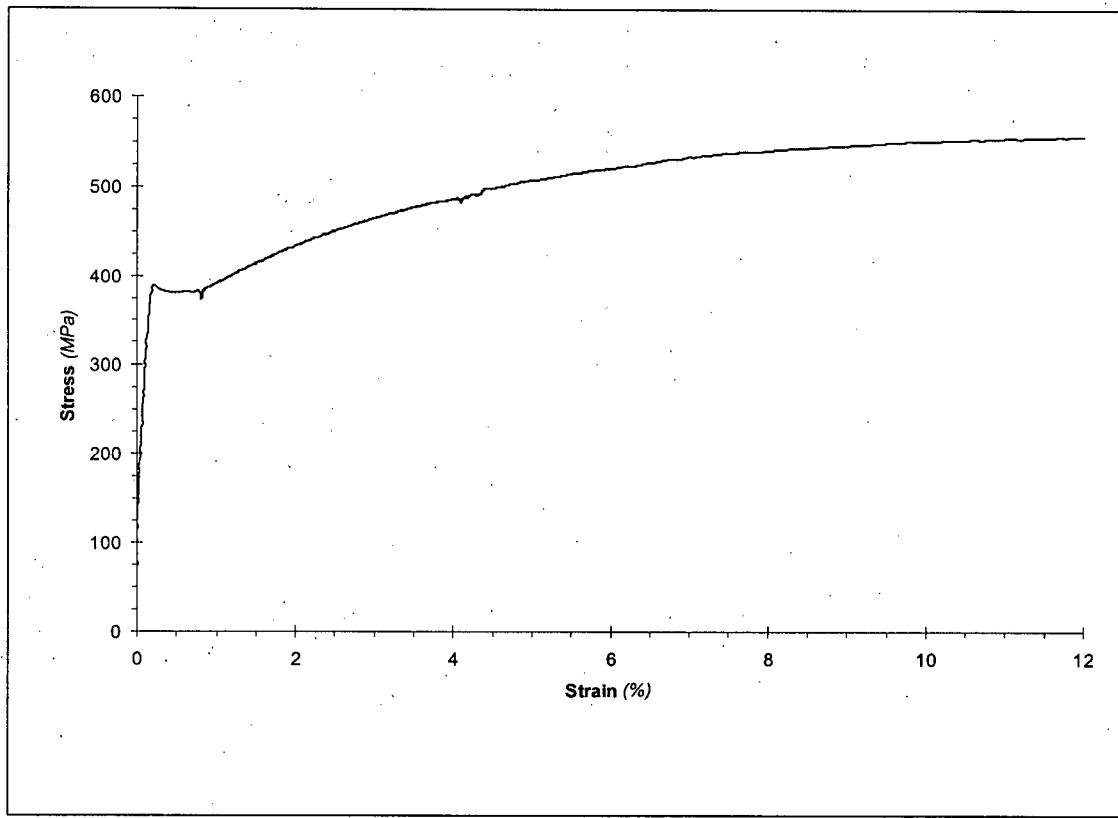


FIGURE A1: Stress strain curve obtained for 'flange' coupon BF

While a limited number of samples were tested, the consistency between members suggested that satisfactory results could be obtained by using these approximate properties for analytical modelling and analysis. No attempt was made to determine the residual stress distribution in the section from the hot rolling process.

A.2 Infill Plate Properties

Tests were conducted to determine the stress-strain relationships of the infill plate material used in the SPSW4 test. A series of coupons were created from each sheet of steel plate received from the supplier. Coupons taken in both orthogonal directions

were used. All tests were conducted on specimens dimensioned as per ASTM E 8M-94a (ASTM, 1994). A summary of the results are presented in Table A2. Figure A2 shows the stress strain curve for a typical infill plate coupon. No attempt was made to determine the residual stress distribution in the plate from the hot rolling process. The orthogonal testing confirmed essentially uniform behaviour regardless of plate orientation.

It is evident from Figure A2 that the material exhibits the classic "hot rolled" properties of a linear elastic range, yield plateau, and strain hardening. These properties were desirable for the infill plate, to allow for large in-plane and buckling deformations of the plate, while minimizing brittle behaviour. It also reflected the sheet steel properties that would be present in a commercial design, using thicker hot rolled plates. The ultimate strain of each coupon exceeded 10 %.

For all calculated quantities presented, a significant amount of scatter in the results is evident. This reflects the relatively poor measuring resolution of the load and strain measuring devices. It is particularly noticeable in the values for Young's Modulus of Elasticity, E . However, all results show a consistent trend, with all tests providing the desired "hot-rolled" properties. There appeared to be no significant influence due to the orientation of the coupon from the plate.

TABLE A2: Summary of infill plate coupon test results

Specimen	σ_y (MPa)	σ_u (MPa)	Strain at ultimate (%)	E (GPa)
A1L	327	391	14	221
A2L	310	—	15+	211
A3L	322	392	18	406
A1S	314	380	22	—
A2S	323	—	16+	238
A3S	—	—	—	—
B1L	—	—	—	—
B2L	335	395	14	303
B3L	311	389	20	523
B1S	324	388	16	174
B2S	312	376	23	1517
B3S	313	388	13	—
C1L	356	415	12	329
C2L	303	383	17	216
C3L	341	414	14	198
C1S	320	394	26	202
C2S	320	387	17	382
C3S	330	387	22	244
TYPICAL	320	370	10+	—

NOTES:
Coupons designated with 'L' and 'S' are from long and short directions, respectively.

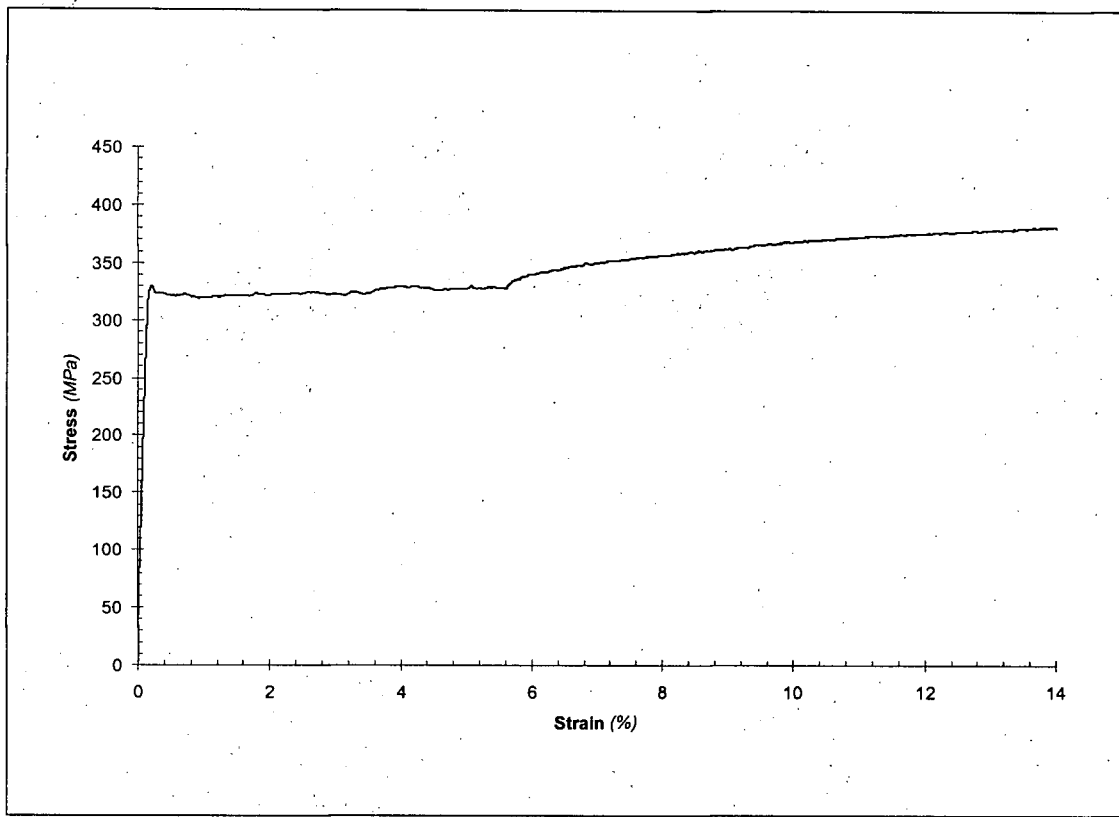


FIGURE A2: Typical stress strain curve, from coupon A2S

A.3 Fish Plate Properties

Tests were conducted to determine the stress-strain relationships of the fish plate material used in construction of the SPSW4 specimen. A series of coupons were created, in both orthogonal directions, from the single sheet of steel plate received from the supplier. All tests were conducted using specimens dimensioned as per ASTM E 8M-94a (ASTM, 1994). A summary of the results are presented in Table A3. Figure A3 shows the stress strain curve for a typical fish plate coupon. No attempt was made to determine the residual stress distribution in the plate from the hot rolling process.

TABLE A3: Summary of fish plate coupon test results

Specimen	σ_y (MPa)	σ_u (MPa)	Strain at ultimate (%)	E (GPa)
F1L	244	333	19	243
F2L	257	340	13	184
F3L	262	346	13	155
F1S	281	351	18	240
F2S	303	360	15	181
F3S	296	357	14	176
TYPICAL	260	350	10+	—

NOTES:
Coupons designated with 'L' and 'S' are from long and short directions, respectively.

It is evident from Figure A3 that the material used exhibits the classic “hot rolled” properties of a linear elastic range, yield plateau, and strain hardening. These properties were desirable for the fish plate, to reflect the sheet steel properties that would be present in a commercial design, using thicker hot rolled plates. The ultimate strain of each coupon exceeded 10 %.

For all calculated quantities presented, some minor scatter in the results is evident. It is particularly noticeable in the values for Young’s Modulus of Elasticity, E, where errors arise from the data acquisition recording resolution. However, all results show a consistent trend, with all tests providing the desired “hot-rolled” properties.

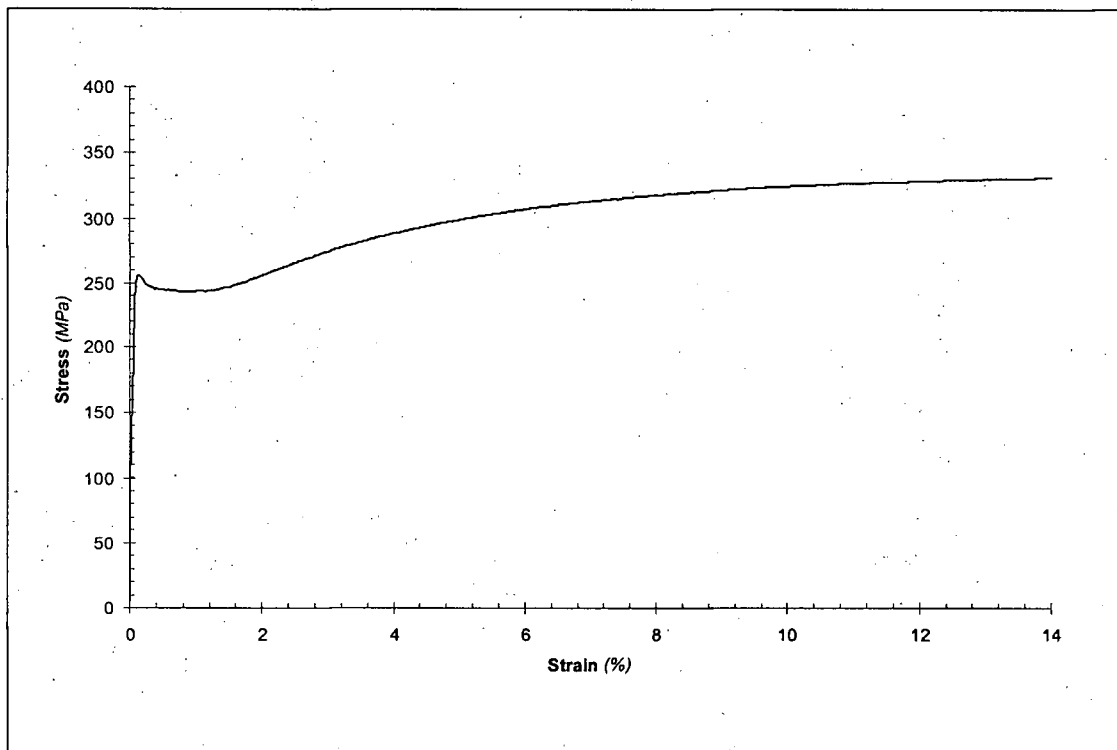


FIGURE A3: Typical fish plate stress strain curve, from coupon F1L

Testing in orthogonal directions revealed that the plate properties are slightly different. It was felt that this would not significantly affect the specimen performance, due to the intended role of the fish plates and their size. All strips used for the fish plates were cut in the short direction, such that the installed configuration had the short direction from the original plate running parallel to the boundary frame.

APPENDIX B

Strain Gauge Analysis Software

B.1 About the Software

A computer program, *ROSETTE*, was developed in the Department of Civil Engineering at the University of British Columbia, to aid in the analysis of recorded strain gauge data. Using a Windows based interface, it was implemented to allow for repetitive analysis of strain gauge data, with an emphasis on data from strain rosettes. Features of the software include the ability to perform basic arithmetic functions on a data set, such as adding a constant, and calculating principle strains and related angle of inclination from strain rosette data.

The software, currently in Version 1.0, permits selection of data records from three active data sources. These correspond to the output data files, in ASCII format, produced by the various data acquisition systems in the UBC Structures Laboratory. Using all three data sources simultaneously permits control channels to be identified when more than 1 data acquisition system was used during a test.

The strain rosette calculation routines make use of the 0 - 45 - 90 configuration selected during the steel plate shear wall project. An explanation of the system of equations necessary to solve for the desired strains from the data collected is provided in Popov

(1990). These respective strains are then used as inputs into Mohr's Circle for Strain, where the principle strains and corresponding angle of inclination are computed.

B.2 Suggested Improvements to the Software

Under low recorded strain levels, the calculation of the principle strain magnitudes and inclination may be significantly affected by the resolution of the data acquisition system. Users of the software should be made aware of this source of error. A potential solution would be to prevent output of numerical results for calculations below preset threshold inputs, with warnings displayed in their place. Further study, potentially on a project-by-project basis is required to establish these threshold magnitudes.

While the software will allow for near immediate processing of the strain gauge data with little effort at the conclusion of a testing sequence, no facility exists to produce output in a graphical form. Other software, such as a spreadsheet application, would be required. The implementation of basic charting abilities, or even animation, may prove useful in interpreting the data in some instances.

Analysis of the data should also include the evaluation of maximum and minimum values in the data set.

APPENDIX C

Sample CANNY-E Input Record

FOR: SPSW2 Monotonic model with $\alpha = 37$ degrees

January 22, 1997

input data for program <CANNY-E>

steel panel specimen analysis, 1 storey, 1-panel replaced by 15 struts
SPSW2 specimen

// analysis assumptions and options

title : SPSW2 Specimen Modelled

title : using building model

title : 15-SPAR at alpha 37-degree

title : CODE -- Push Over

force unit = N

length unit = mm

time unit = sec

static analysis in X-direction (Push over analysis)

Include P-Delta effects

gravity acceleration is 9805 (default 9.8)

output of overall responses at floor level 8F

output of nodal displacement response

output of column response

output of beam response

output of link element response

// control data for static analysis

master DOFs for analysis control: X-translation at 8F

loading direction in 0 degree (global X-direction)

displacement limit 1000.0

output of analysis results at every 0-step

destination at base shear factor 50000 by increment 2000

destination at base shear factor 100000 by increment 1000

destination at base shear factor 140000 by increment 400

destination at base shear factor 160000 by increment 200

destination at base shear factor 180000 by increment 100

destination at base shear factor 225000 by increment 75

//

// ===== floor level data =====

8F(rigid floor, above 7F) Z=900 Lf=1.0

7F(above 6F) Z=801 Lf=0

6F(above 5F) Z=667 Lf=0

5F(above 4F) Z=534 Lf=0

```

4F(above 3F) Z=400 Lf=0
3F(above 2F) Z=267 Lf=0
2F(above 1F) Z=134 Lf=0
1F(footing floor, fixed) Z=0 Lf=0

```

```
// ===== frame locations =====
```

```

frame Y1:Y0 = 0
frame X1:X0 = 0
frame X2:X0 = 26
frame X3:X0 = 74
frame X4:X0 = 100
frame X5:X0 = 126
frame X6:X0 = 174
frame X7:X0 = 200
frame X8:X0 = 226
frame X9:X0 = 274
frame X10:X0 = 300
frame X11:X0 = 326
frame X12:X0 = 374
frame X13:X0 = 400
frame X14:X0 = 426
frame X15:X0 = 474
frame X16:X0 = 500
frame X17:X0 = 526
frame X18:X0 = 574
frame X19:X0 = 600
frame X20:X0 = 626
frame X21:X0 = 674
frame X22:X0 = 700
frame X23:X0 = 726
frame X24:X0 = 774
frame X25:X0 = 800
frame X26:X0 = 826
frame X27:X0 = 874
frame X28:X0 = 900

```

```
// ===== node locations =====
```

```

node at X1 Y1 1F to 8F
node at X2 to X27 Y1 1F
node at X2 to X27 Y1 8F
node at X28 Y1 1F to 8F

```

```
// ===== node displacement degrees of freedom =====
```

```

general node degrees of freedom: all translations, X-Z rotation, Y-Z
rotation

```

```
node X1 to X28 Y1 1F eliminate all components
```

```
// ===== weights at nodes =====
```

```
/* lumped weight 1 N at each corner node
```

```
node X1 Y1 8F, w = 1
```

```
node X28 Y1 8F, w = 1
```

```

// ===== element data : beam =====
/* first story beam
out Y1 X1 to X2 8F LU5 RU5 AU6 0 0
out Y1 X2 to X27 8F LU5 RU5 AU6 0 0
out Y1 X27 to X28 8F LU5 RU5 AU6 0 0

// ===== element data : column =====
/* left column
out Y1 X1 1F to 2F BM10 TM10 SU108 AU109 38 0 /* No torsional
stiffness
out Y1 X1 2F to 7F BM10 TM10 SU108 AU109 0 0 /* for columns
out Y1 X1 7F to 8F BM10 TM10 SU108 AU109 0 38
/* right column
out Y1 X28 1F to 2F BM10 TM10 SU108 AU109 38 0
out Y1 X28 2F to 7F BM10 TM10 SU108 AU109 0 0
out Y1 X28 7F to 8F BM10 TM10 SU108 AU109 0 38

// ===== link element data =====
/* first story
out Y1 X1-X3 7F-8F U100
out Y1 X1-X6 6F-8F U100
out Y1 X1-X9 5F-8F U100
out Y1 X1-X12 4F-8F U100
out Y1 X1-X15 3F-8F U100
out Y1 X1-X18 2F-8F U100
out Y1 X1-X21 1F-8F U100
out Y1 X4-X24 1F-8F U100
out Y1 X7-X27 1F-8F U100
out Y1 X10-X28 1F-7F U100
out Y1 X13-X28 1F-6F U100
out Y1 X16-X28 1F-5F U100
out Y1 X19-X28 1F-4F U100
out Y1 X22-X28 1F-3F U100
out Y1 X25-X28 1F-2F U100
out Y1 X1-X4 2F-1F U100
out Y1 X1-X7 3F-1F U100
out Y1 X1-X10 4F-1F U100
out Y1 X1-X13 5F-1F U100
out Y1 X1-X16 6F-1F U100
out Y1 X1-X19 7F-1F U100
out Y1 X2-X22 8F-1F U100
out Y1 X5-X25 8F-1F U100
out Y1 X8-X28 8F-1F U100
out Y1 X11-X28 8F-2F U100
out Y1 X14-X28 8F-3F U100
out Y1 X17-X28 8F-4F U100
out Y1 X20-X28 8F-5F U100
out Y1 X23-X28 8F-6F U100
out Y1 X26-X28 8F-7F U100

// =====stiffness and hysteresis parameters =====

```

APPENDIX C: Sample CANNY-E Input Record 158

```

/* yielding stress = 380 MPa, maximum 550 MPa for beam and column
/* yielding stress = 320 MPa, maximum 370 MPa for panel
/* top beam (S200*34)
/*U1 15 2e+5 27.0e+6 101080000 101080000 120080000 120080000 -0.04646
-0.04646 0.0015 0.0015 0 0 0 0 0 0.5 0.7
/*U3 1 2e+5 4370 /* elastic axial stiffness of beam
/* single beam (S75*8)
U5 15 2e+5 1.04e+6 25850000 25850000 30901600 30901600 -0.04646 -
0.04646 0.0015 0.0015 0 0 0 0 0 0.5 0.7
U6 1 2e+5 2140 /* elastic axial stiffness of beam
/* axial properties of link element (t = 1.5 mm) fy = 320 MPa
U100 15 2.0e+5 120.0 0 38400 0 44400 0.0015 0.0015 0.00015
0.00015 0 0 0 0 0 0.5 0.7
U101 15 2.0e+5 120.0 38400 38400 44400 44400 0.0015 0.0015 0.00015
0.00015 0 0 0 0 0 0.5 0.7
/* column axial and shear properties
U109 1 2e+5 1070 /* axial
U108 1 0.857e+5 270.9 /* shear
/* column multi-spring model, plastic hinge zone = 0.2*180 = 36 mm
M10 2.0e+5 0.19e+6 1.04e+6 0.2
/* web plate tw = 4.3 mm, 10-spring for total 63 mm
0 -28.35 6.3 10 0 0 0
/* HN Fy dy F'y Nu Ka Alpha Gama Beta Theta
22 14222 0.0945 14222 0.724 21 0 0 0.0015 0.8
/* flange plate tf= 6.6 mm, 5-spring for 59 mm
0 -34.8 69.6 2 -23.6 11.8 5
/* HN Fy dy F'y Nu Ka Alpha Gama Beta Theta
22 40887 0.0945 40887 0.724 21 0 0 0.0015 0.8
//

```